Sound Transmission Analysis of Circular Sandwich Panels Fully and Partially Treated with MR Fluid Core Layer

Masoud Hemmatian

A Thesis

In the Department

of

Mechanical, Industrial and Aerospace Engineering

Presented in Partial Fulfillment of the Requirements

For the Degree of

Doctor of Philosophy (Mechanical Engineering) at

Concordia University

Montreal, Quebec, Canada

September 2017

CONCORDIA UNIVERSITY

SCHOOL OF GRADUATE STUDIES

This is to certify that the thesis prepared

By: Masoud Hemmatian

Entitled: Sound Transmission Analysis Of Circular Sandwich Panels Fully And
                Partially Treated With MR Fluid Core Layer

and submitted in partial fulfillment of the requirements for the degree of

                Doctor of Philosophy (Mechanical Engineering)

complies with the regulations of the University and meets the accepted standards with respect to
originality and quality.

Signed by the final examining committee:

                                                                    Chair
        Dr. Anjali Awasthi

                                                                    External Examiner
        Dr. Ruxandra Botez

                                                                    External to Program
        Dr. Fariborz Haghighat

                                                                    Examiner
        Dr. Rama Bhat

                                                                    Examiner
        Dr. Ion Stiharu

                                                                    Thesis Supervisor
        Dr. Ramin Sedaghati

Approved by _____
            Dr. Ali Dolatabadi, Graduate Program Director

Friday, October 27,
2017
                    _____
                        Dr. Amir Asif, Dean
                        Faculty of Engineering and Computer Science

ABSTRACT

Sound transmission analysis of circular sandwich panels fully and partially treated with MR fluid core layer

Masoud Hemmatian, Ph.D.

Concordia University, 2017

Magnetorheological (MR) fluid is categorized as smart material whose rheological properties can be varied instantaneously under the application of an external magnetic field. Utilization of these smart multifunctional materials into the devices and structures provides a unique opportunity to develop adaptive devices/structures capable of changing their dynamic characteristics in response to wide range of external disturbances. MR fluid have been recently utilized in sandwich panels to provide variable stiffness and damping to effectively control vibrations. The main objective of the present dissertation is to investigate the sound transmission loss (STL) capability of sandwich panels treated with MR fluids at low frequencies. This dissertation contributes in three major parts. First the effect of applied magnetic field on the structural and acoustical behavior of MR fluid sandwich panels is experimentally investigated. An experimental test setup including two anechoic chambers and an electro-magnet has been designed and fabricated to experimentally investigate the effect of applied magnetic field on the STL and natural frequency of sandwich panels having different thicknesses of MR core layer. The magnetic flux density generated inside the electromagnet is simulated using magneto-static finite element analysis and validated with the measured magnetic flux density using Gaussmeter. The results from the magneto-static analysis is used to derive approximate polynomial functions to evaluate the magnetic flux density as a function of the plate's radius and applied current.

In the second part, the sound transmission behavior of MR based-circular sandwich panels is investigated through development of efficient numerical models. The forced vibration equations of motion of the circular sandwich panel fully treated with MR fluid core layer is first derived utilizing Ritz and finite element (FE) methods using circular and annular elements. The transverse velocity in the transmitted side of the panel is then calculated and utilized to obtain the sound radiated from the panel and subsequently the STL. The theoretical models are validated comparing the simulation results with those obtained experimentally. The developed models have been subsequently used to conduct parametric studies in order to investigate the effect of the applied magnetic field, the thickness of the face sheets and the thickness of the MR core layer on the first axisymmetric natural frequency and STL of the MR based-clamped circular panels.

The last part of the present study is devoted to the topology optimization of sandwich panels partially treated with MR fluid and silicone rubber core layer. The FE model of the sandwich panel partially treated with MR fluid and silicone rubber has been developed using circular and 4-node quadrilateral elements. The developed model is then utilized to investigate the vibroacoustic behavior of MR-based sandwich panels and to obtain their natural frequencies, loss factors and STL. Subsequently, systematic parametric studies on the effect of the position of the MR fluid and silicone rubber segments on the first axisymmetric natural frequency, corresponding loss factor and also STL are presented. It has been shown that the vibrational and acoustical behavior of the sandwich panel considerably changes by varying the location of the MR fluid treatment segments. A formal constrained and unconstrained design optimization strategy have been subsequently formulated to identify the optimal location of the MR fluid segments. Due to high computational cost associated with the FE model and considering that in each optimization iteration, FE model requires to be executed several times, approximate meta-models have been developed using

iv

random and D-optimal design points to conduct optimization problems efficiently without using the full FE model. The developed meta-models are then utilized to solve the topology optimization problems using the genetic algorithm (GA) and integer programing (IP) problems. The suitability of the identified optimal candidates are further evaluated using the developed finite element model to determine the true optimized topologies for the constrained and unconstrained problems.

This thesis is dedicated to

my dear and beloved wife

Sheida

ACKNOWLEDGMENT

Foremost, I would like to express my sincere gratitude to my supervisor Professor Ramin Sedaghati for his continuous support and encouragement throughout my PhD study. His remarkable contributions and ideas, motivations, vast knowledge and positive outlook enlighten me all over this thesis which I gratefully and appreciatively acknowledge.

Also, I would like to acknowledge Dan Juras, technical officer of Mechanical, Industrial and Aerospace Engineering at Concordia University, for his great help in my experimental study.

Last but not the least, I would like to extend my sincere thanks and appreciation to my wife Sheida Zolfaghari, my sister Mina Hemmatian, my brothers-in-laws Mohammad Yaghmaei and Shayan Zolfaghari, my parents Abdolhosein Hemmatian and Shahla Zolfaghari, and my parents-in-law Heshmat Zolfaghari and Shahla Haghighat, for their patience, encouragement and constant support.

TABLE OF CONTENTS

NOMENCLATURE

Symbol	Definition
A	Area of circular plate
Amp	Ampere
B	Magnetic flux density
c_0	Speed of sound in the air
D_1, D_3	Elasticity matrices of the front and back face sheets
dB	Decibel
E_1, E_3	Young's modulus of the front and back face sheets
F	Vector of external forces
G	Half-space free field Green's function
G_1, G_3	Shear modulus of the front and back face sheets
G_2	Complex shear modulus of the core layer
G_2', G_2''	Storage and loss moduli of the core layer
G_{MR}', G_{MR}''	Storage and loss moduli of MR fluid
G_{SR}', G_{SR}''	Storage and loss moduli of silicone rubber
Hz	Hertz
h_1, h_3	Thickness of the front and back face sheets
h_2	Thickness of the core layer
I	Applied current to the electromagnet
I_2	Moment of inertia of the core layer
K	Stiffness matrix

k	Radial wave number in medium
k_0	Free wave number in medium
M	Mass matrix
m	Circumferential wave number
mT	Millitesla
Pa	Pascal
P_b	Blocked pressure
P_i	Incident pressure
P_r	Reflected pressure
R	Radial distance to the observation point
r, θ, z	Cylindrical coordinate
r, θ, α	Polar coordinate
R_o	Outer radius of the circular panel
r_ω	Rate of change of natural frequency
r_η	Rate of change of loss factor
STL	Sound transmission loss
u	In-plane radial displacement in r direction
u_1^0, u_3^0	In-plane radial displacements of the mid-plane of the front and back face sheets in in r direction
u_{1n}^0, u_{3n}^0	In-plane radial displacements of the mid-plane of the front and back face sheets in r directions for node n
v	In-plane circumferential displacement in θ direction

v_1^0, v_3^0	In-plane circumferential displacements of the mid-plane of the face sheets in θ direction
$v_{1_n}^0, v_{3_n}^0$	In-plane circumferential displacements of the mid-plane of the front and back face sheets in θ direction for node n
w	Transverse displacement
$\bar{X}$	Binary design vector
X^+	Pseudo inverse of X
z_1, z_3	Transverse coordinate in the local coordinate system of the front and back face sheets considering the origin at the mid-plane of the face sheets
α_i	Incident angle
δ	Nodal displacement vector
δ_e	Nodal displacement vector of element
η_n	nth loss factor
v_1, v_3	Poisson's ratio of the front and back face sheets
$\Pi_{\text{inc}}, \Pi_{\text{rad}}$	Incident and radiated acoustic powers
ρ_1, ρ_3	Mass density of the face sheets
ρ_2	Mass density of the core layer
ρ_f	Density of the medium
ω	Frequency of incident sound
ω_n	nth natural frequency
$\cdot$	Derivation with respect to time
$\dfrac{\partial}{\partial r}, \dfrac{\partial}{\partial \theta}$	Partial derivation with respect to r and θ

LIST OF FIGURES

LIST OF TABLES

CHAPTER 1

INTRODUCTION

1.1. Motivation and General Goal

Acoustical properties of the flexible light-weight structures is often the key feature in the analysis and design of cabin's walls and structures utilized in many engineering systems especially ground and aerospace vehicles. As the external sound meets the cabin's structure, the structure vibrates and transmits the sound into the cavity. Many efforts have been conducted to investigate the acoustical properties of panels (single and multi-layered) in order to passively control the sound transmission with limited success. This is mainly due to the fact that flexible structures are generally inefficient sound barriers especially at low frequencies. Sandwich or multi-layer structures offer superior structural performance including high ratio of flexural stiffness to the weight, good energy absorption and low production cost which make these structures favorable to many industrial applications. Light weight and high flexural stiffness to weight ratio are encouraging properties of sandwich panels when the structural vibration is an issue of primary concern. On the contrary, light weight is less desirable with respect to acoustical properties such as sound transmission. The acoustical characteristics of the structures is directly correlated with its areal density and as the areal density increases, the sound transmission loss (STL) of the structure is enhanced. The main goal of the present research study is to fundamentally investigate the application of controllable magnetorheological (MR) fluids in the improvement of structures' acoustical behavior. The focus will be on sandwich panels with MR fluid as the core layer. While

there are some studies on structural vibration control using MR materials, the research on sound radiation analysis, optimization and control of MR-based adaptive structures is very limited and is in its infancy.

In this chapter, first a review on the pertinent literature in the subject of the sound transmission in sandwich panels with viscoelastic, MR and electrorheological (ER) fluid core layers is presented. Then, the fundamental concepts regarding the sound transmission loss of sandwich structures is described and the MR fluid is introduced. This is followed by the identified research gaps and contributions of the present study. Finally, the organization of the dissertation is demonstrated.

1.2. Fundamental Concepts

This section is devoted to briefly present the fundamental concepts related to the acoustical behavior of sandwich structures and also MR fluid materials. First sandwich structures are briefly discussed. This is followed by fundamental characteristics of sound comprising its frequency and loudness. Then the nature of STL in frequency domain is explained and the effective parameters in each range of frequency are discussed. The compound, operational modes and common models of MR fluid are illustrated in the last part of this section.

1.2.1. Sandwich Structures

Sandwich structures are considered as a class of composite materials and composed of the face sheets and the core layer as shown in Figure 1.1. The core layer is typically a thick, light-weight and low strength material such as foams, viscoelastic rubbers and honeycombs that is

enclosed within two thin and highly stiff face sheets like sheet metals and fiber composite materials. These configuration provide a structure with a high ratio of bending stiffness to weight compared to the one that is consists of a monolithic material with the same weight. In addition, the damping characteristics and the thermal insulation of the structures can be improved by choosing a proper material for the core layer. Cost effectiveness is another advantage of the sandwich structures compared to other composite material making them supreme for industrial applications.
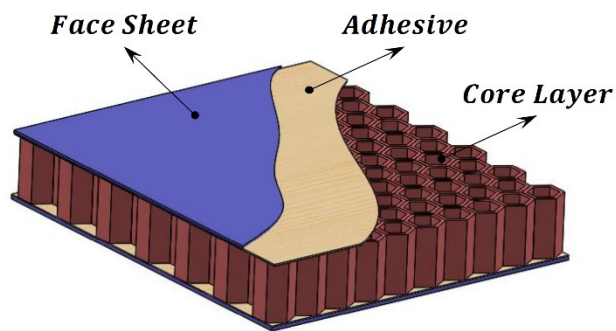
Figure 1.1. Schematic of sandwich structure with honeycomb core layer.

1.2.2. Sound

Sound is basically vibration or oscillations in the pressure that propagates as a wave in a transmission medium like air and water. Sound is typically defined by its frequency and loudness. The frequency of sound is the number of fluctuations in the pressure per second and determines the pitch of the sound. The frequency is measured in Hertz (Hz) in the International Systems of Units (SI). Audio rate is the audible frequency range for humans which is from about $20\ Hz$ to $20000\ Hz$ in the air at standard temperature and pressure. And sub-audio rate and ultrasonic refer to the sounds with the frequencies below $20\ Hz$ and above $20000\ Hz$, respectively. The frequency is the factor that determines the tone of the sound including whether the sound is treble or bass.

For example, musical instruments such as tuba and flute produce low frequency bass and high frequency treble sounds, respectively. Figure 1.2 shows the typical sounds in the audible frequency range.
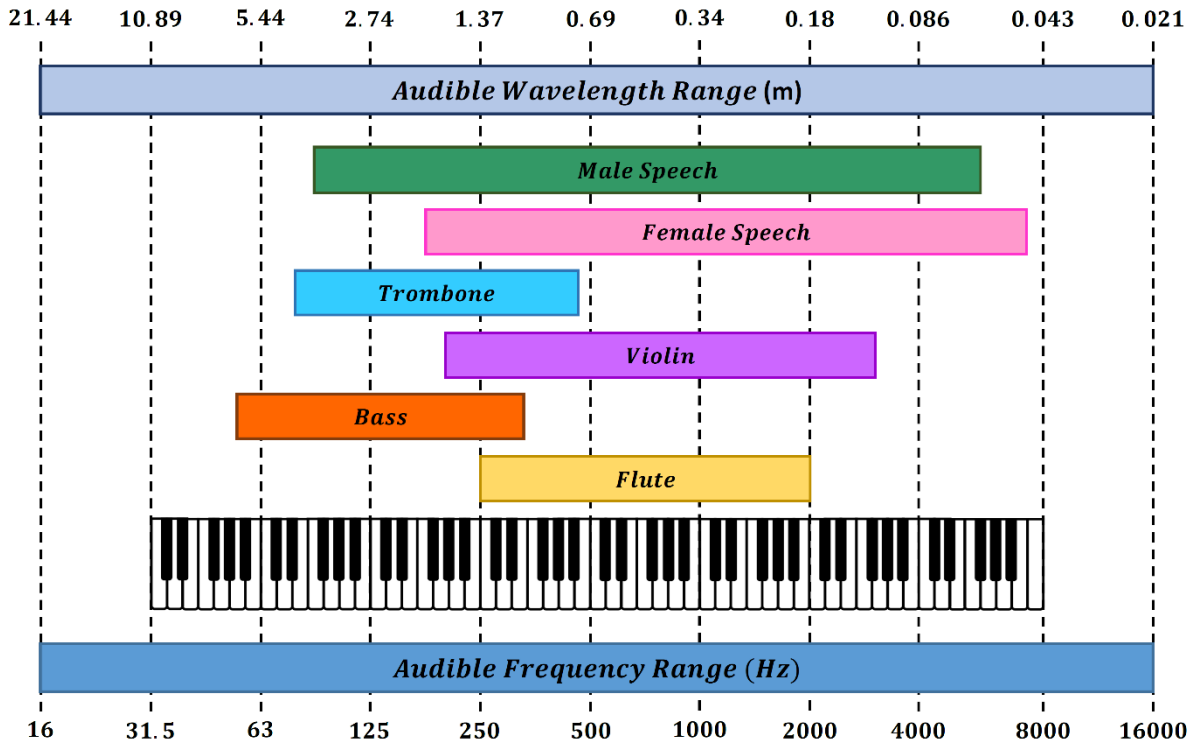
Figure 1.2. Typical sounds in the audible frequency range [1].

The loudness of the sound depends on the amplitude of the pressure variation in which small and large amplitude of the pressure variation correspond to weak and loud sounds, respectively. A human can detect a wide range of pressure variations starting from $20 \, \mu Pa$ which is called the threshold of hearing up to about $200 \, Pa$ which causes actual pain and damage to the ear. Considering that dealing with sound pressure in Pa needs a very large and inconvenience numbers, a logarithmic scale called decibel (dB) is used for the loudness of sound. Sound pressure level (SPL) is evaluated in decibel and defined using the threshold of hearing ($20 \, \mu Pa$) as the reference level (P_0) which is equal to $0 \, dB$ and dB is defined as 20 times of the logarithm of the measured

4

sound pressure (P) to the reference pressure ratio ($SPL = 20\ log_{10}\frac{P}{P_0}$). Table 1.1 shows some typical sound pressure levels in air.

Table 1.1. Some typical sound pressure levels in air [2].

Sources at $1\ m$	Sound Pressure (Pa)	Sound Pressure Level (dB)
Rifle	200 Pa	140 dB
Threshold of pain	20 Pa	120 dB
Pneumatic hammer	2 Pa	100 dB
6 dB = double the Pa	1 Pa	94 dB
Street traffic	0.2 Pa	80 dB
Talking	0.02 Pa	60 dB
Library	0.002 Pa	40 dB
TV Studio	0.0002 Pa	20 dB
Threshold of hearing	0.00002 Pa	0 dB

1.2.3. Sound Transmission Loss

As an acoustic wave strikes the sandwich panel as shown in Figure 1.3, a part of the wave is absorbed, a part is reflected and a part causes the face sheet to vibrate and to transmit the sound. The sound transmission loss (STL) is an index to evaluate the sound transmission performance of structures as the ratio of incident sound pressure to the transmitted sound pressure. The STL depends on the panel's characteristics including material and boundary conditions and the fluid in which the panel is immersed such as air or water.

5
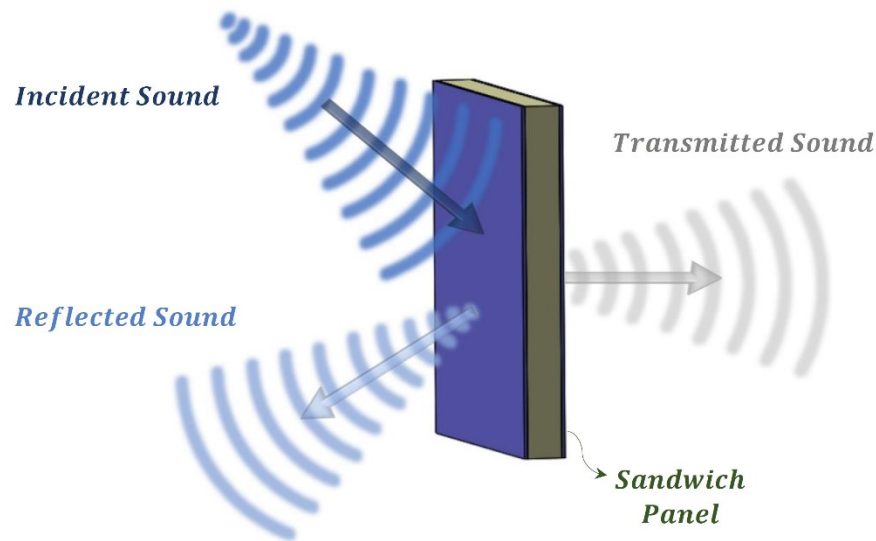
Figure 1.3. Illustration of sound transmission through sandwich panels.

Considering that STL is frequency dependent and human hearing system is unable to distinguish between two separate sounds with frequencies too close to each other, the STL is usually reported for each octave band or for each one-third octave band. As it can be seen in Figure 1.4, the frequency response of STL can be divided into four distinct different regions namely stiffness-controlled, resonance-controlled, mass-controlled and coincidence-controlled. The STL can be increased in stiffness-controlled region by increasing the stiffness of the panel. In the second region, the STL is controlled by the natural frequencies of the panel and the magnitude of the STL oscillation depends on the damping of the structure. In the mass-controlled region, the behavior of the STL is only governed by the mass per unit area of the panel and follows the mass-law. The last region is the coincidence region in which a sudden reduction in the STL occurs at the coincidence frequency. As shown in Figure 1.5 the coincidence occurs when the wavelength of the incident sound wave becomes equal to the wavelength of bending wave in the panel. Both flexural (anti-symmetric) and dilatational (symmetric) motions coexist at the same time in the sandwich panel as shown in Figure 1.6. It should be noted that the bending deformation of the whole panel is

defined as the flexural motion and the thickness deformation of the core in which the face sheets moves out of phase with each other is defined as the dilatational motion.
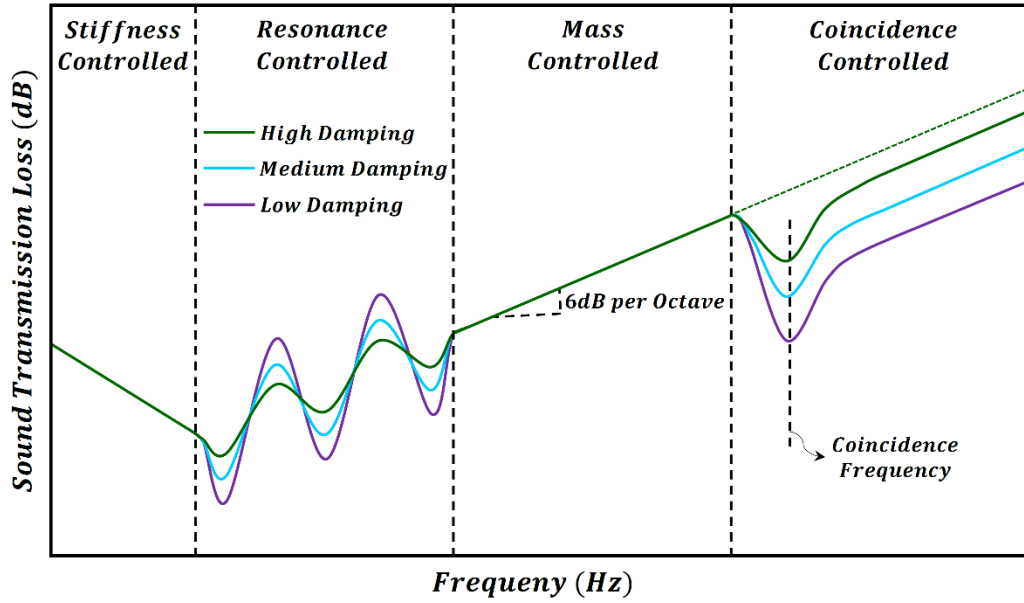
Figure 1.4. Sound transmission loss with respect to frequency [3].
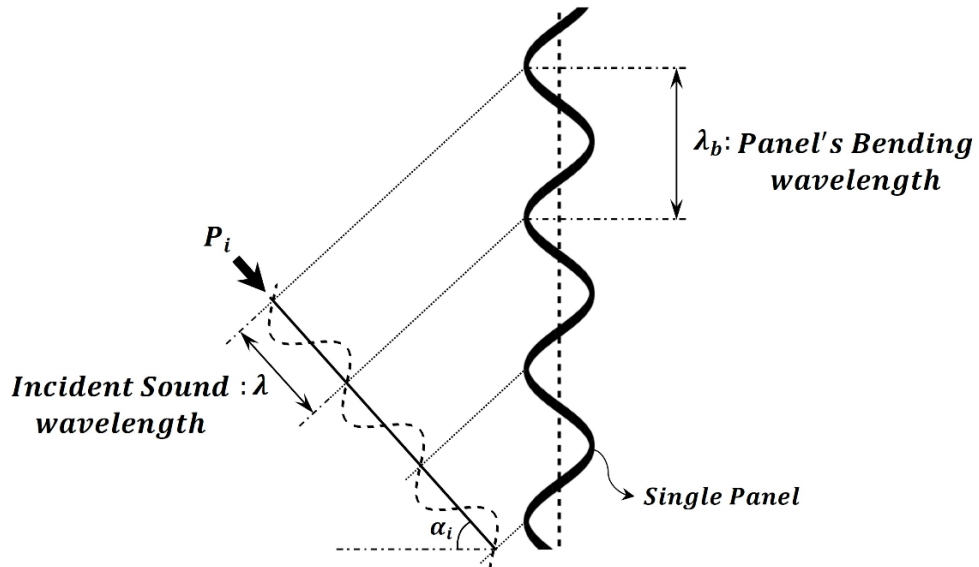
Figure 1.5. Schematic wavelength matching at the coincident frequency [4].
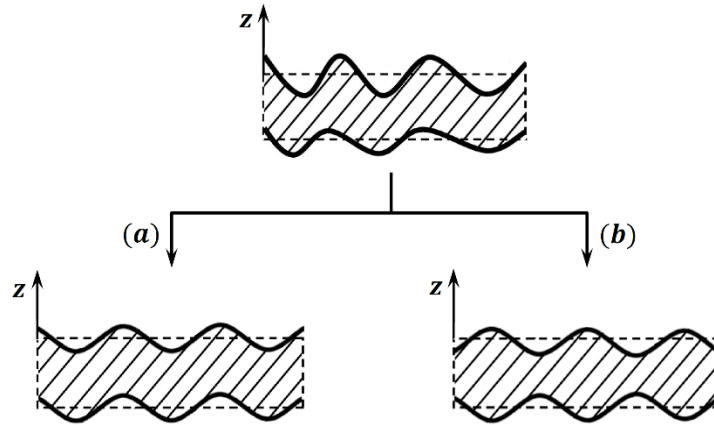
Figure 1.6. Transformation of the general motion of the sandwich panel to the (a) flexural (anti-symmetric) and (b) dilatational (symmetric) motions of the same panel [5].

1.2.4. MR Fluid

MR materials are promising controllable smart materials whose rheological behavior can be instantly changed and controlled through the application of an external magnetic field. MR materials can effectively exploit the structural motion to generate the control forces and offer the reliability of passive treatments, yet maintaining the versatility and adaptability of fully active materials, without requiring large power source and complex control systems. Compared to their Electrorheological (ER) counterparts, MR materials can provide significantly higher yield strength (in order of magnitude), and greater insensitivity to temperature variation and contaminants and also requiring only low power. MR fluids have been efficiently utilized in MR-based devices such as MR dampers and brakes to provide variable damping for the purpose of vibration control. Application of MR materials in sandwich panels, however, can effectively provide variable stiffness and damping which practically enable to semi-actively control the vibration and radiated sound in a wide range of frequencies with minimal power requirement..

A MR fluid contains micron-sized ferromagnetic particles (typically carbonyl iron particles due to its high magnetic saturation) suspended within the non-magnetic carrier fluid (typically silicone oil). As shown in Figure 1.7 in normal circumstances in the absence of the external magnetic field, the ferromagnetic particles are distributed randomly within the carrier oil. As the magnetic field applied to the fluid, the particles are aligned along the lines of magnetic flux and form a chain-like structure which resists the motion.

(a)   (b)
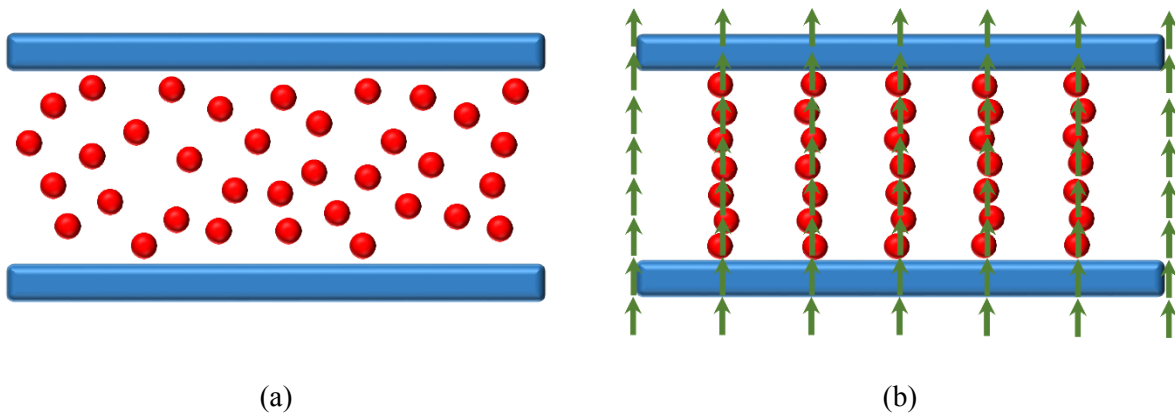
Figure 1.7. Schematic of a MR fluid (a) in absence of magnetic field, where particles are randomly dispersed (b) in presence of magnetic field with parallel chains of carbonyl iron [6].

MR fluid usually used in three operational modes of motion in the devices including flow mode, shear mode and squeeze mode. As shown in Figure 1.8 the pressure-driven flow mode is related to the fixed pole devices such as dampers and shock absorbers in which the fluid moves between two stationary plates and the applied magnetic field is normal to the flow direction. The direct shear mode and squeeze-film mode are related to the devices with relatively movable poles like clutches, brakes and bearings. The applied magnetic field is normal and in parallel to the direction of relative motion of the movable plate in shear and squeeze modes, respectively.
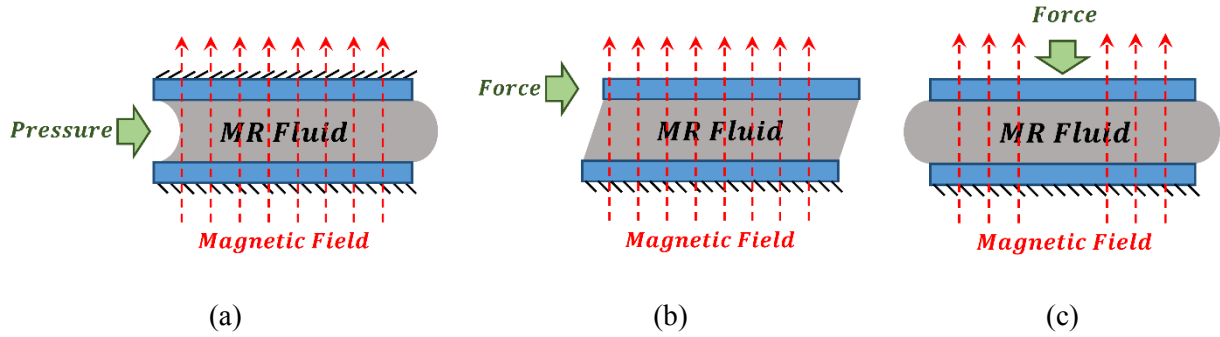
Figure 1.8. Operational modes of MR fluid in devices, (a) pressure-driven flow mode, (b) direct shear mode, (c) squeeze film mode.

In the pre-yield region the shear stress is lower than the apparent yield strength and the fluid behaves as a viscoelastic material with a complex shear modulus which is a function of the applied magnetic field. In the post-yield region, the behavior of the MR fluid is commonly modeled using the Bingham-plastic (BP) and Herschel-Bulkley (HB) in which the shear stress of the fluid is modeled as a function of the yield stress and the shear rate as shown in Figure 1.9. The controllability of MR fluids is due to their field-dependent apparent yield strength which can be instantly changed and controlled by the applied magnetic field.
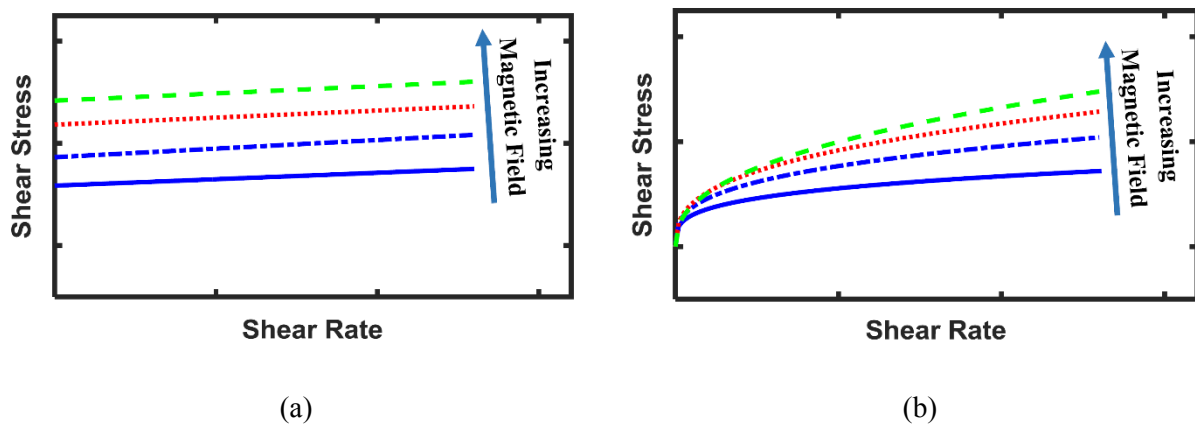
Figure 1.9. (a) Bingham plastic (BP) model for shear stress vs. shear rate (b) Herschel-Bulkley (HB) model for shear stress vs. shear rate [7].

The present research aims to fundamentally investigate the acoustic behavior of sandwich panels treated with MR fluid (MRF) as the core layer and pave the way to design adaptive sandwich structures capable of suppressing noise in wide range of frequencies. Changing the rheological properties of MRF using applied magnetic field provides a unique opportunity to change stiffness and the damping of the structure without affecting the mass unit per area of the sandwich panel.

1.3. State-of-the-Art

This section is devoted to systematically review the previous relevant studies that have been conducted in the area of the acoustical properties of passive and also smart material-based sandwich structures. First, the acoustical properties of sandwich panels treated with passive core layer including viscoelastic, honeycomb and etc. are reviewed. This is followed by the review of studies on the vibration and acoustical properties of structures treated with smart materials. Specifically studies on vibration of sandwich structures treated with ER and MR core layer are presented followed by very limited studies on the sound absorption and transmission characteristics of ME/ER based structures. Finally the research studies focused on the topology optimization of sandwich panels treated with MR and ER fluid core layer are discussed.

1.3.1. Acoustical Performance of Passive Sandwich Structures

Acoustical properties of passive damping treatments of sandwich panels have been widely studied during last decades. Most of these studies focused on the development of analytical and numerical models for sandwich structures treated with viscoelastic and honeycomb core layer to

predict and improve their vibro-acoustic behavior and to passively control the transmitted noise [8-28]. Theoretical approaches such as finite element (FE) method , boundary element method, transfer matrix method and progressive impedance method have been developed to predict the STL of infinite and finite sandwich panels [9, 10, 13, 18, 23, 26, 27]. Narayanan and Shanbhag [9, 10] and Lee and Kondo [18] implemented the governing equations of motion of the sandwich panels with viscoelastic core layer to the noise transmission problem and studied the STL of both infinite and finite sandwich panels. Tang et al. [14, 15] investigated the STL through an infinite cylindrical sandwich shell with honeycomb core layer in context of the transmission of airborne sound into aircraft interiors. They developed an explicit expression for the STL of the shell as a function of the external airflow and two independent incident angles. Veeramani and Wereley [16] studied the sound transmission through a flexible composite sandwich panel into acoustic cavity with the intent of controlling the interior noise. They treated the structure with viscoelastic damping layers for passive attenuation and utilized piezo-electric actuators for active control in the low frequency range. Brouard et al. [13] and Abid et al. [26] developed a general method based on the transfer matrix method (TMM) to predict the STL of infinite multi-layered panels including elastic, solid, fluid and porous layers subjected to a plane wave. Assaf and Guerich [23, 27] used the finite element formulation for the sandwich panel coupled with the boundary element method for the acoustic medium to investigate the STL across the panels with viscoelastic core and elastic face sheets. Kim and Han [28] used hybrid analytical/finite element method (HAFEM) in order to identify the acoustical characteristics of honeycomb sandwich panels. They used FE approximation and analytical solution in the thickness and the in plane directions, respectively and also tackled the problems with the large number of elements using combination of finite element and boundary element methods.

1.3.2. Vibration Performance of MR/ER Sandwich Structures

Passive materials are mainly effective in reducing the transmitted noise within a narrow-band at high frequency ranges. Utilizing semi-active smart materials such as MR/ER fluids and elastomers as the core layer is a new promising approach to control the vibration of sandwich structures by changing the dynamic characteristics (stiffness and damping) of the core layer. There are a number of studies that theoretically and experimentally investigated the vibration response of sandwich beams, plates and also shells treated with MR/ER fluid core layer [29-66]. Multi-layered sandwich beams treated with ER fluid core layer have been primarily studied [29-38]. Choi et al [29] experimentally investigated the vibration characteristics of hollow cantilevered beam filled with an ER fluid. They used the experimental results to derive an empirical model to predict the effect of the electric field on the vibration properties of the beam. Effective stiffness and damping coefficients of a hollow cantilever ER sandwich beam was determined using the experimental data by Berg et al. [31]. It was shown that the frequency response of the beam is dependent of the level of the applied electric field and amplitude of vibration. It was also demonstrated that the apparent damping and stiffness of the beam increases by increasing the applied electric field. Haiqing and King [32] experimentally studied a fully and partially treated ER sandwich beam clamped at both ends. They concluded that the strength of applied electric field has insignificant effect on the loss factor and resonance frequency of the fully treated sandwich beam. In the subject of sandwich beams with ER fluid core layer, some other studies have focused on the dynamic stabilities of the beam subjected to the axial load [33, 34], nonlinear random vibration [35] and optimization study [36, 37]. Yeh et al. [33, 34] investigated the dynamic stability of ER sandwich beam subjected to axial dynamic force. The instability region of the beam has

been evaluated using the finite element and harmonic balance methods. In addition, the effects of electric field and core thickness ratio on the critical load and also the influence of natural frequencies, static buckling and loss factors on the dynamic stability of the ER sandwich beam have been studied. Vaicaitis et al. [35] investigated the nonlinear dynamic response of simply supported ER sandwich beams subjected to random input. The ER fluid was considered to operate in pre-yield region and a three-parameter viscoelastic model has been used to model its rheological behavior.

Free and forced vibration analysis of adaptive rectangular and annular plates treated with ER fluid core layer have also received appropriate attention [39-47]. Yeh et al. [40, 41] used finite element method to study a rectangular sandwich plate with an ER fluid core layer and elastic and orthotropic face layers, respectively. The natural frequencies and loss factor were calculated for different electric fields and their effect on the dynamic behavior of sandwich plates was investigated. Yeh [42] also investigated free vibration of an annular sandwich plates treated with ER fluid core layer. It was reported that ER fluid core layer has a significant effect on the vibrational behavior of the annular plate and both the natural frequency and modal loss factor vary as the applied electric field or thickness of the core layer changes. Furthermore, Yeh [43, 44] studied the free vibration of rotating annular plate treated with ER fluid core layer. The equation of motion of the plate was derived using the finite element method and then used to obtain natural frequencies and modal loss factor of the rotating sandwich annular plate. The effects of the rotational velocity, applied electric field and thickness of the core layer on the natural frequencies and modal loss factor of the structure have been studied. Hasheminejad and Maleki [45] developed a dynamic model for the steady state response of a simply supported rectangular sandwich plate with ER fluid core layer. They determined the natural frequencies and modal loss factors and

14

showed that the natural frequencies depend on the applied electric field and increase with increasing the electric field. However, the lower mode's natural frequencies are more dependent on the applied electric field than the higher modes. Moreover, the force vibration of the panel for different excitation frequencies was investigated and it was presented that applying electric field is more effective in suppressing the vibration amplitude than increasing the thickness of the core layer. Most recent studies on the sandwich structures treated with ER fluid core layer have focused on the cylindrical sandwich shells [48-52]. Mohammadi and Sedaghati [48-50] studied the nonlinear free vibration of cylindrical sandwich shell fully and partially treated with ER fluid core layer. They developed a new technique to represent the equation of motions in a new H-notation in order to reduce the computational costs.

Similar to ER sandwich structures, investigations on the MR fluids-based sandwich structures initiated with research on vibration characteristics of sandwich beams treated with MR fluid core layer [53-63] . Yeh and Shih [34] studied the dynamic stability of a sandwich beam with an ER fluid core layer and then presented a theoretical model for the simply supported MR sandwich beam subjected to axial harmonic load [55]. The buckling load, natural frequency and loss factor of the structure were formulated using Galerkin's method and effects of applied magnetic field, core thickness ratio and beam length were analyzed. Transverse vibration of MR sandwich beam was experimentally and theoretically studied to demonstrate the vibration suppression capabilities of MR adaptive structures [56-59]. Lara-Prieto et al. [56] investigated the stiffness and damping characteristics of MR sandwich beams. They concluded that damping of the structure and its first natural frequency significantly increases as the applied magnetic field strengthened. It was also presented that by applying the magnetic field only to some sections of the beam makes, it is possible to shift the natural frequency of the structure to lower frequencies. Rajamohan et al. [58,

59] used Ritz and finite element methods to formulate the governing equations of a sandwich beam with MR fluid core layer between two elastic face layers. The MR core layer has been considered as a viscoelastic material with complex shear moduli. Using the experiment results, second-order polynomial functions have been presented to estimate the storage and loss moduli as a function of applied magnetic field. Parametric studies on the influence of the applied magnetic field, thickness of MR fluid layer and boundary conditions on the natural frequencies and the loss factor of the structure was conducted. Then, full state dynamic observer based linear quadratic regulator (LQR) was used to suppress the tip vibration of fully and partial treated MR sandwich beam [60]. The significant performance of the semi active controller in reducing vibration of the beam compared to the passive system was then demonstrated. Eshaghi et al. [63] characterized MR fluids in pre-yield region using a finite element (FE) model for a MR sandwich beam with clamped boundary conditions. The frequency response of a cantilevered sandwich beam treated with MR fluid core layer was used to derive the storage and loss moduli of MR fluid as a function of both the magnetic flux density and the excitation frequency.

Most recent investigations have mainly focused on the vibration control of fully and partially treated MR sandwich plates. Eshaghi et al. [64-66] utilized their proposed constitutive equations [63] to formulate the finite element model of the fully and partially treated MR-based sandwich plates to investigate their vibration behavior under varied applied magnetic field. A finite element method was utilized to derive the governing equations of motion of the cantilever sandwich plate treated with MR fluid core layer and the results compared with the experiment measurements [64]. The effect of applied magnetic field on the stiffness and damping of the structure and suppressing vibration of the plate over a broad frequency range was shown. Subsequently, sandwich plates partially treated with MR fluid were investigated [66]. A cantilevered sandwich plate with equal

cavities for the MR fluid treatment was considered and simulation results from finite element model were validated with those obtained experimentally. An optimization problem was then formulated to find the optimal location of the MR fluid treatment that maximize the changes in the first three natural frequencies and corresponding loss factors. Results showed that treating the sandwich plate at locations with relatively higher shear strains maximizes the variations in the natural frequencies and loss factors of the structure. Finally they studied the free vibration of circular sandwich panels treated with MR fluid core layer [65]. Effects of the magnetic flux density on the natural frequencies and damping of a MR circular panel with free-free boundary condition have also been investigated.

1.3.3. Optimization of Sandwich Panels

The quests for improving the performance and reducing the cost have motivated researchers to conduct design optimization of systems and structures. To do so, parametric study is necessary to choose an appropriate objective function, constraints and the design variables to be used in the optimization problem. Sandwich structures with their unique characteristics can be effectively design optimized due to many available design parameters such as the thickness, density, young and shear moduli of the face sheets and the core layer. Considering this, parametric study and design optimization of sandwich panels to improve STL are addressed in a few studies [10, 18, 20, 22, 24, 26, 27] for the past decade. Narayanan and Shanbhag [10] and Lee and Kondo [18] studied the effect of the core shear parameter on the STL of damped sandwich panels. It was shown that the damping treatment increases the performance of the sandwich panel around the resonance and coincidence frequencies. Wang et al [24] studied the optimal design of acoustical and mechanical properties of sandwich panels using genetic algorithm (GA). The influence of various design

variables including thickness of the face sheets and the core, density of the face sheets and the core, young's modulus of the face sheets, compressive and shear moduli of the core were studied. Genetic Algorithm (GA) was also used for optimization study in order to minimize the mass per unit area of the sandwich panel for the specified acoustical and mechanical properties. Abid et al. [26] simulated the effects of the thickness and young modulus of the viscoelastic layer on the STL of infinite multi-layered panels. It was shown that increasing the thickness of the viscoelastic layer improves the insulation especially near the coincidence frequency. In addition, it has been reported that the STL is reduced as the damping effect of the viscoelastic core layer decreased. Guerich and Assaf [27] conducted a parametric study to choose the objective function, the design variables and also the constraints to be used in the optimization problem. The influence of the thickness of the face sheets, the thickness of the core, the shear moduli of the core and the loss factor of the core on the STL of the sandwich panel have been studied. Next, the optimization problem has been defined and solved using sequential quadratic programming (SQP) to minimize the surface mass of the sandwich panel by constraining the acoustical behavior of the panel.

Treating the core layer of the sandwich panels with MR/ER fluids provides an opportunity to semi-actively control the damping and stiffness of the structure simultaneously for the purpose of vibration and noise control. Meanwhile, partial treatment of the core layer of the sandwich panels using MR/ER fluids may enable to change vibrational and acoustical characteristics of sandwich structures while the areal density is kept constant. In other words, the stiffness and damping of the structure changes as the position of the MR/ER fluid segments change in the core layer and this affects the corresponding structural and noise transmission characteristics such as the natural frequencies and loss factors. Moreover, there may be an optimum topology treatment for the core layer in which the influence of the applied magnetic field on the behavior of the sandwich

18

structures is higher than those fully treated. Some research works have been recently conducted on the partial treatment and topology optimization of the sandwich structures treated with MR/ER fluid core layer [32, 49, 59-62, 66]. Haiqing and King [32] investigated the resonance frequency and loss factor of a partially treated ER sandwich beam. They showed that the length of the ER fluid segment considerably affects the resonance frequencies in which resonance frequencies shift to higher values as the length of the ER layer increases. Mohammadi and Sedaghati [49] developed an optimization methodology to optimize the number of unconstrained viscoelastic and constrained electrorheological fluid patches and their distributions, thickness ratios of the electrorheological core and constrained elastic layers to base layers, and the external electric field intensity. They used the genetic algorithm combined with the sequential quadratic programming to achieve the global optimal solution. Rajamohan et al. [59] used Ritz and finite element (FE) methods to formulate the governing equations of a sandwich beam partially treated with MR fluid core layer. The MR core layer has been considered as a viscoelastic material with complex shear moduli. Second-order polynomial functions identified by the authors in their previous studies, have been used to estimate the storage and loss moduli as a function of the applied magnetic field. The developed model for partially treated MR sandwich beams has been validated by comparing the natural frequencies with those obtained experimentally. Parametric studies on the influence of the applied magnetic field, the location of MR fluid segments and their length on the natural frequencies and loss factors of the beam were then conducted. Hu et al. [61] experimentally investigated the vibration characteristics of sandwich beam treated with MR elastomer core layer under non-homogeneous small magnetic field. They fabricated MR elastomer and utilized the MR elastomer as the core layer of a sandwich beam with thin aluminum face layers. They changed the location of the applied magnetic field from the clamped end to the free end of the beam and showed

19

that the first natural frequency decreases as the applied magnetic field moves to the free end. Eshaghi et al. [66] investigated the topology optimization of a sandwich plate partially treated with MR fluid. A cantilevered sandwich plate with equal cavities for the MR fluid treatment was considered and simulation results from FE model were validated with those obtained experimentally. Genetic algorithm (GA) has been used to solve the optimization problem and find the optimal location of the MR fluid treatment that maximizes the changes in first three natural frequencies and the corresponding loss factors. Results showed that treating the sandwich plate at locations with relatively higher shear strains maximizes the variations in the natural frequencies and loss factors of the structure.

1.3.4. Acoustical Properties of ME/ER Sandwich Structures

While there are numerous studies focused on the vibration characteristics of sandwich structures fully and partially treated with MR/ER core layers, limited studies have been conducted on the sandwich panels incorporating MR/ER fluids as the core layer for the treatment of acoustical and noise control problems. In this subject, theoretical studies are mainly limited to the acoustical characteristics of infinite MR/ER sandwich panels [67-70] and other studies experimentally investigated the noise control capability and acoustic absorption of panels and foams treated with MR/ER fluid using impedance tubes [71-75]. Mahjoob et al [67, 68] studied the STL of infinite sandwich panels treated with Newtonian fluid core layer. The STL of a pyrex glass cylindrical tube treated with motor oil, ferromagnetic Nano particles in absence of magnetic field and air has been measured using impedance tube. In addition, progressive impedance method and progressive wave model have been used to predict the STL. Parametric studies on the effect of the density of the core layer and wall surfaces on the STL showed that the STL enhanced as the density of the

core layer and the face sheets increased. They also studied the magnetic field's effect on the STL of multi-layered panels treated with MR fluid as the core layer [69]. They used linear viscoelastic model with complex modulus for the MR layer and developed the acoustic model for the infinite sandwich panel. Simulation results showed that the STL can be increased considerably by increasing the applied magnetic field. In order to validate the theoretical model, the STL of the multi-layer panel with the MR fluid core was measured using impedance tube equipped with a magnetic chamber. Hasheminejad and Shabanimotlagh [70] studied the sound transmission properties of an infinite sandwich panel treated with magnetorheological elastomer core layer. They investigated the effect of applied magnetic field on the STL of the panel for all angles of incident in the audible frequency range. Choi et al. [71] implemented fuzzy control logic to reduce the transmitted sound from a sandwich panel treated with ER fluid core layer. To accomplish this, a rectangular closed cabin was fabricated with the ER sandwich plate fixed in one side. A loudspeaker generated the sound pressure from outside of the cabin and a microphone was used to measure the sound level inside the cavity. The measured sound was then fed back to the microcomputer to determine the appropriate input electric field to the ER fluid. Tang et al. [72-74] studied the STL of the sandwich panels treated with ER fluid as the core layer. They concluded that the tunable characteristics of the flexible and thin ER fluid layer at low frequencies, including the possibility of adjusting the sound pressure level and the phase angle by varying the electrical field, could be used in manufacturing low frequency tunable phononic crystals and other acoustic devices. Zielinski and Rak [75] investigated the acoustical absorption of foams coated with MR fluid as the magnetic field changes. They used polyurethane foams with single and dual porosity and different thicknesses and coated them with the MR fluid. The acoustic absorption of the clean

foams, coated foams and coated foams in the presence of constant magnetic field has then been measured using impedance tube and compared with each other.

1.4. Identified Research Gap and Specific Objectives

As it can be realized from the literature review, although there are some studies to predict the STL of the infinite sandwich panels with fluid core layer including Newtonian fluids, ER fluids and MR fluids, the topic is still in its infancy and no study has been conducted to fundamentally investigate the acoustical behavior of finite sandwich panels treated with MR fluid core layer both analytically and experimentally. Moreover, there is a lack of investigation on the topology optimization of sandwich panels partially treated with MR fluid core layer considering the maximization of acoustical properties as the objective function. Considering this, the specific objectives of the present research study are as follows:

1. Design an experimental set-up to study the STL of sandwich panels treated with MR fluid core layer and investigate the effect of the applied magnetic field on the STL of the structures.

2. Develop analytical/numerical models to accurately predict the STL of finite sandwich panels treated with the MR fluid core layer considering realistic boundary conditions.

3. Formulate an efficient optimization strategy to investigate the topology optimization of the partially treated MR sandwich panels aiming to optimize their acoustical properties.

1.5. Thesis Organization

This dissertation is written according to the chapter-based thesis format following the regulations provided by the Concordia University. The thesis includes 5 chapters which are sequentially arranged to address the objective functions presented before. The fundamental concepts of the sound transmission, review of relevant research works and specific objectives of the present study are presented in the chapter one. The next three chapters provide the methods of accomplishment to fulfill the identified specific objectives. The summery of these chapters are presented in the following. The last chapter is devoted to the main conclusions extracted from this study and the recommendations for the future works.

The fabricated test setup and the electromagnet are introduced in the second chapter. The setup has been designed to be utilized to measure the STL and natural frequencies of a clamped circular sandwich panel treated with the MR fluid core layer. The design procedure, the characteristics of the test setup and also the methodology of measuring the STL and natural frequencies are presented in this chapter. Moreover, the finite element (FE) analysis of the magnetic field inside the fabricated electromagnet is presented in this section. The FE model together with the magnetic field measured using Gaussmeter are employed to developed second and third order polynomial equations for the applied magnetic field as a function of the applied electric current and the radius of the plate. The test setup will then be utilized to validate the models presented for the STL and natural frequencies of the clamped circular sandwich panels in the next chapters.

Chapter three is devoted to the modeling of the STL of sandwich panels fully treated with MR fluid core layer. To do so, the Ritz is utilized to develop the equation of motion of the clamped circular sandwich panel and to calculate the STL using the transverse velocity of the structure. The model is then validated comparing the calculated first axisymmetric natural frequency and STL

with the results experimentally measured. Moreover, the FE model for the axisymmetric motion of the MR sandwich panel is derived using the circular and annular elements. The FE model provides the opportunity consider the changes in the applied magnetic field as a function of the radius of the panel. The FE model is also validated utilizing the experimental results. The effect of the applied magnetic field on the STL and natural frequency of the structure is then investigated. The developed models are then utilized to conduct a parametric study on the influence of the thickness of the core layer and the face sheets on the STL and the first axisymmetric natural frequency of the MR panel.

The topology optimization of the circular sandwich panel partially treated with MR fluid and silicone rubber core layer is investigated in chapter four. First, the equations of motion of the panel is developed using FE model comprising circular and 4-node quadrilateral elements. The developed model is validated comparing the first axisymmetric natural frequency and the STL of the panel with those obtained experimentally and also the results obtained using the Ritz and circular-annular FE model. The developed model is then utilized to conduct parametric studies on the effect of the position of MR fluid and silicone rubber segments on the natural frequency and STL of the panel. Next, a topology optimization problem is then established using the response surface (meta-model) approach due to high computational cost associated with the FE model. The linear and nonlinear topology optimization problems are formulated in both unconstrained and constrained formats. In the unconstrained problem, no limits are considered for the volume of the MR fluid and silicone rubber in the core layer while in the constrained problem the volume of the MR fluid and silicone rubber in the core layer are assumed to be equal. The integer programming and genetic algorithms are utilized to solve the linear and nonlinear topology optimization problems, respectively. The optimal candidates are further examined to determine the true optimal

topology for the core layer of the panel which provides the maximum rates of change in the natural frequency and loss factor due to the applied magnetic field and also maximizes the STL of the structure.

The last chapter is dedicated to the main conclusions achieved from this study and some recommendations for the future works.

CHAPTER 2

DESIGN OF EXPERIMENTAL SETUP AND

EXPERIMENTAL RESULTS

2.1. Introduction

This chapter focuses on the experimental investigation of the effect of applied magnetic field on the structural and acoustical behavior of MR sandwich panels. First, the test setup that has been designed and fabricated is explained. The setup includes two anechoic spaces and an electromagnet that provides the required magnetic field. The magnetic flux density generated inside the electromagnet is simulated using magneto-static finite element analysis and validated with the measured magnetic flux density using Gaussmeter. The results from magneto-static analysis is used to derive an approximate polynomial function to evaluate the magnetic flux density as a function of the plate's radius and applied current. In order to study the effect of the applied magnetic field, two sandwich panels with different thicknesses of the MR fluid core layer have been considered and their first axisymmetric natural frequency and the STL have been measured. Moreover, the influence of the thickness of the core layer on the natural frequency and the STL have been experimentally evaluated utilizing sandwich panels with silicone rubber core layer.

2.2. Experimental Set-up

An experimental setup has been designed to experimentally investigate the STL of circular sandwich panel treated with the MR fluid core layer. The setup includes the wooden anechoic box, power supplies and the analyzer as shown in Figure 2.1.
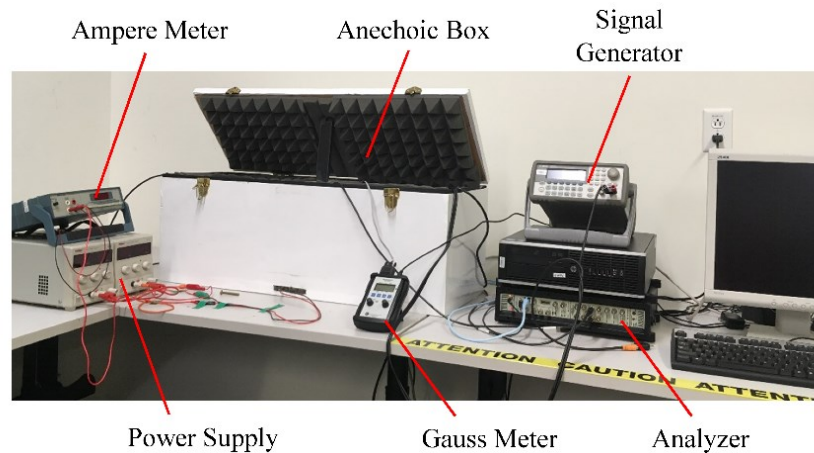
Figure 2.1. Acoustic testing equipment for MR sandwich panel.

The configuration of anechoic box and its elements are shown in Figure 2.2. In the analysis models which will be developed in subsequent chapters, it is assumed that the sound pressure is only a function of the distance travelled and independent of the geometry of the enclosure. This can be achieved by lining up the speaker, microphones and the center of the sandwich panel to form a linear line and absorbing all sounds outside this linear path by the walls of the chambers. To achieve this in the experiment, using a proper fixture the sandwich panel is exactly positioned at the center of the electromagnet which has been located at the center of the anechoic box as shown in the Figure 2.2. The electromagnet basically divides the anechoic box into the source and receiving rooms. Moreover, in order to absorb the sound outside the linear path and also to isolate the box from any exterior noise, interior walls of both the source and receiving rooms were properly insulated using $2\,in.$ acoustic pyramid foams. Acoustic foams are mostly used in

27

recording studios, educational facilities, and buildings where echo effects are undesirable. In addition, the upper lid cover was designed to securely clamp the box. Furthermore, the areas where the lid and box edges meet were lined with sealing foam in order to block any sound leakage through the interfaces. Speaker and microphones are also positioned to be as close to the panel as possible without being affected by the magnetic field. This reduces the errors due to air damping in the results. Hence, the majority of sound produced by the speaker is received by the panel and a minimum of sound from outside or the adjacent room is received by the microphones. The characteristics of the fabricated anechoic box are presented in Table 2.1.
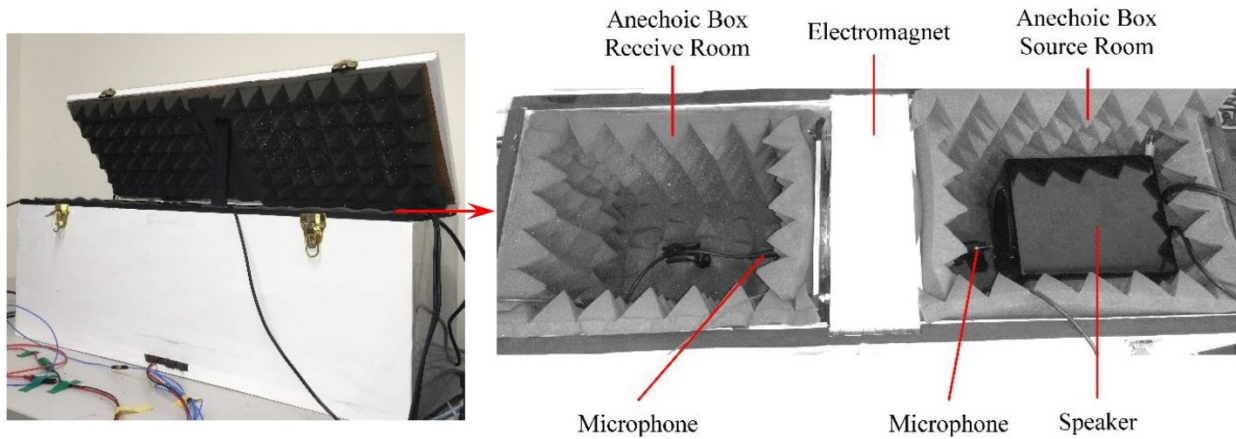
Figure 2.2. Anechoic box.

Table 2.1. The characteristics of the anechoic box.

Material	*Plywood*
Length	91 *cm*
Width	33 *cm*
Height	34.5 *cm*
Thickness of the walls	2.5 *cm*
Length of each of the source and receive rooms	38.5 *cm*

It is noted that a wide frequency range speaker (Behringer C50A Active 30-Watt) and a high precision microphone (PCB Piezotronics, model: 130E20) are placed in the source room to provide and to measure the incident sound wave, respectively. The speaker has a homogenous dispersion pattern and has been placed such that the sound wave hits the MR sandwich panel directly. The microphone was positioned next to the speaker so as not to obstruct the normal sound path from the speaker to the sandwich panel. It would still pick up the sound level because of the spherical nature of the waveform. The same microphone has also been placed in the receiving room in line with the center of the panel to measure the transmitted sound from the panel. The sound measured by two microphones was further analyzed to evaluate the STL using the analyzer (Bruel and Kjaer Pulse LabShop, Type: 2827-002).

To place the MR sandwich panel in the middle of the electromagnet core, it is first clamped at the edge to the end of an aluminum hollow cylinder using 12 $M3$ stainless steel bolts and a circular rim as shown in Figure 2.3. Aluminum has been selected to avoid interfere with the applied magnetic field provided by the electromagnet. The other end of the cylinder has been welded to an aluminum fixture plate. Flushing the fixture plate to the one face of electromagnet allows the hollow cylinder to slip through the electromagnet core placing the MR sandwich plate at the middle of the electromagnet where the magnetic field is nearly uniform and perpendicular to the panel. In addition, the acceleration of the panel is measured using the miniature three-axis accelerometer (PCB Piezotronics, model: 356A03) attached at the center of the circular panel. This acceleration is further analyzed using FFT analyzer to obtain the frequency response and subsequently the natural frequency of the MR sandwich panel.
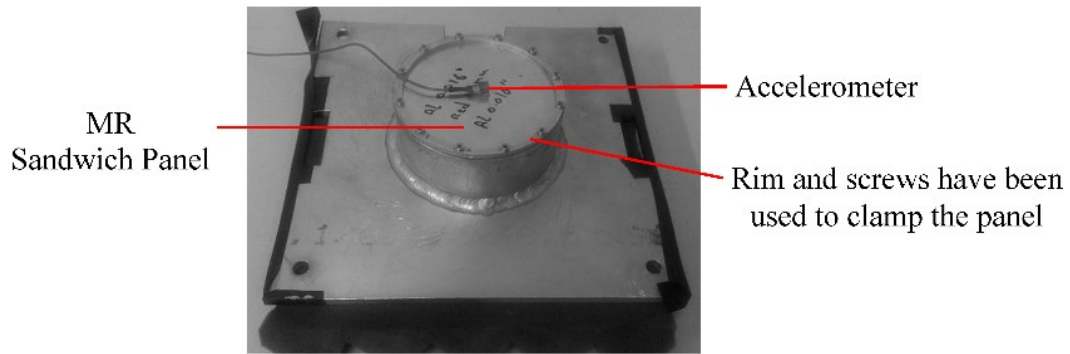
Figure 2.3. Clamped MR sandwich panel.

2.3. Design of Electromagnet

The viscoelastic characteristics of the MR fluid strongly depends on the applied magnetic field. Thus, an appropriate electromagnet is required to provide the sufficient magnetic field. In the present study, the electromagnet coil is fabricated using 4200 turns 18 AWG copper wire coil wound over a hollow core PVC bobbin with the inner and outer radius of 5.75 cm and 6.25 cm, respectively, as shown in Figure 2.4(a). Utilizing magnetic materials such as steel may guide the magnetic field thoroughly into the bobbin thus reducing the magnetic field applied to the MR sandwich panel which is located at the hollow section of the bobbin. Considering this, a non-magnetic core material (PVC) has been used to fabricate the bobbin. The coil has been designed to provide magnetic flux density of about 60 mT at its center for the input current of 2 Amp. It should be noted that the resistance of the electromagnet coil is about 56 Ω which means that about 112 $Vlots$ is needed to provide the 2 Amp required input current. This power is provided by the DC power supplies (TENMA, model: 72-6908) connected in series.
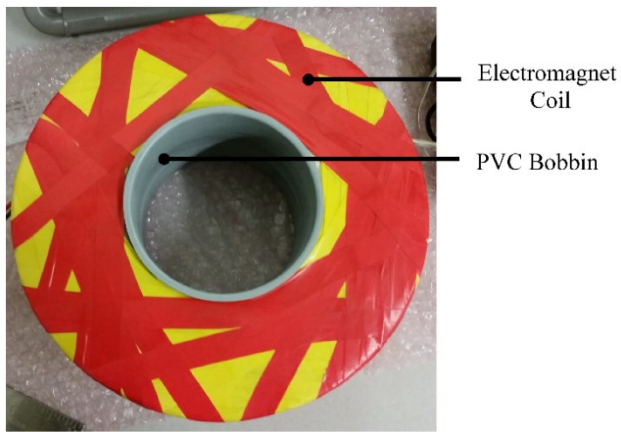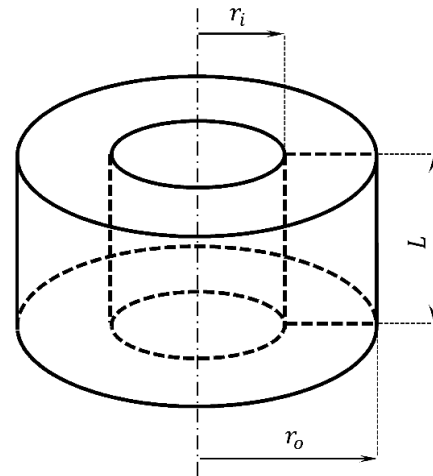
Figure 2.4. The electromagnetic coil (a) the fabricated (b) the schematic.
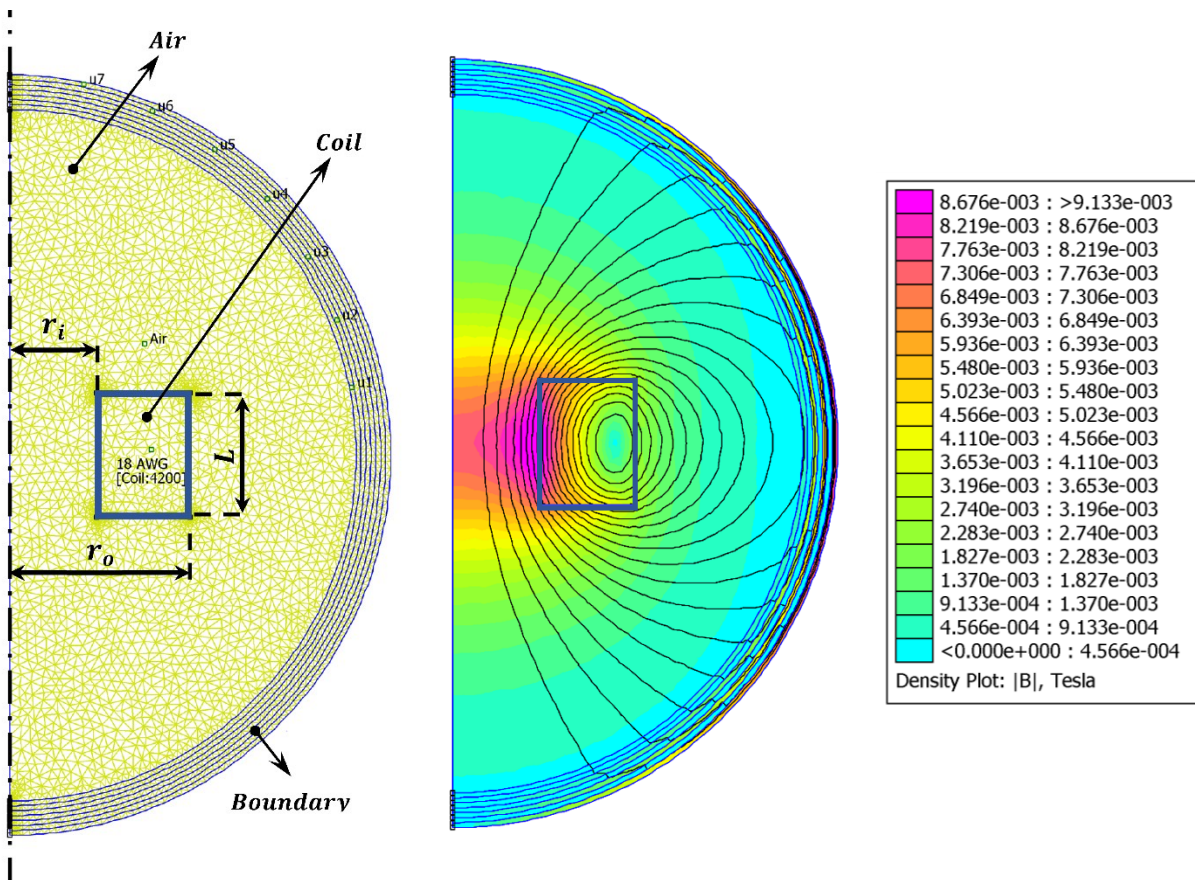
(a)   (b)

Figure 2.5. 2D model of magnetic coil (a) finite element model, (b) magnetic flux density.

31

Table 2.2. Magnetic flux density at the center and edge of the coil.

	Center ($r = 0.0\ cm$)		Edge ($r = 5.0\ cm$)	
	Exp. (mT)	FEM (mT)	Exp. (mT)	FEM (mT)
$I = 0.3\ Amp$	7.3	7.6	8.75	8.9
$I = 0.6\ Amp$	15.0	15.3	17.7	17.8
$I = 0.9\ Amp$	22.6	22.9	26.7	26.7
$I = 1.2\ Amp$	30.3	30.5	35.4	35.6
$I = 1.5\ Amp$	38.0	38.2	44.5	44.5
$I = 1.8\ Amp$	45.5	45.8	53.5	53.4

Measuring the magnetic flux density of the fabricated electromagnet using Gaussmeter shows that the flux density varies about 14 percent from center to the edge of the coil. To have better understanding of the flux density variation, a magneto-static analysis of the electromagnet has been conducted using the finite element method. For this purpose, a magneto-static FE model has been developed using an open source finite element software designed for solving low frequency electromagnetic problems on 2D planer and axisymmetric domain [76]. Figure 2.4(b) shows the schematic of the coil and its dimensions that has been used in the model. The electromagnet coil has been modeled as 4200 turn of 18 AWG copper wire which provides a cylinder with the inner and outer radius of $r_i = 6.25\ cm$ and $r_o = 13\ cm$, respectively, and the height of $L = 9\ cm$. In order to approximate an unbound domain which is required to solve the field of the electromagnet coil, an open boundary with the radius of 55 cm is considered as shown in Figure 2.5(a). The medium is considered as air and triangular mesh including 4824 nodes has been generated to establish the finite element model in order to evaluate the magnetic flux density around the coil as shown in Figure 2.5(b). Table 2.2 shows the magnetic flux density for different input currents obtained experimentally and using the developed finite element model. As it can be realized, the

estimated magnetic flux densities are in excellent agreement with the experimental results obtained using Gaussmeter. It should be mentioned that $r = 5\ cm$ was the maximum radius that was accessible to measure the magnetic flux density.

Figure 2.6 and 2.7 show the variation of the magnetic flux density in the middle of electromagnet with respect to the radius and input current, respectively. Results show that the magnetic flux density depends on the radius as a polynomial of 2nd or 3rd order and linearly changes with respect to the input current. Considering this, following polynomial functions are suggested to represent magnetic flux density as a function of $r\ (cm)$ and $I\ (Amp)$:

$$B_A(r, I) = A_{00} + A_{01}I + A_{10}r + A_{11}rI + A_{20}r^2 + A_{21}r^2I \qquad (2.1)$$

$$B_C(r, I) = C_{00} + C_{01}I + C_{10}r + C_{11}rI + C_{20}r^2 + C_{21}r^2I + C_{30}r^3 + C_{31}r^3I \qquad (2.2)$$

where A_{ij} and C_{ij} are the constant coefficients. These coefficients are identified using least square method by minimizing the errors between the finite element results and those obtained explicitly using the proposed functions in Eqs. (2.1) and (2.2). Table 2.3 shows the identified coefficients, the maximum absolute error percentage and the coefficient of determination. The maximum error and the coefficient of determination are acceptable for both identified functions. However, $B_C(r, I)$ provides more accurate function to estimate the magnetic flux density in the electromagnet coil as a function of both current and radius.
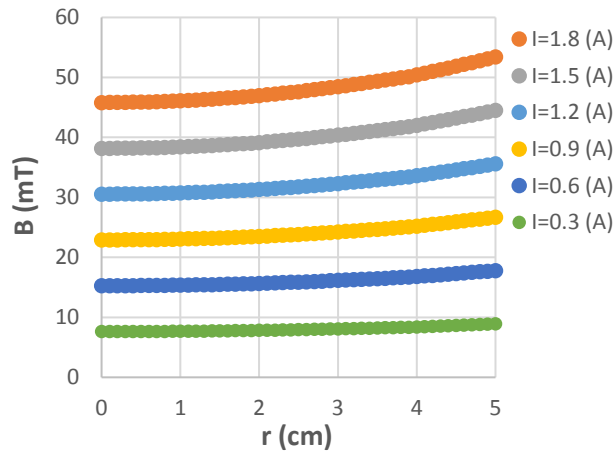
Figure 2.6. Magnetic flux density with respect to radius for different input current.
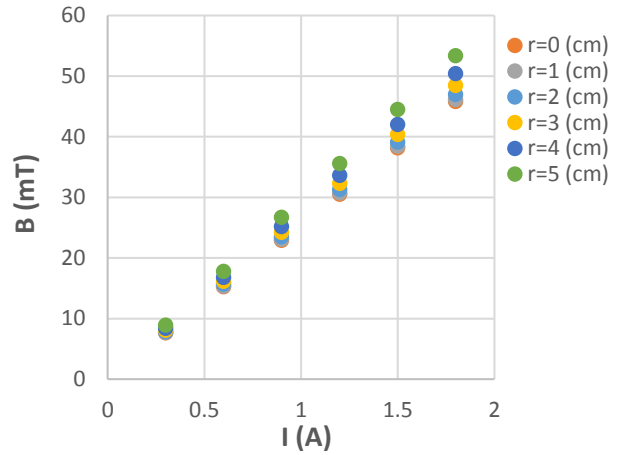
Figure 2.7. Magnetic flux density with respect to current for different radiuses.

Table 2.3. The identified coefficients, the maximum absolute error percentage and the coefficient of determination.

$B_A(r,I)$		$B_C(r,I)$	
A_{00}	6.48×10^{-9}	C_{00}	6.74×10^{-10}
A_{01}	0.0254	C_{01}	0.0254
A_{10}	-7.72×10^{-9}	C_{10}	1.035×10^{-8}
A_{11}	-4.96×10^{-5}	C_{11}	8.395×10^{-5}
A_{20}	1.50×10^{-9}	C_{20}	-7.619×10^{-9}
A_{21}	1.74×10^{-4}	C_{21}	1.074×10^{-4}
		C_{30}	1.217×10^{-9}
		C_{31}	8.993×10^{-6}
$|e|_{max}$ (%)	0.36	$|e|_{max}$ (%)	0.27
$\mathcal{R}^2$	0.999	$\mathcal{R}^2$	0.999

2.4. Effect of the Magnetic Field

In order to investigate the effect of applied magnetic field on the structural and acoustical properties of MR sandwich panel, sandwich panels consisting of $0.4\ mm$ thickness aluminum face sheets and MR fluid core layer with thicknesses of $1.35\ mm$ and $1.8\ mm$ have been fabricated. $MRF\ 132DG$ manufactured by Lord Corporation [77] has been utilized as the core layer and the edge of the circular panel has been sealed using silicone rubber with $1.35\ mm$ and $1.8\ mm$ thicknesses. The natural frequency is evaluated by exciting the panel using pulse sound with the duration of $2.5\ Seconds$. The acceleration is measured using a miniature accelerometer attached at the center of the panel. The measured time domain acceleration was then transferred to frequency domain using FFT analyzer. The frequency resolution and sampling frequency were considered to be $1\ Hz$ and $800\ Hz$, respectively. Table 2.4 provides the first axisymmetric natural frequency of the MR sandwich panel for different input currents. Examination of results reveal that intensifying the applied magnetic field causes the natural frequency of the MR sandwich panel to considerably increase with the rate of increase of about $13.3\ Hz/A$. This clearly shows the effect of MR fluid in stiffening the panel by increasing the applied magnetic field. Moreover, the CPB analyzer is utilized to examine the incident and transmitted sounds measured by the microphones and determine the STL of the panel. Table 2.4 also provides STL of the MR-based sandwich panel at the resonance frequency for different input currents. As it can be realized the STL increases as the input current increases. This can be explained as a result of the damping effect of the MR core layer which is strengthened as the magnetic field increases. Above observation clearly shows that by distributing the MR fluid within the structure (MR-bases sandwich structure) provides the opportunity to simultaneously change both structural damping and stiffness for effective vibration/noise control applications.

Table 2.4. Experimental results for the panel with 0.4 mm aluminum face sheets and 1.35 mm MR fluid core layer.

Current (Amp)	Natural Frequency (Hz)	STL (dB)
0	248	12.4
0.3	248	13.6
0.6	252	14.5
0.9	255	15.1
1.2	262	15.8
1.5	266	16.2
1.8	270	15.6

Figure 2.8 (a) shows the natural frequency of the MR sandwich panel with respect to the applied magnetic field (current) for two MR layer thicknesses of 1.35 mm and 1.8 mm. Results show that the natural frequency of the sandwich panels linearly increases with increasing the applied magnetic field. In addition, the rate of change in natural frequency with respect to the applied magnetic field has been increased from 13.3 Hz/A for the panel with 1.35 mm MR core layer to 17.0 Hz/A for the panel with 1.8 mm core layer. This fact might be explained as the increase of the thickness of the core layer enhances the influence of the shear deformation on the panel's response. Consequently, increasing the shear strength of the MR core layer by strengthening the applied magnetic field has a further effect on the natural frequency of the panel. It is noted that increasing the thickness of the core layer causes the natural frequency to decrease as increase in mass is more dominant than increase in stiffness.
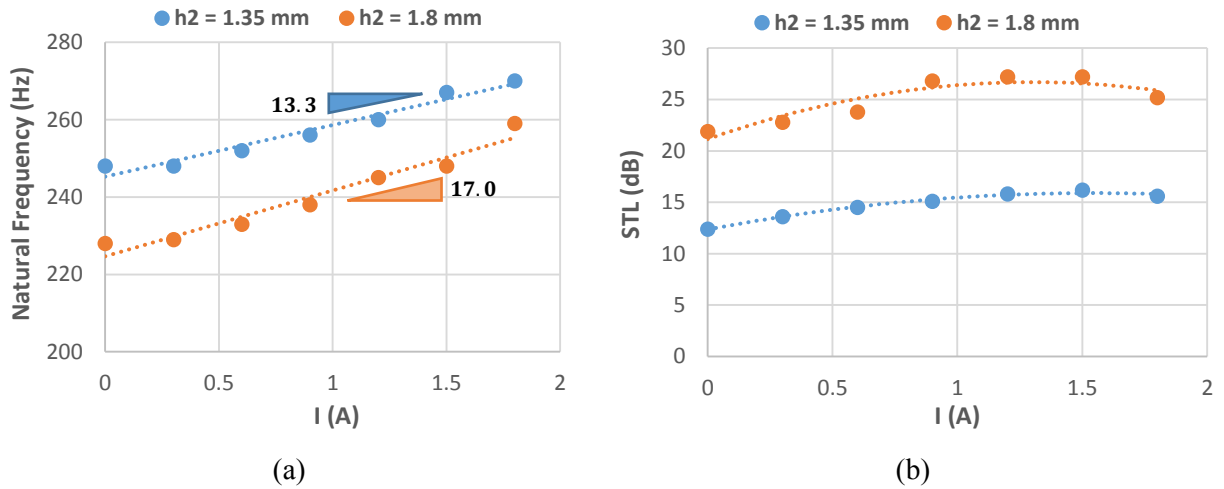
Figure 2.8. (a) Natural frequencies and (b) STL of MR sandwich panel with 1.35 mm and 1.8 mm thickness of MRF 132DG core layer.

The STL of the MR sandwich panel at resonance frequency with respect to applied magnetic field for MR layer thicknesses of 1.35 mm and 1.8 mm is also shown in Figure 2.9 (b). As it can be realized, in contrast to the natural frequency, STL increases by almost 10 dB by increasing the MR fluid layer thickness from 1.35 mm to 1.8 mm, irrespective of the applied current, which is mainly attributed to the mass effect. Moreover for given thickness, the STL increases by increasing the applied current while showing saturation effect at high applied current.

To investigate further, STL of the MR-based sandwich panel with core thickness of 1.35 mm has been evaluated experimentally for different applied current. The results are provided in Figure 2.9. As expected there is a notch (significant reduction) in the STL of the panel at the resonance frequencies identified in Table 2.4 and the notch shifts to higher frequencies as the magnetic field increases. This clearly shows that the stiffness and thus sound absorption capability of the MR sandwich panel can be varied using the applied magnetic field. It is also interesting to note that the STL of the panel at the resonance frequency increases from 12.4 dB at the natural frequency of 248 Hz to 15.6 dB at the natural frequency of 270 Hz as the input current increases from 0 Amp

37

to 1.8 *Amp*. This can be attributed to the influence of the magnetic field on the loss factor of the MR fluid and consequently the damping of the MR sandwich panel. As a matter of fact, the vibration of the structure at the resonance frequency decreases as its damping increases and causes the STL to increase. As discussed before, this clearly shows the adaptability of the MR sandwich panels through changing their stiffness and damping. In addition, further examination of results reveal that depending on the excitation frequency, the STL of the panel can be increased or decreased as the input current increases. The STL increases as the input current increases for the frequencies below the natural frequency, however increasing the input current causes the STL to decrease for the frequencies above the natural frequency of the panel. This shows the potential to improve the sound absorption of panels adaptively through development of appropriate semi-active control strategies to maximize the STL by determining the appropriate input current based on the excitation frequency and some other feedback from the structure such as the acceleration of the panel.
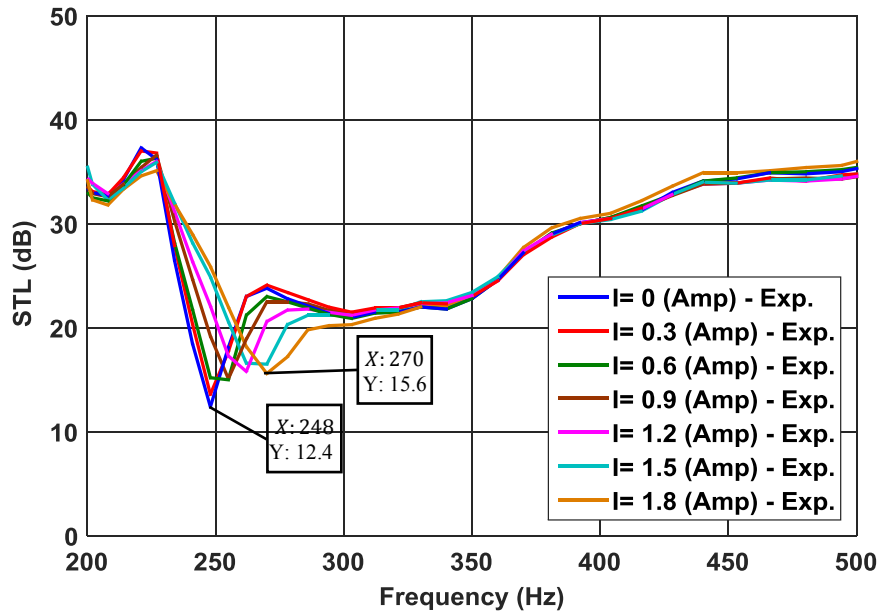
Figure 2.9. STL of panel with 0.4 *mm* aluminum face sheets and 1.35 *mm* MR fluid core layer (a) measured STL, (b) predicted STL using FEM.

2.5. Effect of the Core Layer's Thickness

Further investigation on the effect of the thickness of the core layer on the STL has been conducted experimentally on four types of sandwich panels with silicone rubber core layer. The first axisymmetric natural frequency of the fabricated sandwich panels with respect to the thickness of the core layer are presented in Figure 2.10(a). As it can be realized the natural frequency decreases as the thickness of the core layer increases. This results may be attributed to the increase in mass per unit area of the structure that leads the natural frequency to reduce. In addition, the rate of the reduction in the natural frequency also decreases as the thickness of core layer increases and increasing the thickness above 4 mm does not considerably affect the first axisymmetric natural frequency. The STL of the panels at the resonance frequency is also presented in Figure 2.10 (b). The results show that STL increases almost linearly with respect to the thickness of the core layer.

(a)   (b)
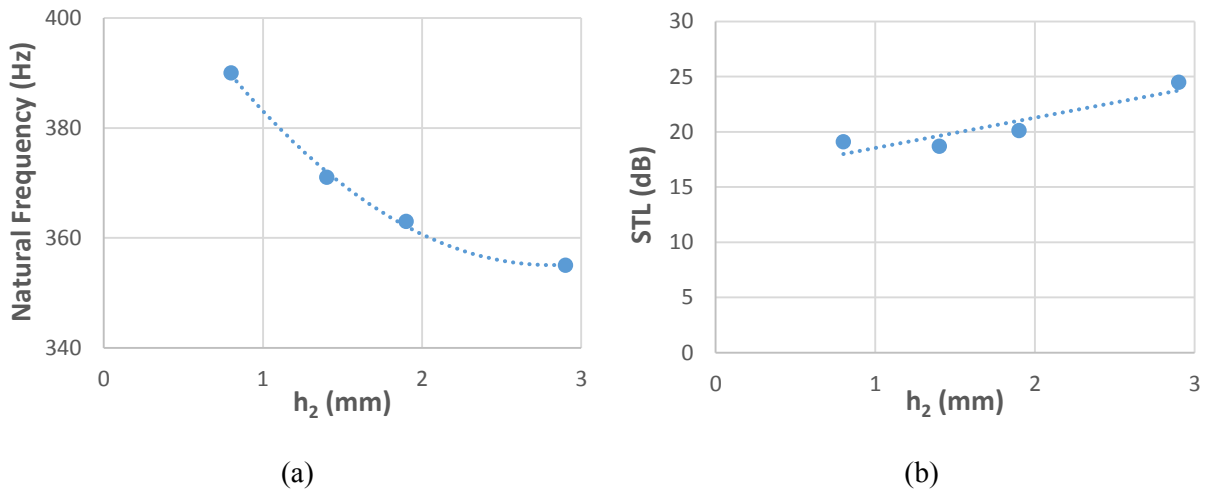
Figure 2.10. Sandwich panel with 0.4 mm thickness aluminum face sheets and silicone rubber core layer (a) natural frequency (b) STL.

2.6. Conclusions

An experimental test setup including an anechoic chamber and electromagnet has been designed and fabricated in order to investigate the effect of the applied magnetic field on the structural and acoustical properties of MR sandwich panels. Natural frequency and the STL of the panel were measured utilizing the microphones and accelerator, respectively. Considering that the magnetic flux density inside the electromagnet varies as a function of the radius, finite element method was also used to model the magnetic flux density of the electromagnet and validated with the experimental measurements. The magnetic finite element model was then utilized to develop polynomial functions to estimate the magnetic flux density as a function of the input current and the radius which can then be incorporated into the numerical models of the MR-based sandwich panels to be discussed in the following chapters. The influence of the applied magnetic field on the STL and the first axisymmetric natural frequency of the panel were investigated. It was shown that the effect of the applied magnetic field increases as the thickness of the MR core layer increases. Moreover, the effect of the thickness of the core layer on the natural frequency and the STL at the resonance frequency were studied for sandwich panels with silicone rubber core layer.

CHAPTER 3

SOUND TRANSMISSION LOSS OF MR- BASED SANDWICH PANELS USING RITZ AND FINITE ELEMENT METHODS

3.1. Introduction

This chapter is devoted to theoretically investigate the STL of circular sandwich panel fully treated with MR fluid core layer. A clamped circular sandwich panel with elastic face sheets and MR Fluid as the core layer has been considered and the governing equations of motion are formulated using the Ritz and FE methods. Circular and annular elements have been utilized to develop the FE model. Evaluating the transverse velocity of the sandwich panel, the sound radiated from the panel has been calculated using Rayleigh's integral and subsequently utilized to estimate the STL. In order to validate the models, the first axisymmetric natural frequency and the STL of the sandwich panel with silicone rubber core layer have been compared with those obtained experimentally. The effect of the applied magnetic field on the natural frequency and STL of the MR sandwich panel are then investigated. Moreover, parametric study on the effect of the thickness of the MR core layer and the thickness of face sheets on the natural frequency and STL of the MR sandwich panel are presented.

3.2. Mathematical Formulations

In the following first the Ritz method has been used to formulate the problem. This is followed by the development of FE models.

3.2.1. Equation of Motion using Ritz Method

A multilayered uniform circular panel comprising two elastic face sheets and MR fluid core layer as shown in Figure 3.1 is considered in this study. Figure 3.2 shows the assumed displacement field components. Considering small thickness to radius ratio for the face sheets and neglecting their transverse shear deformation and rotary inertia (Kirchhoff hypothesis), the classical plate theory may be used to obtain the displacements of the face layers as:

$$u_i = \left(u_i^0 - z_i \frac{\partial w}{\partial r} \right) \quad \& \quad i = 1,3 \tag{3.1}$$

$$v_i = \left(v_i^0 - z_i \frac{\partial w}{r \partial \theta} \right) \quad \& \quad i = 1,3 \tag{3.2}$$

$$w_1 = w_2 = w_3 = w \tag{3.3}$$

where u and v are the in-plane radial and circumferential displacements in r and θ directions, respectively. The subscripts 1 (front) and 3 (back) refer to the two face sheets and u_i^0 and v_i^0 are the in-plane radial and circumferential displacements of the mid-plane of the face sheets in r and θ directions, respectively. w is the transverse displacements which is assume to be the same for the face sheets and the core layer and z_i denotes the transverse coordinate in the local coordinate

system of each layer considering the origin at the mid-plane of each layer. Assuming that there is no slippage between the face sheets and core layer (perfect bonding), the compatibility conditions can be described as:

$$
\begin{cases}
u_1 \Big|_{\left(z_1=-\frac{h_1}{2}\right)} = u_2 \Big|_{\left(z_2=\frac{h_2}{2}\right)} \\
\\
v_1 \Big|_{\left(z_1=-\frac{h_1}{2}\right)} = v_2 \Big|_{\left(z_2=\frac{h_2}{2}\right)}
\end{cases}
\tag{3.4}
$$

$$
\begin{cases}
u_3 \Big|_{\left(z_3=\frac{h_3}{2}\right)} = u_2 \Big|_{\left(z_2=-\frac{h_2}{2}\right)} \\
\\
v_3 \Big|_{\left(z_3=\frac{h_3}{2}\right)} = v_2 \Big|_{\left(z_2=-\frac{h_2}{2}\right)}
\end{cases}
\tag{3.5}
$$

where subscript (2) refers to the core layer. It is noted that using Eqs. (3.4) and (3.5), the radial and circumferential displacements of the core layer can be obtained in terms of those of the face sheets.

The strain-displacement relationships for the normal and in-plane shear strain of the face sheets and also the transverse shear strain of the core layer can now be described as:

$$\begin{cases} \varepsilon_{i_r} = \dfrac{\partial u_i}{\partial r} \\[3mm] \varepsilon_{i_\theta} = \dfrac{u_i}{r} + \dfrac{\partial v_i}{r\partial \theta} \qquad\qquad \& \qquad i = 1,3 \\[3mm] \gamma_{i_{r\theta}} = \dfrac{\partial v_i}{\partial r} + \dfrac{\partial u_i}{r\partial \theta} - \dfrac{v_i}{r} \end{cases} \qquad\qquad (3.6)$$

$$\begin{cases} \gamma_{2_{rz}} = \dfrac{u_{1_0} - u_{3_0}}{h_2} + \dfrac{d}{h_2}\dfrac{\partial w}{\partial r} \\[3mm] \gamma_{2_{\theta z}} = \dfrac{v_{1_0} - v_{3_0}}{h_2} + \dfrac{d}{h_2}\dfrac{\partial w}{r\partial \theta} \end{cases} \qquad\qquad (3.7)$$

where $d = \frac{h_1}{2} + h_2 + \frac{h_3}{2}$ and h_1 and h_3 are the thickness of the face sheets and h_2 is the thickness

of the core layer as shown in Figure 3.2.
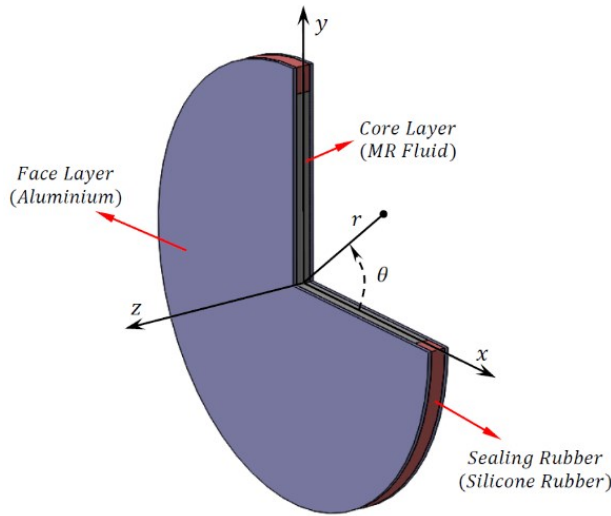
| Figure 3.1. Schematic of sandwich panel treated with MR fluid core layer. | Figure 3.2. Assumed displacement field components. |
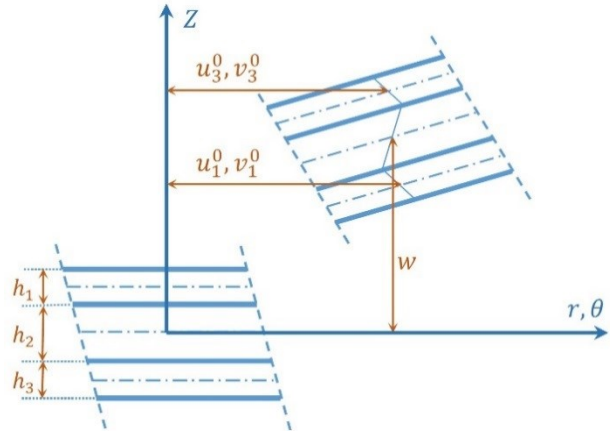
The stress-strain relationships are given by Hooke's law as follows:

$$\begin{cases} \sigma_{i_r} = \dfrac{E_i}{1 - v_i^2}\left(\varepsilon_{i_r} + v_i \varepsilon_{i_\theta}\right) \\[2mm] \sigma_{i_\theta} = \dfrac{E_i}{1 - v_i^2}\left(\varepsilon_{i_\theta} + v_i \varepsilon_{i_r}\right) \quad \& \quad i = 1,3 \\[2mm] \tau_{i_{r\theta}} = G_i \gamma_{i_{r\theta}} \end{cases} \tag{3.8}$$

$$\begin{cases} \tau_{2_{rz}} = G_2 \gamma_{2_{rz}} \\[1mm] \tau_{2_{\theta z}} = G_2 \gamma_{2_{\theta z}} \end{cases} \tag{3.9}$$

where E_i, G_i and v_i are the Young's modulus, the shear modulus and the Poisson's ratio of the face sheets, respectively. The MR fluid core layer is considered to experience small shear deformation and thus operate mainly in pre-yield region in which the MR fluid exhibit linear viscoelastic behavior. G_2 is the complex shear modulus of the MR core layer which can be written in terms of the storage and loss moduli as:

$$G_2 = G_2' + jG_2'' \tag{3.10}$$

where G_2' and G_2'' are the storage and loss moduli of the MR core layer, respectively. The storage and loss moduli of MR layer are functions of the applied magnetic field and the excitation frequency. It is noted that field-dependent constitutive models for the storage and loss moduli which have been developed and experimentally validated by Eshaghi et al. [63] are utilized in the present study.

The total strain and kinetic energies can be subsequently expressed as:

$$T = T_1 + T_2 + T_3 \tag{3.11}$$

$$V = V_1 + V_2 + V_3 \tag{3.12}$$

where

$$\begin{cases} T_i = \dfrac{1}{2} \iint_A \int_{-\frac{h_i}{2}}^{\frac{h_i}{2}} \rho_i(\dot{u}_1^2 + \dot{v}_1^2 + \dot{w}^2) dz\, dA \\[3mm] T_2 = \dfrac{1}{2} \iint_A \left[\rho_2 h_2 \dot{w}^2 + I_2\left((\dot{\gamma}_{2rz})^2 + (\dot{\gamma}_{2\theta z})^2 \right) \right] dA \end{cases} \tag{3.13}$$

$$\begin{cases} V_i = \dfrac{1}{2} \iint_A \int_{-\frac{h_i}{2}}^{\frac{h_i}{2}} (\sigma_{i_r}\varepsilon_{i_r} + \sigma_{i_\theta}\varepsilon_{i_\theta} + \tau_{i_{r\theta}}\gamma_{i_{r\theta}}) dz\, dA \\[3mm] V_2 = \dfrac{1}{2} \iint_A \int_{-\frac{h_2}{2}}^{\frac{h_2}{2}} (\tau_{2rz}\gamma_{2rz} + \tau_{2\theta z}\gamma_{2\theta z}) dz\, dA \end{cases} \tag{3.14}$$

where $i = 1,3$ refers to the two face sheets. ρ_1 and ρ_3 are the mass density of the face sheets and ρ_2 is the mass density of the core layer. I_2, the moment of inertia of the core layer which can be expressed as:

$$I_2 = \frac{\rho_2 h_2^3}{12} \tag{3.15}$$

The work done by the acoustic pressure on the panel can be written as:

$$W = \iint_A P_b w\, dA \tag{3.16}$$

where P_b is blocked pressure. Neglecting the radiated pressure on the incident side due to the vibration of the plate, the blocked pressure is the sum of the incident, P_i, and the reflected pressure, P_r, on the incident side of the panel. Assuming $P_i=P_r$, the blocked pressure is obtained as $P_b = 2P_i$.

Considering the circumferential symmetry of annular plate about the coordinate θ, the radial and circumferential displacements of the mid-plane and transverse displacement can be expressed as:

$$u_i^0 = \bar{u}_i^0(r)\cos(m\theta) \tag{3.17}$$

$$v_i^0 = \bar{v}_i^0(r)\sin(m\theta) \tag{3.18}$$

$$w = \bar{w}(r)\cos(m\theta) \tag{3.19}$$

where $i = 1,3$. $\bar{u}_i^0$, $\bar{v}_i^0$ and $\bar{w}$ are the functions for amplitude of radial, circumferential and transverse displacements, respectively, and m is the non-negative integer that identifies the circumferential wave number.

Ritz method developed by Walter Ritz in 1908 assumes that the desired function can be approximately represented as a linear combination of known functions [78]. In this method, the solution is estimated as an approximated weighted functions, each satisfying essential boundary conditions. The displacement amplitude functions in Eqs. (3.17) to (3.19) might be written as:

$$\bar{u}_i^0(r) = B_U(r)\sum_{k=0}^{N} b_{i_k}r^k \quad \& \quad i = 1,3 \tag{3.20}$$

47

$$\bar{v}_i^0(r) = B_V(r) \sum_{k=0}^{N} c_{i_k} r^k \qquad \& \qquad i = 1,3 \tag{3.21}$$

$$\bar{w}(r) = B_W(r) \sum_{k=0}^{N} l_k r^k \tag{3.22}$$

where $B_U(r)$, $B_V(r)$ and $B_W(r)$ are the boundary functions defined to satisfy the geometrical boundary conditions. b_{i_k}, c_{i_k} and l_k are unknown coefficients and N is the highest degree of the polynomials. For a circular panel with camped edges the boundary functions are defined as:

$$B_U(r) = r - R_o \tag{3.23}$$

$$B_V(r) = r - R_o \tag{3.24}$$

$$B_W(r) = (r - R_o)^2 \tag{3.25}$$

where R_o is the outer radius of the circular panel.

Using the strain and kinetic energies described previously in Eqs. (3.11)-(3.14) and the work done by the acoustic pressure on the panel provided in Eq. (3.16), the total potential of the system can be written as:

$$\Pi = V - T - W \tag{3.26}$$

In Ritz method, the stationary condition is applied to the total potential energy with respect to the unknown coefficients b_{i_k}, c_{i_k} and l_k to obtain the governing equations of motion of the panel:

$$\begin{cases} \dfrac{\partial \Pi}{\partial b_{i_k}} = 0 \\[2mm] \dfrac{\partial \Pi}{\partial c_{i_k}} = 0 \\[2mm] \dfrac{\partial \Pi}{\partial l_k} = 0 \end{cases}$$

(3.27)

which leads to the following system of algebraic equations:

$$[K - M\omega^2]\{C\} = \{F\}$$

(3.28)

where K, M, F are the system stiffness and mass matrices and vector of external forces, respectively. C is the vector of arbitrary coefficients which can be written as:

$$\{C\} = \begin{Bmatrix} \{b_1\} \\ \{c_1\} \\ \{l\} \\ \{b_3\} \\ \{c_3\} \end{Bmatrix}$$

(3.29)

where

$$\{b_i\} = \begin{Bmatrix} b_{i_1} \\ b_{i_2} \\ \vdots \\ b_{i_N} \end{Bmatrix} \quad , \quad \{c_i\} = \begin{Bmatrix} c_{i_1} \\ c_{i_2} \\ \vdots \\ c_{i_N} \end{Bmatrix} \quad , \quad \{l\} = \begin{Bmatrix} l_1 \\ l_2 \\ \vdots \\ l_N \end{Bmatrix}$$

(3.30)

where $i = 1,3$. Solving Eq. (3.28) yields the arbitrary coefficients $\{C\}$ which are then used to calculate the in-plane and transverse displacements of the sandwich panel.

49

3.2.2. Finite Element Method

In the Ritz formulation, the applied magnetic field was considered to be constant with respect to the radius of the circular panel. However, it was shown in Chapter 2 that the applied magnetic field is different at the different radiuses. Moreover, the Ritz formulation is not applicable for the panels partially treated with MR fluid core layer and the core layer was assumed to be uniform. The Finite element method provides the opportunity to formulate the equations of motion of the sandwich panel partially treated with MR fluid core layer. The equation of axisymmetric motion of the circular sandwich panel is developed in this section using FE method. Figure 3.3 shows the circular and annular elements utilized in development of the FE model. Due to the symmetry, the circular element is defined by one circular node j and the annular element is defined by two i and j nodes at the inner and outer edges of the element, respectively. Here, the displacements of the face sheets and the compatibility conditions are similar to those presented for Ritz method in Eqs. (3.1) to (3.5). It should be noted that the strain-displacement relations presented in Eqs. (3.6) and (3.7) are for general motion of the panel including both axisymmetric and nonaxisymmetric modes. Thus, for the axisymmetric motion, they can be simplified as:

$$
\begin{cases}
\varepsilon_{i_r} = \dfrac{\partial u_i}{\partial r} \\[3mm]
\varepsilon_{i_\theta} = \dfrac{u_i}{r} \qquad \& \quad i = 1,3 \\[3mm]
\gamma_{i_{r\theta}} = 0
\end{cases}
\tag{3.31}
$$

$$
\begin{cases}
\gamma_{2_{rz}} = \dfrac{u_1^0 - u_3^0}{h_2} + \dfrac{d}{h_2}\dfrac{\partial w}{\partial r} \\[3mm]
\gamma_{2_{\theta z}} = 0
\end{cases}
\tag{3.32}
$$
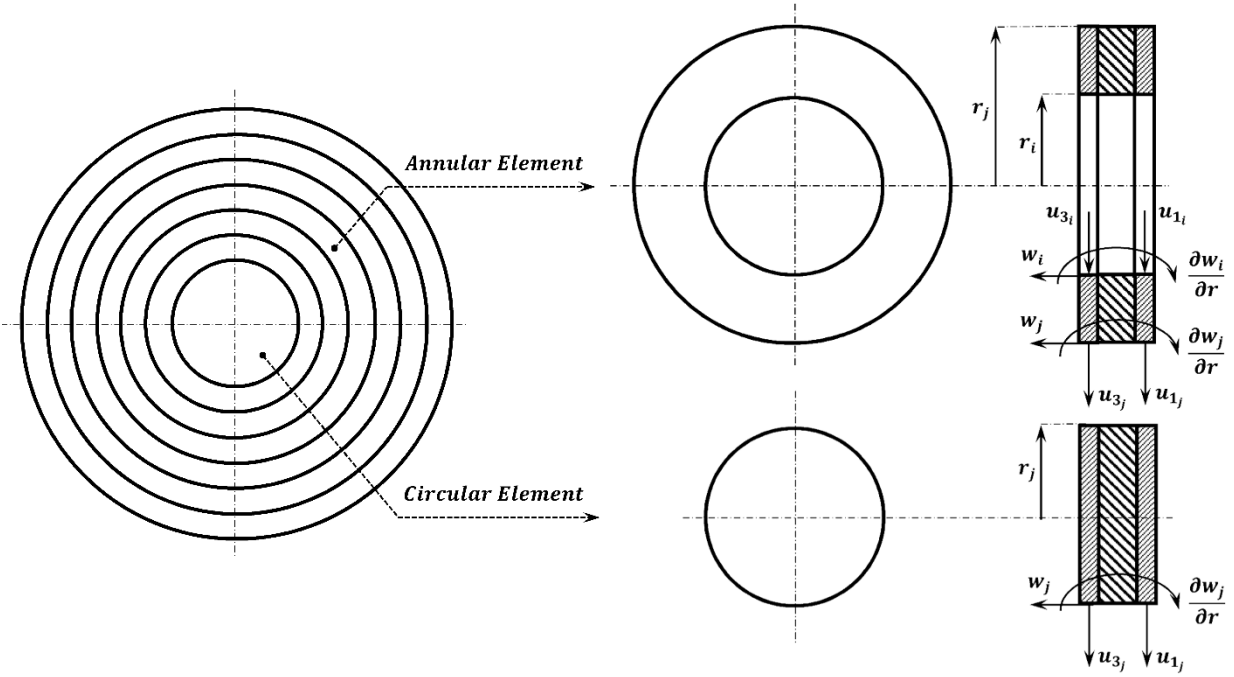
Figure 3.3. Schematic of the finite element model.

Four degrees of freedom have been considered for each of the nodes as follows:

$$
\delta_i = \begin{Bmatrix} w_i \\[1mm] \dfrac{\partial w_i}{\partial r} \\[2mm] u_{1_i}^0 \\[1mm] u_{3_i}^0 \end{Bmatrix}
\quad \& \quad
\delta_j = \begin{Bmatrix} w_j \\[1mm] \dfrac{\partial w_j}{\partial r} \\[2mm] u_{1_j}^0 \\[1mm] u_{3_{ij}}^0 \end{Bmatrix}
\tag{3.33}
$$

51

where w and $\frac{\partial w}{\partial r}$ are the transverse displacement and the rotation, respectively. $u_{1_i}^0$, $u_{3_i}^0$ and $u_{1_j}^0$, $u_{3_j}^0$ are the in-plane radial displacements of the mid-plane for the nodes i and j of the front and back face sheets, respectively. Now considering Figure 3.3, the nodal displacement vector for the circular and annular elements is expressed as:

$$\delta_e^c = \{\delta_j\} \tag{3.34}$$

$$\delta_e^a = \begin{Bmatrix} \delta_i \\ \delta_j \end{Bmatrix} \tag{3.35}$$

where superscripts c and a refer to the circular and annular elements, respectively. Defining the dimensionless parameter $y = \frac{r}{r_j}$ as the ratio of the radius r over the outside radius of the element, r_j, the transverse and in-plane displacement functions may be described as [79]:

$$\begin{cases} w_c = c_1 + c_2 y^2 \\ u_{c_1}^0 = c_3 y \\ u_{c_3}^0 = c_4 y \end{cases} \tag{3.36}$$

$$\begin{cases} w_a = a_1 + a_2 y^2 + a_3 \ln y + a_4 y^2 \ln y \\ u_{a_1}^0 = a_5 y + a_6 y^2 \\ u_{a_3}^0 = a_7 y + a_8 y^2 \end{cases} \tag{3.37}$$

where c_1 to c_4 and a_1 to a_8 are the constant coefficients which must be determined. Using relations (3.36) and (3.37), the nodal displacement vectors of the circular and annular elements in Eqs. (3.34) (3.33)and (3.35) are formulated in matrix form as follows:

$$\delta_e^c = [C^c]\{\alpha^c\} \tag{3.38}$$

$$\delta_e^a = [C^a]\{\alpha^a\} \tag{3.39}$$

where $[C^c]$ and $[C^a]$ are 4×4 and 8×8 matrices whose elements depends on the coordinates of the nodal points of the circular and annular elements defined in Figure 3.3, respectively. These matrices are provided in Appendix A. $\{\alpha^c\}$ and $\{\alpha^a\}$ are the vector of coefficients which can be written as:

$$\{\alpha^c\} = [c_1 \quad c_2 \quad c_3 \quad c_4]^T \tag{3.40}$$

$$\{\alpha^a\} = [a_1 \quad a_2 \quad a_3 \quad a_4 \quad a_5 \quad a_6 \quad a_7 \quad a_8]^T \tag{3.41}$$

The transverse and in-plane displacement functions of the face sheets' mid-plane for circular and annular elements can then be related to the nodal displacement vectors using shape functions as:

$$\begin{Bmatrix} w_c \\ u_{c_i}^0 \end{Bmatrix} = [N_i^c]\{\alpha^c\} = [L_i^{*c}]\delta_e^c \quad \& \quad i = 1,3 \tag{3.42}$$

$$\begin{Bmatrix} w_a \\ u_{a_i}^0 \end{Bmatrix} = [N_i^a]\{\alpha^a\} = [L_i^{*a}]\delta_e^a \quad \& \quad i = 1,3 \tag{3.43}$$

where $[L_i^{*c}]$ and $[L_i^{*a}]$ are the shape functions of the circular and annular finite elements, respectively, and can be expressed as:

$$[L_i^{*c}] = [N_i^c][C^c]^{-1} \quad \& \quad i = 1,3 \tag{3.44}$$

$$[L_i^{*a}] = [N_i^a][C^a]^{-1} \quad \& \quad i = 1,3 \tag{3.45}$$

$[N_i^c]$ and $[N_i^a]$ are provided in Appendix A. Substituting Eqs. (3.42) and (3.43) into Eqs. (3.31) and (3.32), the strain-displacement relations can be written as functions of nodal displacement vectors as:

$$\varepsilon_i^c = \begin{Bmatrix} \varepsilon_r \\ \varepsilon_\theta \\ \gamma_{r\theta} \end{Bmatrix}_i^c = [B_i^c]\delta_e^c \quad \& \quad i = 1,3 \tag{3.46}$$

$$\gamma_2^c = \begin{Bmatrix} \gamma_{rz} \\ \gamma_{\theta z} \end{Bmatrix}_2^c = [B_2^c]\delta_e^c \tag{3.47}$$

$$\varepsilon_i^a = \begin{Bmatrix} \varepsilon_r \\ \varepsilon_\theta \\ \gamma_{r\theta} \end{Bmatrix}_i^a = [B_i^a]\delta_e^a \quad \& \quad i = 1,3 \tag{3.48}$$

$$\gamma_2^a = \begin{Bmatrix} \gamma_{rz} \\ \gamma_{\theta z} \end{Bmatrix}_2^a = [B_2^a]\delta_e^a \tag{3.49}$$

where $[B_{1,2,3}^c]$ and $[B_{1,2,3}^a]$ are given in Appendix A.

The strain and kinetic energies can then be described as the sum of those for each of the layers of sandwich panel as:

$$T_e^{c,a} = \mathrm{T}_{e_1}^{c,a} + T_{e_2}^{c,a} + T_{e_3}^{c,a} \tag{3.50}$$

$$V_e^{c,a} = \mathrm{V}_{e_1}^{c,a} + V_{e_2}^{c,a} + V_{e_3}^{c,a} \tag{3.51}$$

where subscripts 1, 2 and 3 refer to the front face sheet, the core layer and back face sheets, respectively. $\mathrm{T}_{e_1}^{c,a}$, $T_{e_2}^{c,a}$, $T_{e_3}^{c,a}$ and $\mathrm{V}_{e_1}^{c,a}$, $V_{e_2}^{c,a}$, $V_{e_3}^{c,a}$ are defined as:

$$T_{e_i}^{c,a} = \frac{1}{2} \int\limits_{-\frac{h_i}{2}}^{\frac{h_i}{2}} \iint\limits_{A_e^{c,a}} \rho_i \{\dot{\delta}_e^{c,a}\}^T [L_i^{c,a}]^T [L_i^{c,a}] \{\dot{\delta}_e^{c,a}\} dA \, dz \quad \& \quad i = 1,3 \tag{3.52}$$

$$T_{e_2}^{c,a} = \frac{1}{2} \iint\limits_{A_e^{c,a}} I_2 \{\dot{\delta}_e^{c,a}\}^T [B_2^{c,a}]^T [B_2^{c,a}] \{\dot{\delta}_e^{c,a}\} dA$$

$$+ \frac{1}{2} \iint\limits_{A_e^{c,a}} \rho_2 h_2 \{\dot{\delta}_e^{c,a}\}^T [L_1^{c,a}]^T \begin{bmatrix} 1 & 0 \\ 0 & 0 \end{bmatrix} [L_1^{c,a}] \{\dot{\delta}_e^{c,a}\} dA \tag{3.53}$$

$$V_{e_i}^{c,a} = \frac{1}{2} \int\limits_{-\frac{h_i}{2}}^{\frac{h_i}{2}} \iint\limits_{A_e^{c,a}} [\varepsilon_i^{c,a}]^T [D_i] [\varepsilon_i^{c,a}] dA \, dz \quad \& \quad i = 1,3 \tag{3.54}$$

$$V_{e_2}^{c,a} = \frac{1}{2} \int\limits_{-\frac{h_2}{2}}^{\frac{h_2}{2}} \iint\limits_{A_e^{c,a}} [\gamma_2^{c,a}]^T [G_2] [\gamma_2^{c,a}] dA \, dz \tag{3.55}$$

where $[L_i^{c,a}]$ is given in Appendix A. ρ_1 and ρ_3 are the mass density of the face sheets. ρ_2 and I_2 are the mass density and the moment of inertia of the core layer, respectively. $[D_i]$ and $[G_2]$ are the elasticity matrices of the face sheets and the core layer, respectively, and defined as:

$$[D_i] = \frac{E_i}{1-v_i^2}\begin{bmatrix} 1 & v_i & 0 \\ v_i & 1 & 0 \\ 0 & 0 & \dfrac{1-v_i}{2} \end{bmatrix} \quad \& \quad i = 1,3 \tag{3.56}$$

$$[G_2] = \begin{bmatrix} G_2' + jG_2'' & 0 \\ 0 & G_2' + jG_2'' \end{bmatrix} \tag{3.57}$$

where E_i and v_i are the Young's modulus and the Poisson's ratio of the face sheets, respectively. G_2' and G_2'' are the storage and loss moduli of the core layer, respectively, and $j = \sqrt{-1}$. As it was mentioned before, the MR fluid is considered to operate in pre-yield region whose behavior is similar to that of linear viscoelastic material with complex shear modulus

The incident sound hits the front face sheet as shown in Figure 3.4. The work done by the acoustic pressure on the MR sandwich panel might then be described as a function of the pressure affected on the front panel and the transverse displacement as:

$$\pi_{ext}^{c,a} = \{\delta_e^{c,a}\} \iint_{A_e^{c,a}} P_b [L_1^{c,a}]^T \begin{bmatrix} 1 \\ 0 \end{bmatrix} dA \tag{3.58}$$

where P_b is the blocked pressure obtained as twice of the incident pressure. It should be mentioned that the radiated pressure at the incident side of the panel is neglected and the reflected pressure is considered to be equal to the incident pressure at this side.
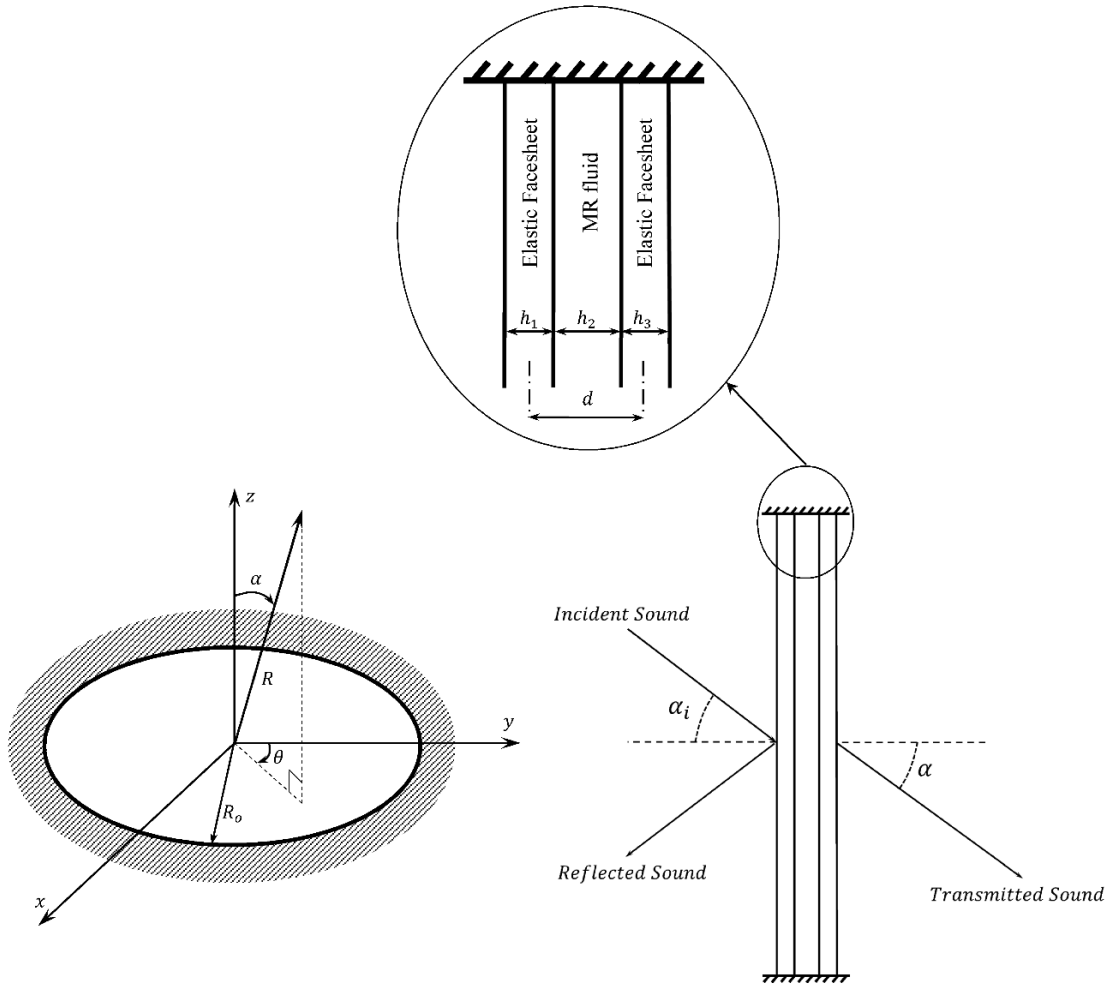
Figure 3.4. Schematic of the clamped MR sandwich panel.

Considering the strain and kinetic energies and the work done by the acoustic pressure and using Lagrange's equations, the governing equations of motion in the FE format for the circular and annular element of MR sandwich panel can be finally written as:

$$[M_e^{c,a}]\{\ddot{\delta}_e^{c,a}\} + [K_e^{c,a}]\{\delta_e^{c,a}\} = \{f_e^{c,a}\} \tag{3.59}$$

where $[M_e^{c,a}]$, $[K_e^{c,a}]$ and $\{f_e^{c,a}\}$ are the mass and stiffness matrices and the vector of nodal forces for the circular and annular elements, respectively. The mass, stiffness and nodal force matrices

57

should then be assembled to obtain the system governing equations of motion for the MR sandwich

panel as:

$$[M]\{\ddot{\delta}\} + [K]\{\delta\} = \{f\} \qquad (3.60)$$

where $[M]$, $[K]$ and $\{f\}$ are the mass, stiffness and force vector of the system, respectively, and

$\{\delta\}$ is the global displacement vector. After applying the appropriate boundary conditions,

Eq. (3.60) can be solved to evaluate the in-plane and transverse displacements of the circular

sandwich panels treated with MR fluid core layer. Clamped boundary condition is considered in

the present study in which the in-plane, transverse displacements and their slopes of the outer edge

of the panel is considered to be zero.

3.2.3. Sound Transmission Loss

The transverse velocity of the panel can be used to calculate the sound radiated from the panel

using the Rayleigh integral approach as [80]:

$$P_{rad} = \int_0^{2\pi} \int_0^{R_o} j\omega\rho_f v \, G \, r dr \, d\theta \qquad (3.61)$$

where R_o, ρ_f and ω are the panel's radius, density of the medium and the incident sound frequency,

respectively. v is the velocity of the panel which is substituted by $j\omega w$ for harmonic excitation. G

is the half-space free field Green's function which is defined as:

$$G = \frac{e^{jkR}}{2\pi R} \tag{3.62}$$

where R is the radial distance to the observation point as shown in Figure 3.4. Considering k_0 as the free wave number in the medium which is air in the present study, the wave number k is expressed as $k = k_0 \sin \alpha$.

The STL is calculated as the ratio of incident and radiated sound acoustic powers as follows:

$$STL = 10 \, \log_{10} \frac{\Pi_{\text{inc}}}{\Pi_{\text{rad}}} \tag{3.63}$$

where Π_{inc} and Π_{rad} are the incident and radiated acoustic powers, respectively. The incident acoustic power is expressed as a function of incident plane wave amplitude as [81]:

$$\Pi_{\text{inc}} = \frac{A|P_i|^2}{2\rho_f c_0} \cos(\alpha_i) \tag{3.64}$$

where c_0 is the speed of sound in the air and α_i is the incident angle as shown in Figure 3.4. The radiated acoustic power is also evaluated as [81]:

$$\Pi_{\text{rad}} = \frac{\iint |P_{rad}|^2 R_o^2 \sin(\alpha) \, d\alpha d\theta}{2\rho_f c_0} \tag{3.65}$$

59

3.3. Validation

In order to validate the analytical models developed using Ritz and FE methods, first the fundamental natural frequency and STL of sandwich panels treated with silicone rubber core layer are compared with those obtained experimentally. A $0.1\ m$ diameter clamped circular sandwich panel has been fabricated. The panel consists of face sheets made of aluminum and the silicone rubber core layer. The storage modulus of the silicone rubber is $1.34\ MPa$ and its frequency dependent loss modulus can be described as [63]:

$$G''_{SR} = 152511 + 68.31\omega + 0.475\omega^2 \qquad (3.66)$$

where ω is the excitation frequency in Hz and G''_{SR} is in Pa. The properties of the sandwich panel are presented in Table 3.1.

The FE model composed of n finite elements including one circular element and $n-1$ annular elements assembled with each other as shown in Figure 3.3. In order to determine the appropriate number of elements, finite element models with different number of elements have been examined. Figure 3.5 shows the first axisymmetric natural frequency of the sandwich panel with respect to different number of finite elements. As it can be seen, for $n \geq 16$, the finite element model converges almost to the same result. Considering this, 20 finite elements including one circular element and 19 annular elements have been utilized in the present study.
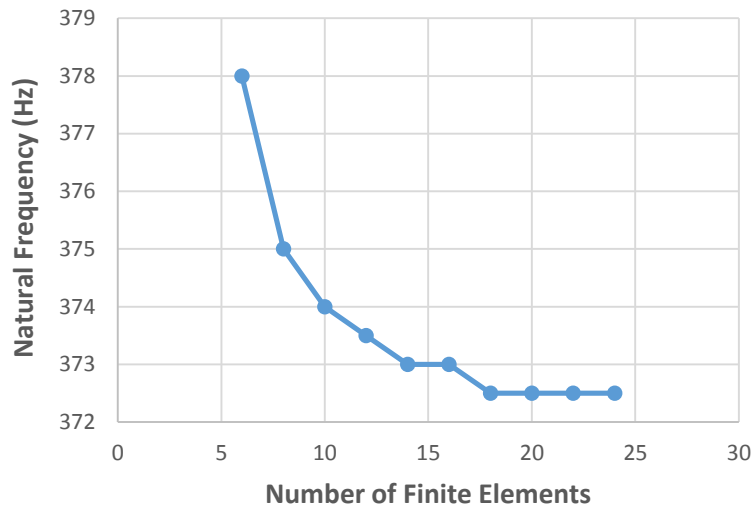
Figure 3.5. The first axisymmetric natural frequency of panel with
0.4 mm aluminum face sheets and 1.35 mm silicone rubber core layer.

The first axisymmetric natural frequency of the clamped circular panel obtained using the Ritz and FE models is compared with the experimental results in Table 3.2. Two symmetric sandwich panels with the 0.4 mm thickness aluminum face sheets and 1.35 mm and 1.8 mm silicone rubber core layer have been examined. As it was mentioned before, in order to obtain the natural frequency of the panel, the speaker has been set to provide pulse sound with the duration of 2.5 $Seconds$ hitting the panel. The acceleration was measured using a miniature accelerometer attached at the center of the panel. The measured time domain acceleration was then transferred to frequency domain using FFT analyzer. The frequency resolution and sampling frequency were considered to be 1 Hz and 800 Hz, respectively. Results show good agreement between the predicted natural frequencies obtained using Ritz and FE methods and the measured data with the error percentage less than3 %.

Table 3.1. Properties of aluminum face sheets, silicone rubber and MR fluid core layers.

Aluminum Face Sheets	
Mass Density (Kg/m^3)	2712
Young's modulus (GPa)	69
Poisson's ratio	0.33
Core Layer	
Silicone Rubber - Mass Density (Kg/m^3)	1460
MRF 132DG - Mass Density (Kg/m^3)	3500

Table 3.2. The first axisymmetric natural frequency of the panel with aluminum face sheets and silicone rubber core layer.

Panel			Natural Frequency (Hz)		
h_1 (mm)	h_2 (mm)	h_3 (mm)	Ritz	FEM	Exp.
0.4	1.35	0.4	377	373	371
0.4	1.8	0.4	362	358	366

The predicted STL of the test panels using Ritz and FE methods are compared with the experimental results in Figure 3.6. It should be mentioned that the speaker is placed such that the incident sound hits perpendicularly to the panel. Considering this, the incident wave angle (α_i) is considered to be zero in the simulations. The predicted STL of clamped circular sandwich panel with viscoelastic core layer using developed Ritz and FE models is generally in good agreement with the measured STL especially for the frequencies higher than the first natural frequency of the panels. As it can be realized, there is a notch in the STL at the resonance frequency in which the resonance effect causes the STL to significantly decrease.
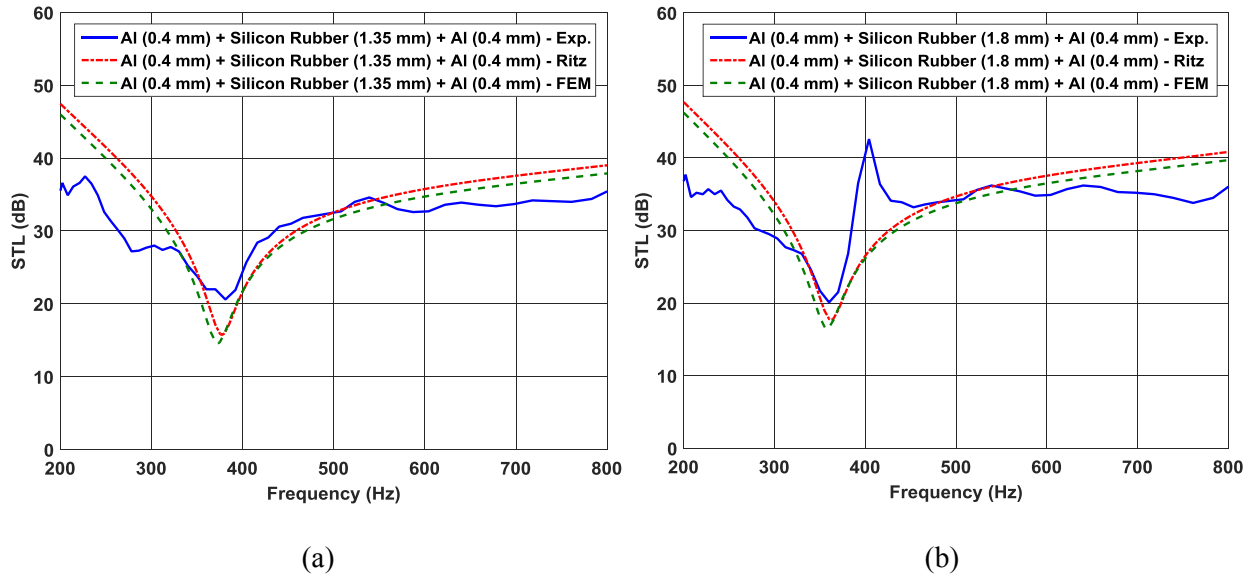
Figure 3.6. STL of panel with 0.4 mm aluminum face sheets and (a) 1.35 mm silicone rubber core layer (b) 1.8 mm silicone rubber core layer.

Moreover, the STL of the MR sandwich panel in absence of applied magnetic field is presented in Figure 3.7. This figure compares the STL of the MR sandwich panel obtained using Ritz and FE methods with the experimental results previously presented in Chapter 2. Sandwich panel with 0.4 mm thickness aluminum face sheets and 1.35 mm thickness MR fluid core layer is considered. The properties of the sandwich panel are presented in Table 3.1. As it was mentioned before, the MR fluid behaves like a viscoelastic material with complex shear modulus in pre-yield region. The field dependent storage and loss moduli of MRF $132DG$ have been previously identified as a function of the magnetic flux density and excitation frequency by Eshaghi et al. [63] as:

$$G'_{MR} = (192160.6 + 30663.56B + 243.6247B^2)(1 - e^{-0.004080\omega}) \qquad (3.67)$$

$$G''_{MR} = (45524.40 + 6757.977B + 6.441200B^2)(1 - e^{-0.007416\omega}) \qquad (3.68)$$

where B and ω are the magnetic flux density in mT and excitation frequency in Hz, respectively. These relations are used as G'_2 and G''_2 in Eq. (3.57).
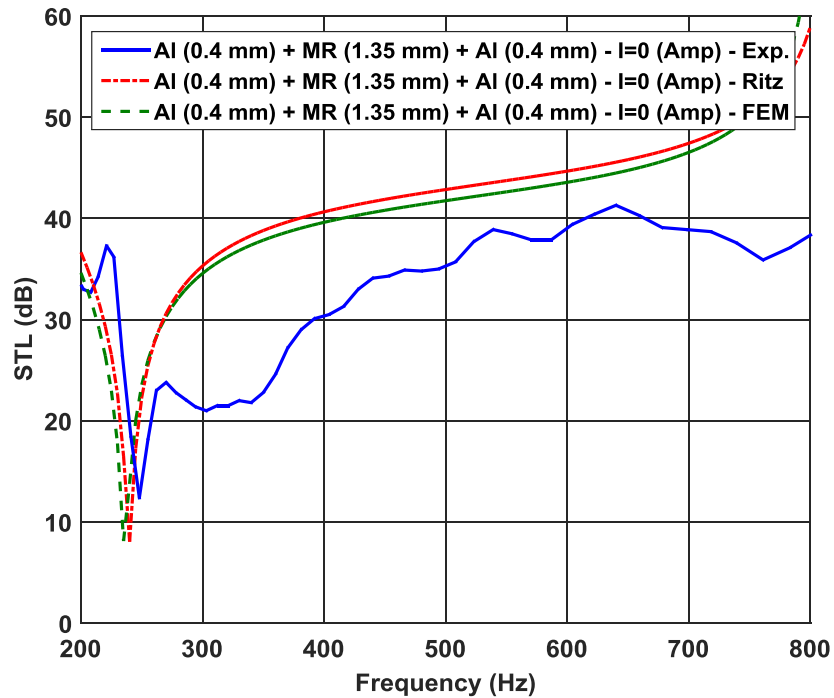
Figure 3.7. STL of panel with 0.4 mm aluminum face sheets and 1.35 mm MR fluid core layer in absence of applied magnetic field.

As it can be seen in Figure 3.7, the predicted STLs obtained using Ritz and FE models are in good agreement with the experimental results around resonance frequency. There is a notch in the STL at the resonance frequency in which the resonance effect causes the STL to significantly decrease. The resonance frequencies of the panel identified by the Ritz and FE model is close to that of experiment with error percentage around 5 %. It should be noted that in this study the radiated sound from the sandwich panel has been measured using one microphone. Also the STL

of the sandwich panel has been evaluated by subtracting the pressure of the radiated sound from the pressure of the incident sound and it was assumed that the radiated sound pressure is the same for different positions with the same distance from the center of the MR sandwich panel. Moreover all low frequency sound waves hitting the anechoic chamber's wall may not be completely absorbed by acoustic pyramid foam. Difference between the predicted and measured STL may thus be attributed to these assumptions. The comparison between the natural frequency of MR sandwich panel obtained using Ritz and FE models and those experimentally measured is presented in next section.

3.4. Results and Discussion

3.4.1. Effect of the Magnetic Field

Here, the effect of applied magnetic field on the STL of the sandwich panel with MR fluid core layer is studied. Table 3.3 represents simulation results and experimental measurements of the first axisymmetric natural frequency and also the STL at the natural frequency of the MR sandwich panel for different input currents to the electromagnet. As it was mentioned before, the magnetic field has been considered to be uniform across the panel from the center to the edge in the Ritz model. However, in the experiment, the applied magnetic field is different at different radius of the panel. For example for 1.8 Amp input current, the applied magnetic field varies from 44 mT at the center of the panel to 52 mT at edge with average of 48 mT. Thus the average magnetic fields as presented in Table 3.3 have been used for the simulations of the Ritz model. For the FE model, the simulations have been conducted utilizing the third order polynomial

function presented in Eq. (2.2) to calculate the magnetic field with respect to the radius and the input current. Comparing the results for the first axisymmetric natural frequency and also the STL at the resonance frequency obtained using the Ritz method with those evaluated using FE model show that they are in good agreement and the slight difference may be attributed to the consideration of uniform magnetic field in the Ritz method. Moreover, the simulation results for natural frequency and STL at resonance frequency are also generally in good agreement with those obtained experimentally for all current excitations and the maximum error is about 11 %. The difference between simulation and experimental results may be associated with the clamped boundary condition. In experiment the MR plate is clamped using multiple closely spaced bolts which cannot represent the ideal boundary condition in simulation. In addition, the panel becomes stiffer as the magnetic field increases and this further enhances the boundary condition effect. Thus the percentage error between the predicted resonance frequency and those measured using experiment increases as the magnetic field increases. Moreover, the wooden anechoic box cannot completely insulate the incident sound in the source chamber and part of the sound wave may reach the receiving chamber passing through the box or reflect back from the wall and hit the plate. While this has no noticeable influence on the natural frequency measured using the accelerometer, it is one of the major source of errors in the measurement of STL. Considering this, the STL is expected to be fairly predicted for the frequencies near the resonance frequency of the panel and to follow the trend for other frequencies. As it was mentioned before in Chapter 2, enhancing the stiffness and also damping of the MR sandwich panel by increasing the input current while the areal density is kept constant causes the first axisymmetric natural frequency and the corresponding STL to increase, respectively.

Table 3.3. The first axisymmetric natural frequency of the panel with 0.4 mm thickness aluminum face sheets and 1.35 mm thickness MRF 132DG core layer.

Current (Amp)	Average Magnetic Field (mT)	Natural Frequency (Hz)			STL (dB)		
		Ritz	FEM	Exp.	Ritz	FEM	Exp.
0	0	240	235	248	8.1	8.1	12.4
0.3	7.85	247	245	248	15.1	13.2	13.6
0.6	15.5	255	255	252	17.4	16.5	14.5
0.9	24	267	265	255	19.3	18.4	15.1
1.2	32	277	275	262	20.5	19.7	15.8
1.5	40	290	285	266	21.8	20.8	16.2
1.8	48	300	300	270	22.6	21.4	15.6

The STL of the MR sandwich panel with respect to the incident sound frequency for different applied input currents obtained using the developed FE model is also shown in Figure 3.8. Considering that the results obtained using the Ritz and FE models are very close to each other, the results of the FE model is presented and discussed. As expected, increasing the magnetic field causes the notch in the STL at resonance frequency to shift to higher frequencies. Moreover, enhancing the magnetic field causes the damping of the structure to increase and consequently the STL of the panel at the resonance frequency. Figure 3.8 also show that depending on the incident sound frequency, increasing the magnetic field causes the STL to increase or decrease. For the frequencies below the resonance frequency, the STL increases as the magnetic field enhances, while the STL decreases as the magnetic field increases for the frequencies above the resonance frequency. This shows the possibility of using semi-active control strategy to automatically determine the appropriate magnetic field to maximize the STL for the frequency range of interest.
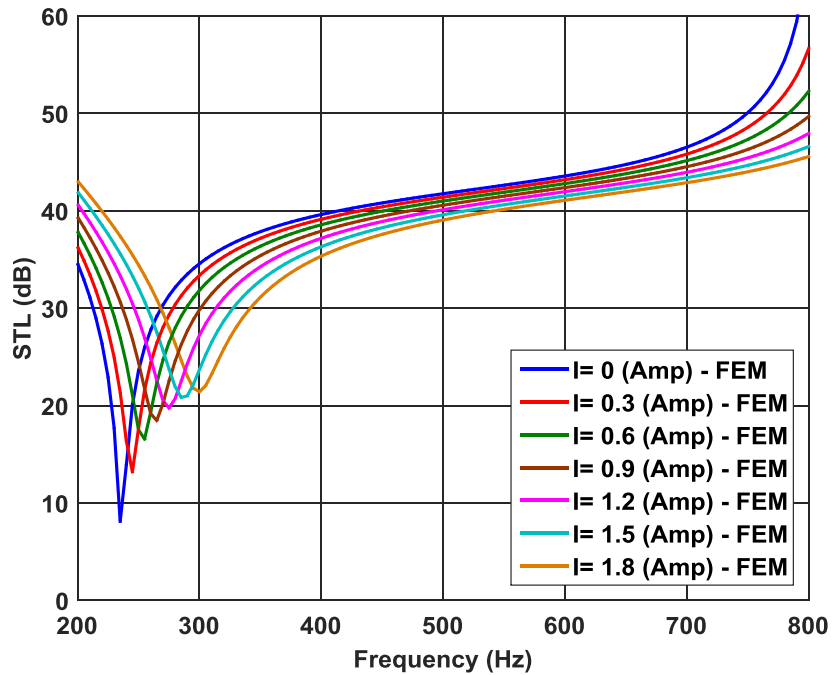
Figure 3.8. STL of panel with 0.4 mm aluminum face sheets and 1.35 mm MR fluid core layer predicted using FE model.

3.4.2. Effect of the Thickness of the Face Sheets and Core Layer

The variation of the first axisymmetric natural frequency of the MR circular sandwich panel with respect to the thickness of the face sheets is shown in Figure 3.9. The sandwich panel is considered to be symmetric with same thickness for front and back face sheets and 1.35 mm MR core layer with zero input current. As it can be seen, the natural frequency of the panel increases almost in proportion to the thickness of the face sheets which is due to the increase in the sandwich panel's stiffness as the thickness of the face sheets increases. Figure 3.10 shows the effect of the thickness of the MR core layer on the first axisymmetric natural frequency and STL of the circular sandwich panel with 0.4 mm aluminum face sheets. As it can be realized in Figure 3.10 (a), the natural frequency of the panel decreases quadratically as the thickness of the core layer increases.

68

This is due to the fact that the mass per unit area of the panel increases and causes the natural frequency to decrease. With respect to the STL, Figure 3.10 (b) shows that STL of the MR sandwich panel increases quadratically as the thickness of the MR layer increases which could be explained as the effect of damping provided by the thicker MR core layer.
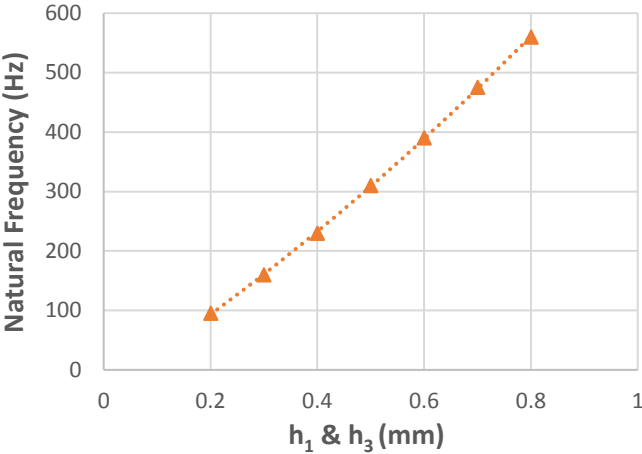
Figure 3.9. First axisymmetric natural frequency of the panel with and 1.35 mm MR fluid core layer in absence of magnetic field.

(a)   (b)
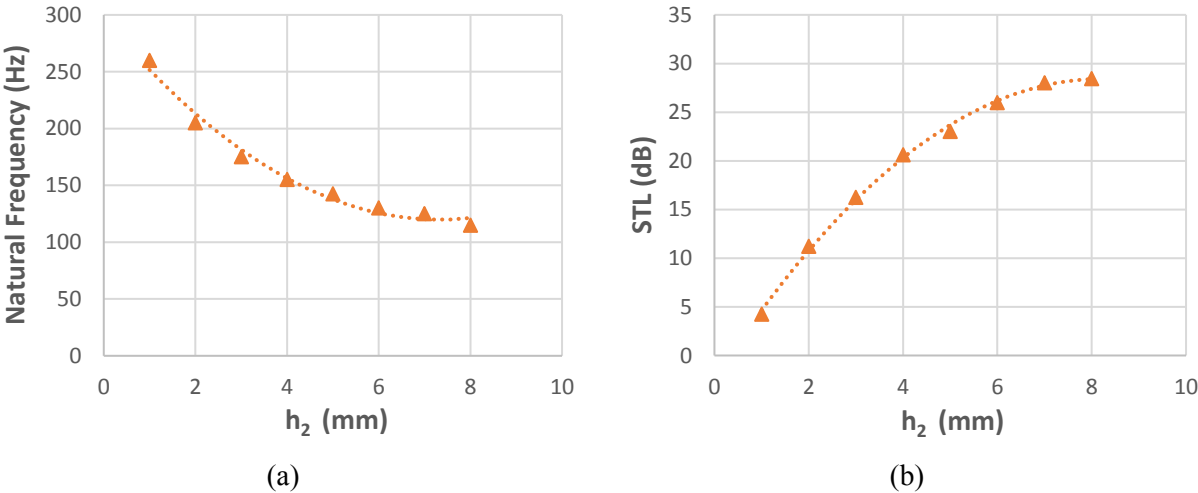
Figure 3.10. MR sandwich panel with 0.4 mm aluminum face sheets in absence of magnetic field (a) first axisymmetric natural frequency, (b) STL.

3.5. Conclusions

The STL of circular sandwich panel fully treated with MR fluid core layer was investigated in this chapter. MR sandwich panel with clamped boundary conditions and elastic face sheets was considered and the governing equation of motions were derived using both Ritz and FE methods. Two circular and annular finite elements were used to derive the finite element model. The developed models were validated comparing the first axisymmetric natural frequency and STL of the sandwich panels with silicone rubber core layer with those experimentally measured. The effects of the applied magnetic field on the natural frequency and the STL of MR sandwich panel were investigated. It was shown that the damping of the structure enhances as the magnetic field increases and consequently the sudden reduction in the STL at the response frequency can be significantly improved by increasing the applied current. Moreover the notch in STL at the resonance frequency can be considerably shifted by changing the applied current. In addition, the effect of the applied magnetic field on the STL of the MR sandwich panel depends on the frequency of the incident sound. For the frequencies below and above the resonance frequency, the STL increase and decreases, respectively, as the input current increases. Thus, it is possible to employ an appropriate control strategy to determine the proper magnetic field to maximize the STL. Parametric study on the effect of the face sheets' and the core layer's thicknesses on the natural frequency and the STL of the MR sandwich panel showed that the natural frequency shifts to higher frequencies as the thickness of the face sheets increases. Increasing the thickness of the MR core layer causes the natural frequency to decrease while increasing the thickness of the core layer causes the STL of the panel at the resonance frequency to increase.

CHAPTER 4

VIBRO-ACOUSTIC ANALYSIS AND TOPOLOGY OPTIMIZATION OF PARTIALLY TREATED MR-BASED SANDWICH PANELS

4.1. Introduction

This chapter aims to investigate the STL of sandwich panels partially treated with MR fluid. Considering that the models developed in Chapter 3 are mostly effective for the sandwich panels with uniform core layer, in the present study a 4-node quadrilateral element is developed to derive the FE model for a clamped circular sandwich panel with partially treated core layer. The developed FE model is validated through comparing the results for the fully treated configuration with those of experimental and analytical results previously reported in Chapter 3. Using the established FE model, systematic parametric study is then presented to investigate the influence of different partial treatments on the natural frequencies, loss factors and the STL of the sandwich panels. The meta-model technique based on the developed FE model and D-optimal technique is then utilized to derive approximate and efficient models to evaluate the response of the sandwich panels including the first natural frequency and corresponding loss factor and also the rate of their changes as a result of changes in applied magnetic field. The topology optimization problem is finally formulated using the developed meta-models and solved using genetic algorithm (GA) and

integer programing (IP) methods in absence and presence of mass constraint. The optimal candidates are further evaluated using the developed FE model to identify the true optimized topology. The STL and the rate of changes in natural frequencies and loss factors of the constraint and non-constraint optimal topologies are also compared.

4.2. Finite Element Model

Figure 4.1 shows a circular sandwich panel comprising two elastic face sheets and the core layer which has been partially treated with MR fluid and silicone rubber. The FE model is developed considering following assumptions: (1) the ratio of the thickness to radius of the face sheets is considered to be small and the classical plate theory is used to obtain the displacements of the face sheets, (2) The transverse displacements are the same for the face sheets and the core layer, (3) There is no slippage between the face sheets and core layer and the compatibility conditions is used to obtain the displacements of the core layer in terms of those of the face sheets, (4) The stress components of the face sheets and the core layer are obtained utilizing the Hooke's law. The schematic of the finite element model and the degrees of freedom of each element is shown in Figure 4.2. The circular panel is divided into a circular element at the center and 4 node quadrilateral elements circumferentially and radially connected to each other. The circular element has a node at the edge with four degrees of freedom, $\left[w \quad \frac{\partial w}{\partial r} \quad u_1^0 \quad u_3^0 \right]^T$, as it was presented in Chapter 3. The 4-node element is defined by two i_1 and i_2 nodes at the inner radious and two j_1 and j_2 nodes at the outer radius. Seven degrees of freedom have been considered for each of the nodes as follows:
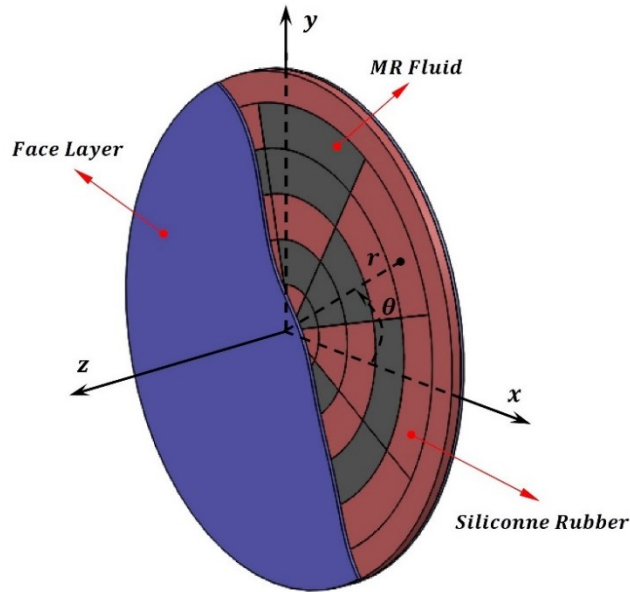
Figure 4.1. Schematic of sandwich panel partially treated with MR fluid and silicone rubber core layer.
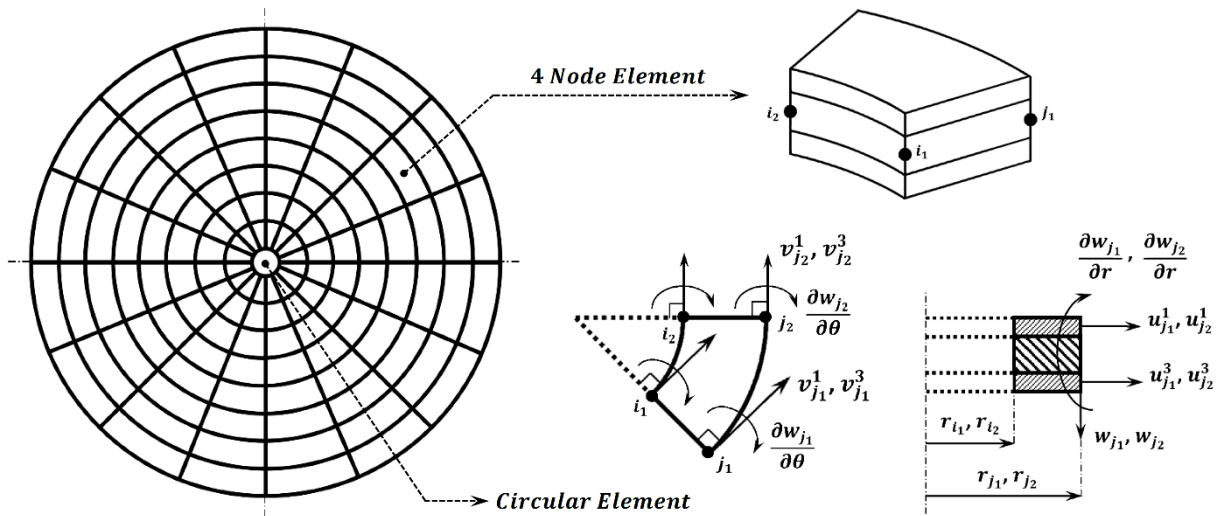
Figure 4.2. Schematic of the finite element model.

$$\delta_n = \begin{bmatrix} w_n & \dfrac{\partial w_n}{\partial r} & \dfrac{\partial w_n}{\partial \theta} & u^0_{1_n} & u^0_{3_n} & v^0_{1_n} & v^0_{3_n} \end{bmatrix}^T \qquad n = i_1, i_2, j_1, j_2 \tag{4.1}$$

where w_n, $\dfrac{\partial w_n}{\partial r}$ and $\dfrac{\partial w_n}{\partial \theta}$ are the transverse displacement, radial and circumferential rotations, respectively. $u^0_{1_n}$, $u^0_{3_n}$ and $v^0_{1_n}$, $v^0_{3_n}$ are the in-plane radial and circumferential displacements of the mid-plane of the face sheets in r and θ directions, respectively. Now considering Figure 4.2, the nodal displacement vector can be expressed as:

$$\delta_e = \begin{Bmatrix} \delta_{i_1} \\ \delta_{i_2} \\ \delta_{j_1} \\ \delta_{j_2} \end{Bmatrix} \tag{4.2}$$

The nodal displacement vector can then be utilized to express the transverse and in-plane displacements of the face sheets' mid-plane as a function of shape functions:

$$\begin{Bmatrix} w \\ u^0_i \\ v^0_i \end{Bmatrix} = \begin{bmatrix} L_w \\ L^0_{u_i} \\ L^0_{v_i} \end{bmatrix}_{3\times28} \{\delta_e\}_{28\times1} \quad \& \quad i = 1,3 \tag{4.3}$$

where L_w, $L^0_{u_i}$ and $L^0_{v_i}$ are the shape functions presented in Appendix B. The strain-displacement relations are then written using Eq. (4.3) to obtain the strain and subsequently kinetic and strain energies of the 4-node element:

$$T_e = T_{e_1} + T_{e_2} + T_{e_3} \tag{4.4}$$

$$V_e = V_{e_1} + V_{e_2} + V_{e_3} \tag{4.5}$$

where subscripts 1, 2 and 3 refer to the front face sheet, the core layer and back face sheet, respectively. T_{e_1}, T_{e_2}, T_{e_3} and V_{e_1}, V_{e_2}, V_{e_3} are defined as:

$$T_{e_i} = \frac{1}{2} \int_{-\frac{h_i}{2}}^{\frac{h_i}{2}} \iint_{A_e} \rho_i \{\dot{\delta}_e\}^T [L_i]^T [L_i] \{\dot{\delta}_e\} dA\, dz \quad \& \quad i = 1,3 \tag{4.6}$$

$$T_{e_2} = \frac{1}{2} \iint_{A_e} I_2 \{\dot{\delta}_e\}^T [B_2]^T [B_2] \{\dot{\delta}_e\} dA + \frac{1}{2} \iint_{A_e} \rho_2 h_2 \{\dot{\delta}_e\}^T [L_w]^T [L_w] \{\dot{\delta}_e\} dA \tag{4.7}$$

$$V_{e_i} = \frac{1}{2} \int_{-\frac{h_i}{2}}^{\frac{h_i}{2}} \iint_{A_e} \{\dot{\delta}_e\}^T [B_i]^T [D_i] [B_i] \{\dot{\delta}_e\} dA\, dz \quad \& \quad i = 1,3 \tag{4.8}$$

$$V_{e_2} = \frac{1}{2} \int_{-\frac{h_2}{2}}^{\frac{h_2}{2}} \iint_{A_e} \{\dot{\delta}_e\}^T [B_2]^T [G_2] [B_2] \{\dot{\delta}_e\} dA\, dz \tag{4.9}$$

where ρ_i and h_i are the mass density and the thickness of the face sheets, respectively, and ρ_2, h_2 and I_2 are the mass density, the thickness and the moment of inertia of the core layer, respectively. $[L_i]$, $[B_i]$, $[D_i]$ and $[G_2]$ are defined as:

$$[L_i] = \begin{bmatrix} L_w \\ L_{u_i}^0 - z_i \dfrac{\partial L_w}{\partial r} \\ L_{v_i}^0 - z_i \dfrac{\partial L_w}{r \partial \theta} \end{bmatrix} \quad \& \quad i = 1,3 \tag{4.10}$$

$$[B_i] = \begin{bmatrix} -z_i \dfrac{\partial^2}{\partial r^2} & \dfrac{\partial}{\partial r} & 0 \\[2ex] -\dfrac{z_i}{r^2}\dfrac{\partial^2}{\partial \theta^2} - \dfrac{z_i}{r}\dfrac{\partial}{\partial r} & \dfrac{1}{r} & \dfrac{1}{r}\dfrac{\partial}{\partial \theta} \\[2ex] -\dfrac{2z_i}{r}\dfrac{\partial^2}{\partial r\partial\theta} + \dfrac{2z_i}{r^2}\dfrac{\partial}{\partial \theta} & \dfrac{1}{r}\dfrac{\partial}{\partial \theta} & \dfrac{\partial}{\partial r} - \dfrac{1}{r} \end{bmatrix} \begin{bmatrix} L_w \\ L_{u_i}^0 \\ L_{v_i}^0 \end{bmatrix} \quad \& \quad i = 1,3 \tag{4.11}$$

$$[B_2] = \begin{bmatrix} \dfrac{d}{2h_2}\dfrac{\partial}{\partial r} & 1 & 0 \\[2ex] \dfrac{d}{2h_2}\dfrac{\partial}{r\partial\theta} & 0 & 1 \end{bmatrix} \begin{bmatrix} L_w \\ L_{u_1}^0 \\ L_{v_1}^0 \end{bmatrix} + \begin{bmatrix} \dfrac{d}{2h_2}\dfrac{\partial}{\partial r} & -1 & 0 \\[2ex] \dfrac{d}{2h_2}\dfrac{\partial}{r\partial\theta} & 0 & -1 \end{bmatrix} \begin{bmatrix} L_w \\ L_{u_3}^0 \\ L_{v_3}^0 \end{bmatrix} \tag{4.12}$$

$$[D_i] = \dfrac{E_i}{1 - v_i^2} \begin{bmatrix} 1 & v_i & 0 \\ v_i & 1 & 0 \\ 0 & 0 & \dfrac{1 - v_i}{2} \end{bmatrix} \quad \& \quad i = 1,3 \tag{4.13}$$

$$[G_2] = \begin{bmatrix} G & 0 \\ 0 & G \end{bmatrix} \tag{4.14}$$

where E_i and v_i are the Young's modulus and the Poisson's ratio of the face sheets, respectively. As it can be seen in Figure 4.3, z_i denotes the transverse coordinate in the local coordinate system of each layer considering the origin at the mid-plane of each layer and $d = \frac{h_1}{2} + h_2 + \frac{h_3}{2}$. G is the complex shear modulus of the core layer comprising the silicone rubber and MR fluid in the present study. As MR fluid core layer experiences small shear strain, it is considered to operate in pre-yield region. Thus, both MR fluid and silicone rubber can be described as a linear viscoelastic material with complex shear modulus.
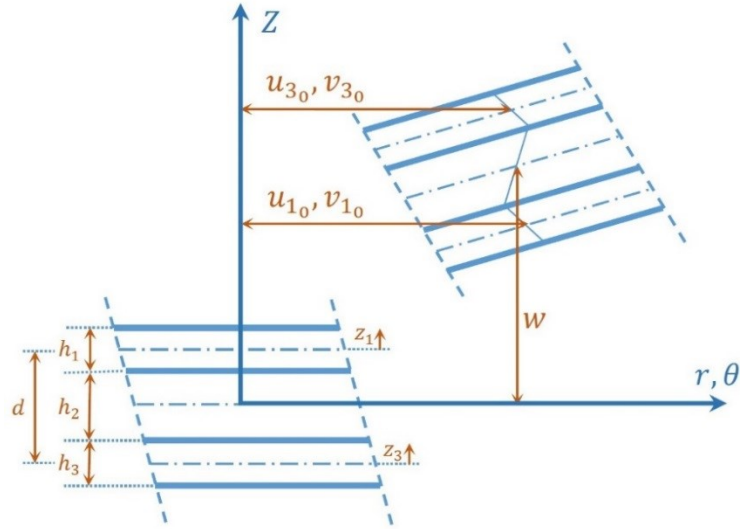
Figure 4.3. Assumed displacement field components.

The mass and stiffness matrices for the 4-node element are obtained based on Lagrange's equations using the strain and kinetic energies. Assembling the mass and stiffness matrices of the 4-nodes and also the circular elements, the free governing equations of motion of the circular sandwich panel can be represented in the finite element form as:

$$[M]\{\ddot{\delta}\} + [K]\{\delta\} = \{0\} \tag{4.15}$$

where $[M]$, $[K]$ and $\{\delta\}$ are the mass, stiffness and the global nodal displacement vector, respectively. The free vibration equations of motion of the structure may then be expressed as:

$$(-\omega^2[M] - [K])C = \{0\} \tag{4.16}$$

where ω and C are the natural frequency and the associate nodal mode shape vector, respectively. The complex eigenvalues of this equation can be used to calculate the natural frequencies and the associated loss factor as follows:

$$\omega_n = \sqrt{\lambda'_n} \tag{4.17}$$

$$\eta_n = \frac{\lambda''_n}{\lambda'_n} \tag{4.18}$$

where ω_n and η_n are the nth natural frequency and the corresponding loss factor, respectively, and $\lambda_n = \lambda'_n + j\lambda''_n$ is the nth complex eigenvalue of the system.

The work done by the acoustic pressure on the MR sandwich panel may also be described as:

$$\pi_{ext} = \{\dot{\delta}_e\} \iint_{A_e} P_b [L_w]^T dA \tag{4.19}$$

where P_b is the blocked pressure obtained as twice of the incident pressure. Considering the work done by the acoustic pressure, the vector of nodal forces for the 4-node element are obtained. Thus, the forced vibration governing equations of motion of the sandwich panel can be expressed as:

$$[M]\{\ddot{\delta}\} + [K]\{\delta\} = \{F\} \tag{4.20}$$

where $\{F\}$ is the force vector of the system. Solving Eq. (4.20), provides the transverse velocity of the panel which can then be used to calculate the STL following Eqs. (3.61) to (3.65).

4.3. Validation of the FE Model

The developed circular-4 node quadrilateral FE model provides a unique opportunity to investigate the wide variety of partial treatment configurations and also can be effectively utilized to identify the optimal topological arrangements of MR fluid and Silicone rubber segments.

Here in this section, first the results for natural frequency and STL of a fully treated clamped circular sandwich panel obtained using the developed circular-4-node quadrilateral FE model (C-4NQ FE) have been compared with those obtained experimentally and also numerically using Ritz and circular-annular FE model (C-A FE) presented in Chapter 3 for the purpose of validation. To do so, a $100\ mm$ diameter circular sandwich panel with $0.4\ mm$ aluminum face sheets and $1.35\ mm\ MRF\ 132DG$ manufactured by Lord Corporation [77] as the core layer is considered. MR fluid in the core layer generally operates in pre-yield region and thus behaves as a viscoelastic material with complex shear modulus [63]. The field dependent storage and loss moduli of $MRF\ 132DG$ which have been identified by Eshaghi et al. [63] and presented in Eqs. (3.67) and (3.68) are used in the present study. The properties of the aluminum face sheets and MR fluid core layer are similar to those provided in Table 3.1 which is again repeated in Table 4.1 for the sake of clarity. For the convergence analysis and also to find optimal number of elements in radial direction, the fist axisymmetric natural frequency of the panel have been examined using the C-4NQ FE model with different number of elements. The results are shown in Figure 4.4. As it can be realized, the developed FE model has converged to the same natural frequency when the number of elements in radial direction is nearly over 25.

Table 4.1. Properties of aluminum, MRF 132DG and silicone rubber.

Aluminum Face Sheets			MRF 132DG	Silicone Rubber
Mass Density (Kg/m^3)	Young's Modulus (GPa)	Poisson's Ratio	Mass Density (Kg/m^3)	Mass Density (Kg/m^3)
2712	69	0.33	3500	1460
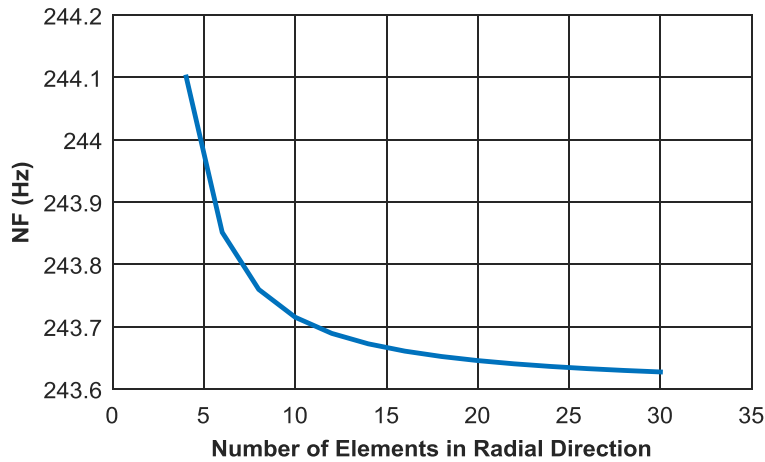
Figure 4.4. The effect of number of elements in radial direction on the first axisymmetric natural frequency of panel with 0.4 *mm* aluminum face sheets and 1.35 *mm* MR fluid core layer considering 30 elements in circumferential direction.

Table 4.2 compares the first axisymmetric natural frequency of the panel with clamped boundary condition obtained using the developed FE model (C-4NQ FE) with those presented in Chapter 3 for Ritz, C-A FE model and experimental results. The natural frequencies of the panel for zero and 1.8 *Amp* current input to the electromagnet are presented. The error percentage between the resonance frequencies obtained using C-4NQ FE model and those based on Ritz and C-A FE models is about 2 % and less than 10 % comparing to the results. Therefore, there is a good agreement between the predicted and reported natural frequencies. Figure 4.5 also shows the STL of the panel in absence of magnetic field obtained using the C-4NQ FE, Ritz, C-A FE models and also experiment. This figure shows that the results based on the developed C-4NQ FE model are in good agreement with those previous numerical results and also experiment in the vicinity of the resonance frequency. It is noted that matching the incident sound frequency with the natural frequency of the panel causes the panel to resonate yielding drastic reduction in the STL. The

80

difference between the predicted and measured STL may be attributed to the fact that STL has been measured by subtracting the radiated sound pressure from the incident sound pressure in which it was assumed that the radiated sound pressure is the same for different positions with the same distance from the center of the MR panel.

Table 4.2. The first axisymmetric natural frequency of the panel with 0.4 mm thickness aluminum face sheets and 1.35 mm thickness MRF 132DG core layer.

Input Current (Amp)	Natural Frequency (Hz)			
	C-4NQ FE	Ritz	C-A FE	Exp.
$I = 0$	235	240	235	248
$I = 1.8$	295	300	300	270
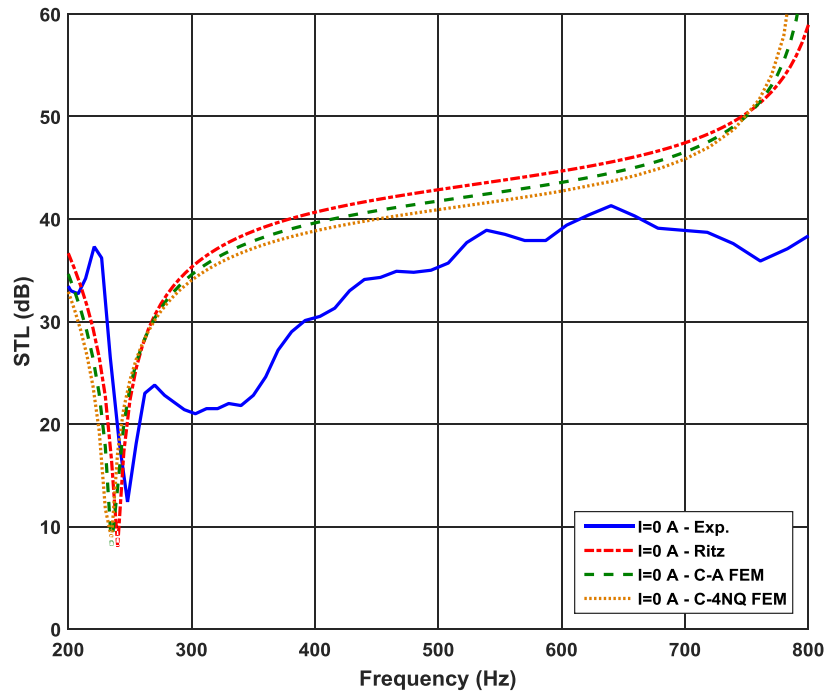
Figure 4.5. STL of panel with 0.4 mm aluminum face sheets and 1.35 mm MR fluid core layer.

81

4.4. Parametric Study

In order to investigate the effect of the position of MR fluid and silicone rubber on the STL, first axisymmetric natural frequency and the corresponding loss factor of the sandwich panel have been investigated for 9 different cases representing different positions of the MR fluid and silicone rubber in the core layer. Figure 4.6 shows the cases in which the MR fluid and silicone rubber radially and circumferentially distributed in the core layer. It should be noted that the segmentation has been done in such a way that the MR fluid and silicone rubber have the same area in all the cases, thus the mass of all 9 cases are equal and the distribution of the MR fluid and silicone rubber just affects the stiffness and damping of the structure. The STL of the partially treated panels in absence of magnetic field is presented in Figure 4.7. Figure 4.7 (a) compares the STL for cases 1-6 in which the MR fluid and silicone rubber circumferentially distributed to form annular pattern. It can be seen that as the position of MR fluid changes in the core layer, the stiffness of the panel is considerably affected and consequently the first natural frequency shifts. Moreover, the damping of the structure changes and causes the STL of the panel at the resonance frequency to increase or decrease for different cases. For example the first axisymmetric natural frequency of the sandwich panel (sudden notch in the STL shown in Figure 4.7) changes from 250 Hz for case 1 to 340 Hz for case 4. This confirms that changing the position of the MR fluid from the center to the outer circumferential edge of the core layer stiffens the structure causing the natural frequency to increase. Moreover, Figure 4.7 shows that for the frequencies above the resonance frequencies, the STL for cases 1 to 3 are more than those for cases 4 to 6. Given that MR fluid is denser than silicone rubber and maximum shear deformation occurs at center of plate, it may be concluded that the presence of denser material at the center of the panel causes the STL to increase. The STL of

the cases 7 to 9 in which the MR fluid and silicone rubber radially distributed among the core layer are presented in Figure 4.7(b). This figure shows that radial distribution of the MR fluid and silicone rubber does not considerably affect the first axisymmetric natural frequency and also the STL of the structure. On the other hand, the asymmetric distribution of the MR fluid in Case 7 causes the STL to reduce at the second natural frequency of the panel.
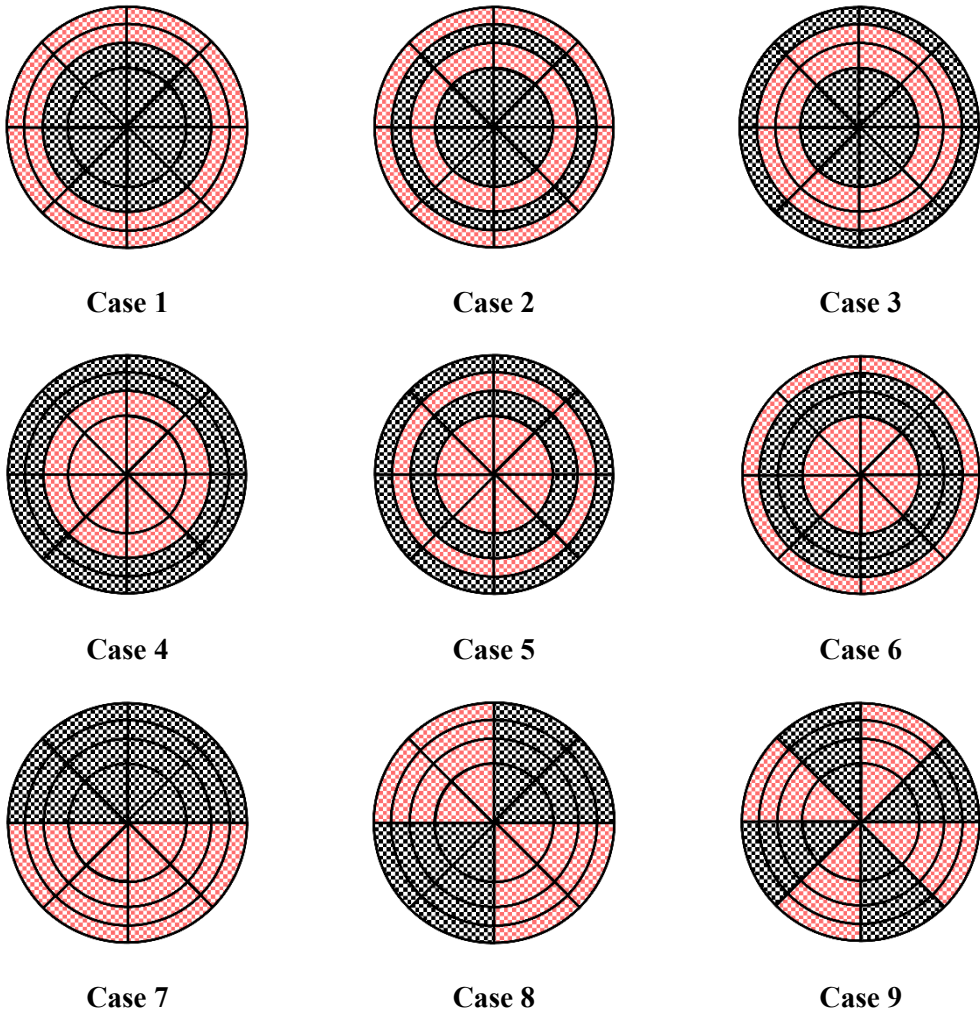
Figure 4.6. Schematic of circular sandwich panel partially treated with MR fluid and silicone rubber; MR fluid: ▨, silicone rubber: ▨.

(a)   (b)
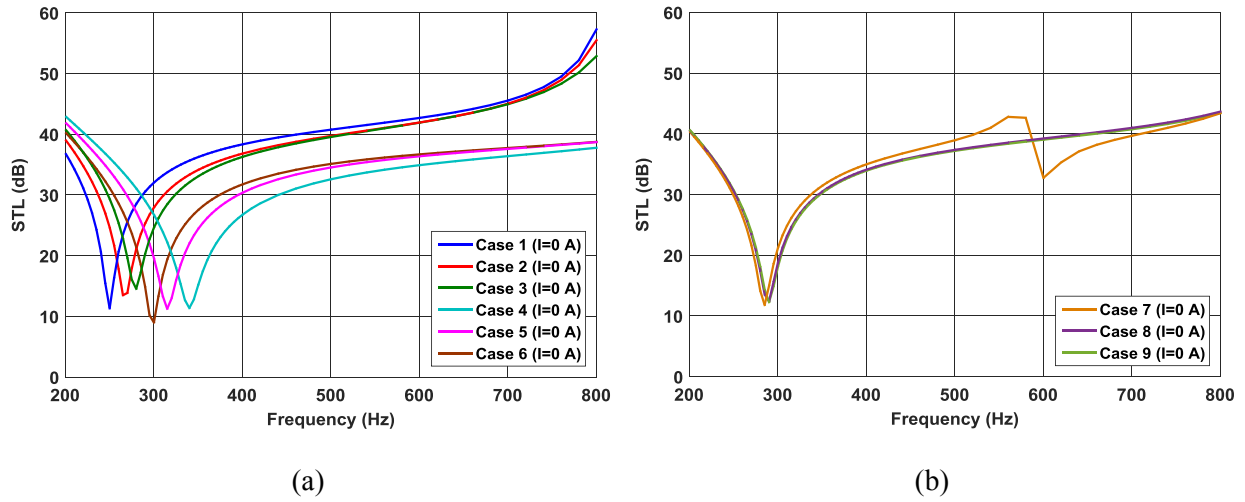
Figure 4.7. STL of partially treated MR sandwich panels in absence of magnetic field ($I = 0\ Amp$) (a) cases 1 to 6 (b) cases 7 to 9.

Table 4.3 shows the first axisymmetric natural frequencies and loss factors for zero and 1.8 Amp current input to the electromagnet. In order to investigate the effect of applied magnetic field on the natural frequency and loss factor, the rates of their changes due to applying magnetic field are also calculated and provided in Table 4.3. Comparing the rates, it can be realized that the maximum and minimum rates of change in natural frequency are corresponding to cases 1 and 4, respectively. This shows that the influence of applied magnetic field on the first axisymmetric natural frequency increases as the MR fluid shifts from the boundary edge toward the center of the panel. This can be attributed to the fact that for the first axisymmetric mode shape of the clamped circular sandwich panel, the maximum and minimum shear deformation locations coincide with the location of MR fluid segments in cases 1 and 4, respectively. Comparing the rates of the change in the loss factor, case 6 shows the maximum rate of nearly 114 %. It is clear from Eq. (4.18) that by increasing the stiffness of the structure (increasing the natural frequency), the loss factor decreases. Considering this, the higher loss factor rate for the case 6 compared with that for the

84

case 1 can be interpreted as a result of higher rate of changes in the stiffness for the case 1 which causes the rate of loss factor to decrease. Comparing the rates for the cases 7 to 9, it can be realized that the radial distribution of the MR fluid and silicone rubber does not significantly affect the rate of changes of first axisymmetric natural frequency and loss factors. However, the maximum rate between these cases belongs to case 7 in which the concentration of MR fluid in a large segment enhances its effectiveness.

Table 4.3. The first axisymmetric natural frequencies and loss factors (Cases 1-9) for zero and 1.8 Amp current input

	$\omega_{I=0\ Amp}$	$\omega_{I=1.8\ Amp}$	$\left\|\dfrac{\omega_{I=1.8\ Amp} - \omega_{I=0\ Amp}}{\omega_{I=0\ Amp}}\right\|$ %	$\eta_{I=0\ Amp}$	$\eta_{I=1.8\ Amp}$	$\left\|\dfrac{\eta_{I=1.8\ Amp} - \eta_{I=0\ Amp}}{\eta_{I=0\ Amp}}\right\|$ %
Case 1	250.97	301.26	20.04	0.0394	0.0843	113.97
Case 2	268.11	309.13	15.30	0.0513	0.0852	65.95
Case 3	279.52	305.23	9.20	0.06290	0.0838	33.21
Case 4	343.38	372.55	8.50	0.0627	0.0843	34.31
Case 5	318.47	357	12.10	0.0566	0.0832	47.06
Case 6	301.86	360.88	19.55	0.0395	0.0846	114.22
Case 7	287.43	330.74	15.07	0.0498	0.0844	69.66
Case 8	291.49	331.61	13.76	0.0544	0.0844	55.10
Case 9	292.58	331.89	13.44	0.0557	0.0844	51.63

4.5. Optimization Strategy

Partial treatment of sandwich panel with MR fluid core layer provides the opportunity to control the stiffness and damping of the structure while its mass per unit area is minimized. In addition, in some cases the partial treatment may further increase the influence of the applied magnetic field on the stiffness and damping of the structure compared with the fully treatment

configuration. In this section, a strategy for topology optimization of the core layer of the clamped MR-based circular sandwich panel is presented. Figure 4.8 shows the schematic of the segmented core layer. As it can be seen, a tiny circular segment is considered at the middle. The diameter of this segment is $1\ mm$. The rest of the core layer is divided into eight 45° radial and 4 circumferential sections. The diameter of the annular sections shown in Figure 4.8 are selected in a way that the area of all the 32 sections to be equal. It should also be mentioned that the size of the elements of the developed FE model are selected in such a way that none of the elements are placed in common between two sections. Table 4.4 provides the diameter of each four annular sections and also the number of 4-node quadrilateral elements distributed radially and circumferentially in each section. Finer mesh has been used at the center area due to the presence of higher shear deformation. As it can be realized, the finite element model comprises of $(12 + 5 + 4 + 3) \times 72 = 1728$ 4-node quadrilateral elements and 1 circular element for a total of 12600 degrees of freedom.

It should be noted that evaluation of the rate of changes of natural frequency and loss factors using the developed high fidelity FE model is computationally very expensive and takes about $11\ hours$ on a $64\ bit$ operating system with $Intel(R)Core(TM)i7 - 4770\ CPU\ @\ 3.40\ GHz$ and $8.00\ GB\ RAM$. Thus, due to iterative nature of the optimization process in which at each iteration the FE model may be called several times, it would be impractical to use the full finite element model in optimization formulation. Considering this, in this study the response surface methods (meta-model technique) is utilized to develop approximate response models which can accurately predict the desired output responses. Subsequently, the developed approximate response models have been effectively utilized in the defined optimization problems to find the

optimal topology with respect to arrangement of MR fluid and silicone rubber segments in the core layer of the circular sandwich structure.
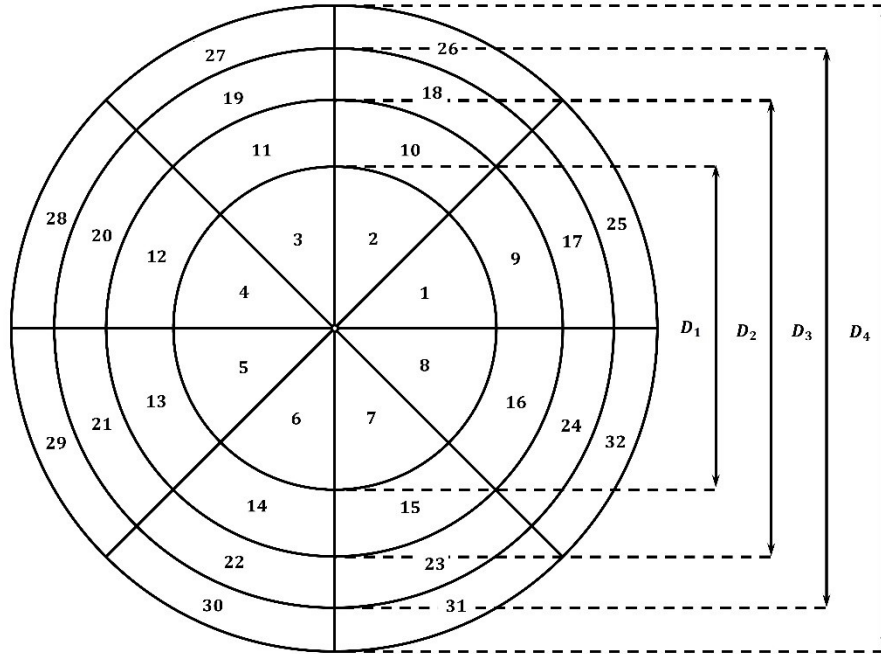
Figure 4.8. Schematic of the segmented core layer.

Table 4.4. Diameter and the number of annular elements in each of the annular sections.

Diameter of annular element (mm)	Number of elements in radial direction	Number of elements in circumferential direction
50	12	72
70.7	5	72
86.6	4	72
100	3	72

4.5.2. Development of Meta-Models

In order to build the meta-models, it is required to have a sample design points within the feasible design space of interest that can be utilized as inputs for the simulation tool (FE model) or physical experiment in order to provide the desired responses of the system. The point is that the designer should try to select minimum number of design points in order to minimize the number of expensive experiments or simulations while providing enough information to accurately construct the approximate meta-model. In this subject, there are some statistical techniques that helps the designer to identify the appropriate design points such as Factorial, D-optimal, Taguchi and also random numbers. As it was explained before, in the present study there are 32 segments of the core layer which could be filled with either MR fluid or silicone rubber. Therefore, 32 binary variables is considered for the present topology optimization problem in which each of the variables represent one segment of the core layer. All of the variables are binary, zero or one, in which zero represents silicone rubber in the relevant segment of the core layer and one represents the MR fluid. It should be mentioned that due to the small size of the circular element at the center, this element is neglected as a variable in the optimization problem and the core layer of this circular element is considered to be silicone rubber. Considering the high number of design variables and also due to binary nature of variables, a linear model is considered for the meta-model as follows:

$$Y = a_0 + a_1 x_1 + a_2 x_2 + \ldots + a_{32} x_{32} = a_0 + \sum_{i=1}^{32} a_i x_i \qquad (4.21)$$

where a_0 to a_{32} are the coefficients that should be identified using the selected design points. The design point have been selected using the D-optimal and random approaches. The D-optimal

method is an algorithm that provides the design points for both continuous and discrete problems. There are different criteria for a D-optimal design such as D-Optimality, A-Optimality and V-Optimality. Among these criteria, D-Optimality is the most common and widely used criterion in which the determinant of the information matrix, $X'X$, is maximized. In the present study the STATGRAPHICS Centurion XVII software has been used to obtain the D-optimal design points. Due to the limitation of the software, the design points for a problem with 16 variables have been determined. These 16 design points are then utilized to obtain the design points for a current problem with 32 design variables as follows:

$$x_{2i-1} = x_{2i} = x_i^{D\_Optimal} \quad \& \quad i = 1 \ to \ 16 \tag{4.22}$$

where $x_i^{D\_Optimal}$ is the design variables obtained using the D-optimality criterion software.

The 200 D-optimal design points generated using the software provide 200 configurations of MR based-sandwich panel with different core-layer topology which can then be used as inputs to determine the desired response outputs (first axisymmetric natural frequency and loss factor in the absence of current and for the applied current of 1.8 Amp) using the developed FE models. Using evaluated natural frequencies and loss factors, the rate of changes in the natural frequencies and loss factors are then evaluated as:

$$r_\omega^j = \left| \frac{(\omega^j)_{I=1.8 \ Amp} - (\omega^j)_{I=0 \ Amp}}{(\omega^j)_{I=0 \ Amp}} \right| \quad \& \quad j = 1 \ to \ 200 \tag{4.23}$$

$$r_\eta^j = \left| \frac{(\eta^j)_{I=1.8\ Amp} - (\eta^j)_{I=0\ Amp}}{(\eta^j)_{I=0\ Amp}} \right| \quad \& \quad j = 1\ to\ 200 \tag{4.24}$$

where r_ω^j and r_η^j are the rate of the changes of the first axisymmetric natural frequency and loss

factor due to the increase of applied current from 0 *Amp* to 1.8 *Amp* obtained using the jth design

point, respectively. These ratios are then assessed as the influence of the applied magnetic field

(MR effect) on the vibration behavior of the structure. The binary design input points and the

simulated outputs (natural frequencies, loss factors and the corresponding rates) are then utilized

to construct the approximate linear response functions as follows:

$$(\omega')_{I=0\ Amp} = a_{\omega_0} + \sum_{i=1}^{32} a_{\omega_i} x_i \tag{4.25}$$

$$(\omega')_{I=1.8\ Amp} = b_{\omega_0} + \sum_{i=1}^{32} b_{\omega_i} x_i \tag{4.26}$$

$$r_\omega' = c_{\omega_0} + \sum_{i=1}^{32} c_{\omega_i} x_i \tag{4.27}$$

$$(\eta')_{I=0\ Amp} = a_{\eta_0} + \sum_{i=1}^{32} a_{\eta_i} x_i \tag{4.28}$$

$$(\eta')_{I=1.8\ Amp} = b_{\eta_0} + \sum_{i=1}^{32} b_{\eta_i} x_i \tag{4.29}$$

$$r_\eta' = c_{\eta_0} + \sum_{i=1}^{32} c_{\eta_i} x_i \qquad (4.30)$$

where a_{ω_i}, b_{ω_i}, c_{ω_i}, a_{η_i}, b_{η_i} and c_{η_i} are the coefficients which are identified using the least square method to minimize the error between the responses obtained using developed approximate meta-models and those obtained using the full FE mode. These coefficients collectively can be expressed in matrix as follows:

$$[A_\omega]_{33\times1} = [X^+]_{33\times200} \times \left[(\Omega)_{I=0\ Amp}\right]_{200\times1} \qquad (4.31)$$

$$[B_\omega]_{33\times1} = [X^+]_{33\times200} \times \left[(\Omega)_{I=1.8\ Amp}\right]_{200\times1} \qquad (4.32)$$

$$[C_\omega]_{33\times1} = [X^+]_{33\times200} \times [R_\omega]_{200\times1} \qquad (4.33)$$

$$\left[A_\eta\right]_{33\times1} = [X^+]_{33\times200} \times \left[(H)_{I=0\ Amp}\right]_{200\times1} \qquad (4.34)$$

$$\left[B_\eta\right]_{33\times1} = [X^+]_{33\times200} \times \left[(H)_{I=1.8\ Amp}\right]_{200\times1} \qquad (4.35)$$

$$\left[C_\eta\right]_{33\times1} = [X^+]_{33\times200} \times \left[R_\eta\right]_{200\times1} \qquad (4.36)$$

where

$$[A_\omega]_{33\times1} = [a_{\omega_0} \quad a_{\omega_1} \quad \cdots \quad a_{\omega_{32}}]^T \qquad (4.37)$$

$$[B_\omega]_{33\times1} = [b_{\omega_0} \quad b_{\omega_1} \quad \cdots \quad b_{\omega_{32}}]^T \qquad (4.38)$$

$$[C_\omega]_{33\times1} = [c_{\omega_0} \quad c_{\omega_1} \quad \cdots \quad c_{\omega_{32}}]^T \qquad (4.39)$$

$$[A_\eta]_{33\times1} = [a_{\eta_0} \quad a_{\eta_1} \quad \cdots \quad a_{\eta_{32}}]^T \tag{4.40}$$

$$[B_\eta]_{33\times1} = [b_{\eta_0} \quad b_{\eta_1} \quad \cdots \quad b_{\eta_{32}}]^T \tag{4.41}$$

$$[C_\eta]_{33\times1} = [c_{\eta_0} \quad c_{\eta_1} \quad \cdots \quad c_{\eta_{32}}]^T \tag{4.42}$$

$$[(\Omega)_{I=0\ Amp}]_{200\times1} = [(\omega^1)_{I=0\ Amp} \quad (\omega^2)_{I=0\ Amp} \quad \cdots \quad (\omega^{200})_{I=0\ Amp}]^T \tag{4.43}$$

$$[(\Omega)_{I=1.8\ Amp}]_{200\times1} = [(\omega^1)_{I=1.8\ Amp} \quad (\omega^2)_{I=1.8\ Amp} \quad \cdots \quad (\omega^{200})_{I=1.8\ Amp}]^T \tag{4.44}$$

$$[R_\omega]_{33\times1} = [r_\omega^1 \quad r_\omega^2 \quad \cdots \quad r_\omega^{200}]^T \tag{4.45}$$

$$[(H)_{I=0\ Amp}]_{200\times1} = [(\eta^1)_{I=0\ Amp} \quad (\eta^2)_{I=0\ Amp} \quad \cdots \quad (\eta^{200})_{I=0\ Amp}]^T \tag{4.46}$$

$$[(H)_{I=1.8\ Amp}]_{200\times1} = [(\eta^1)_{I=1.8\ Amp} \quad (\eta^2)_{I=1.8\ Amp} \quad \cdots \quad (\eta^{200})_{I=1.8\ Amp}]^T \tag{4.47}$$

$$[R_\eta]_{33\times1} = [r_\eta^1 \quad r_\eta^2 \quad \cdots \quad r_\eta^{200}]^T \tag{4.48}$$

$$[X]_{200\times33} = \begin{bmatrix} 1 & x_1^1 & \cdots & x_{32}^1 \\ 1 & x_1^2 & \cdots & x_{32}^2 \\ \vdots & \vdots & \ddots & \vdots \\ 1 & x_1^{200} & \cdots & x_{32}^{200} \end{bmatrix} \tag{4.49}$$

where $[X^+]$ is the pseudo inverse of the $[X]_{200\times33}$ design point matrix.

In addition to the design points obtained using D-optimal method, another method based on the random approach, in which 200 topologies are randomly designed, is utilized to build the approximate meta-model following Eqs. (4.23) to (4.49).

In order to evaluate the correctness of the identified models, 100 random topologies have been selected and the first axisymmetric natural frequencies and loss factors have been calculated using the developed FE model. Then the accuracy of the proposed meta-models is assessed by calculating the coefficient of determination, $\mathcal{R}^2$, in which $\mathcal{R}^2$ varies between zero and 1 with one means excellent accuracy indicating perfect agreement between results generated by FE and meta-models.

The identified coefficients of A_ω, B_ω, C_ω, A_η, B_η and C_η are presented in Appendix C. Table 4.5 shows the coefficient of determination calculated for the first axisymmetric natural frequencies and loss factors. Examination of results reveals that the linear models identified using the D-optimal and random design points are accurate enough for the evaluation of the natural frequency and loss factor corresponding to the first axisymmetric motion of the circular sandwich panel.

Table 4.5. Coefficient of determination for the first three natural frequencies and loss factors.

	$\left(\mathcal{R}^2\right)_{\omega_n}$			$\left(\mathcal{R}^2\right)_{\eta_n}$	
	$D-Optimal$	$Random$		$D-Optimal$	$Random$
$(\omega')_{I=0\ Amp}$	0.9957	0.9951	$(\eta')_{I=0\ Amp}$	0.9618	0.9831
$(\omega')_{I=1.8\ Amp}$	0.9927	0.9931	$(\eta')_{I=1.8\ Amp}$	0.9621	0.9767
r'_ω	0.9904	0.9940	r'_η	0.8167	0.9345

4.5.3. Optimization Formulation

The topology optimization problem is defined to determine the optimized treatment of the core layer in such a way that the effect of magnetic field on the vibrational and acoustical behavior of the structure is maximized. Considering that changing the treatment of the core layer affects the

stiffness and damping of the sandwich structure, the natural frequencies and the relevant loss factors are selected as the desired indices addressing the vibrational and acoustical behavior. Then, the rate of changes in these factors due to the change in the applied magnetic field are considered to represent the influence of applied magnetic field on the structural and acoustical behavior of the panel. Therefore two optimization problems are formally formulated as follows:

$$\begin{cases} maximize \quad r_\omega(\bar{X}) = \left| \dfrac{(\omega)_{I=1.8\ Amp} - (\omega)_{I=0\ Amp}}{(\omega)_{I=0\ Amp}} \right| \\ subject\ to \quad \bar{x}_i\ is\ 0\ or\ 1 \end{cases} \tag{4.50}$$

$$\begin{cases} maximize \quad r_\eta(\bar{X}) = \left| \dfrac{(\eta)_{I=1.8\ Amp} - (\eta)_{I=0\ Amp}}{(\eta)_{I=0\ Amp}} \right| \\ subject\ to \quad \bar{x}_i\ is\ 0\ or\ 1 \end{cases} \tag{4.51}$$

where

$$\bar{X} = [\bar{x}_1 \quad \bar{x}_2 \quad ... \quad \bar{x}_{32}]^T \tag{4.52}$$

As it can be seen, Eq. (4.50) shows the topology optimization problem which maximizes the changes in the first axisymmetric natural frequency of the panel while Eq. (4.51) maximizes the changes in the corresponding loss factor. $\bar{X}$ is the design vector composed of the 32 binary elements determining which segments of the core layer should be filled with MR fluid or silicone rubber. The topology optimization problems formulated in Eqs. (4.50) and (4.51) have not any constraints on the numbers of the MR fluid or silicone rubber segments in the core layer and it is left to optimizer to determine the optimal number as well as the location of the MR fluid and silicone rubber segments.

The optimization problem is linear if the rate of changes of the natural frequencies and loss factors (r_ω' and r_η') presented in Eqs. (4.27) and (4.30) are utilized as the objective functions. In the present study, the integer programing algorithm (IP) is employed to solve the following linear topology optimization problems:

$$IP_1: \begin{cases} maximize \quad r_\omega'(\bar{X}) \\ subject\ to \quad \bar{x}_i\ is\ 0\ or\ 1 \end{cases} \tag{4.53}$$

$$IP_2: \begin{cases} maximize \quad r_\eta'(\bar{X}) \\ subject\ to \quad \bar{x}_i\ is\ 0\ or\ 1 \end{cases} \tag{4.54}$$

The problem becomes nonlinear if the models presented in Eqs. (4.25), (4.26), (4.28) and (4.29) for natural frequencies and loss factors are individually used. These nonlinear optimization problems are then formulated as:

$$GA_1: \begin{cases} maximize \quad \left| \dfrac{(\omega_n')_{I=1.8\ Amp} - (\omega_n')_{I=0\ Amp}}{(\omega_n')_{I=0\ Amp}} \right| \\ subject\ to \quad \bar{x}_i\ is\ 0\ or\ 1 \end{cases} \tag{4.55}$$

$$GA_2: \begin{cases} maximize \quad \left| \dfrac{(\eta_n')_{I=1.8\ Amp} - (\eta_n')_{I=0\ Amp}}{(\eta_n')_{I=0\ Amp}} \right| \\ subject\ to \quad \bar{x}_i\ is\ 0\ or\ 1 \end{cases} \tag{4.56}$$

which have been solved using the genetic algorithm (GA).

Figure 4.9 shows the results obtained solving the topology optimization problems using IP and GA for the meta-models identified using the D-optimal and random design points. As it can

be seen, the GA evaluated the sandwich panel fully treated with MR fluid as the panel with maximum MR effect. The IP suggested the fully treated panel as well except for one of the cases in which there is a segment that IP recommends to be filled with silicone rubber. In order to confirm the optimum solution, the rate of change in the first axisymmetric natural frequency and loss factor of the panels suggested in Figure 4.9 have been calculated using the full FE model and the results are presented in Table 4.6. As it can be realized, the maximum rate of changes for both the natural frequency and loss factor is associated with the clamped sandwich panel fully treated with MR core layer. The reason for the difference between the optimized topology identified by the GA and the one suggested by IP can be interpret to the inherent approximation in linear optimization problems in Eq. (4.53) and (4.54) and possibly premature termination of the IP algorithm.
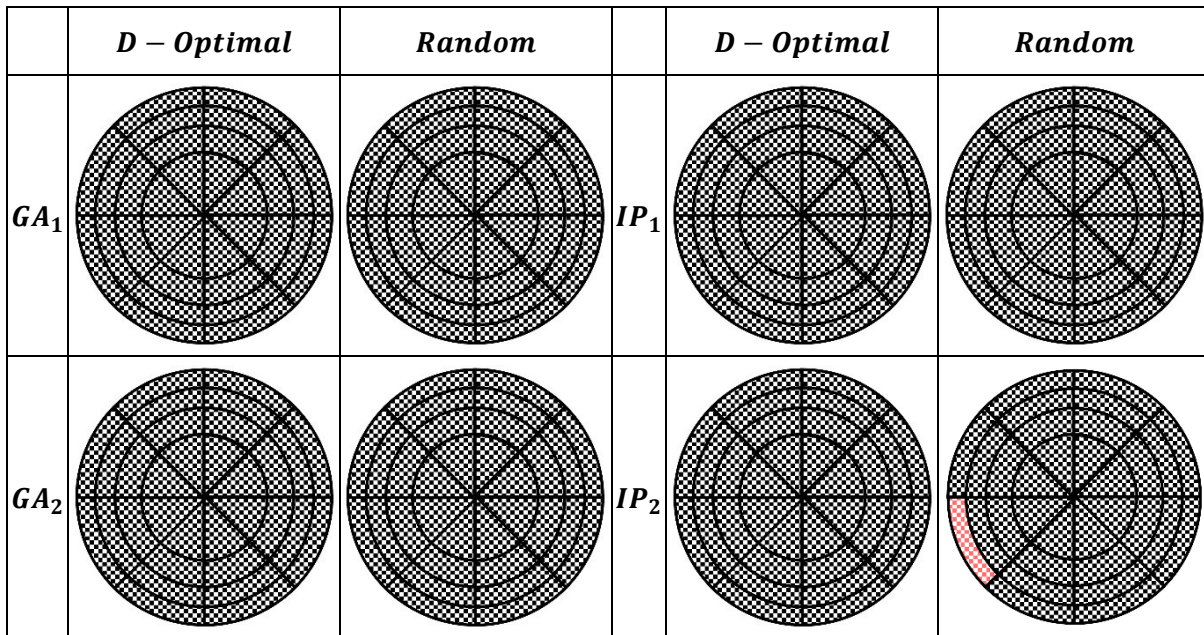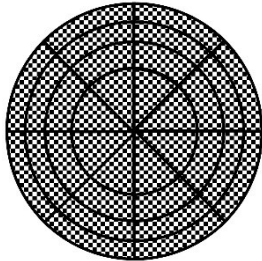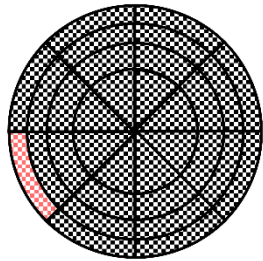
Figure 4.9. The results of topology optimization based on the first axisymmetric natural frequency and loss factor without any constraint; MR fluid: ▨, silicone rubber: ▨.

96

Table 4.6. The rate of changes in the first axisymmetric natural frequency and loss factor due to change in applied magnetic field for optimized topologies; MR fluid: ⊠, silicone rubber: ⊠.

r_ω	0.3060	0.3040
r_η	3.9295	3.8086

In order to investigate which part of the core layer mostly affects the MR effect, the topology optimization problem is also solved in the presence of the constraint in which the total volume of the MR fluid and silicone rubber segments should be equal. Therefore, the optimal solution should provide arrangement of MR fluid and silicone rubber segments that have maximum influence on the stiffness and damping of the structure as the magnetic field changes. Considering that the segmentation has been done in such a way that the area of all the 32 segments is equal, the equal volume constraint for MR fluid and rubber means that half of the segments should be filled with MR fluid and the other half with silicone rubber. Then the topology optimization problem may be formulated as:

$$\begin{cases} maximize \quad r_\omega(\bar{X}) = \left| \dfrac{(\omega)_{I=1.8\ Amp} - (\omega)_{I=0\ Amp}}{(\omega)_{I=0\ Amp}} \right| \\[4mm] subject\ to \quad \bar{x}_i\ is\ 0\ or\ 1 \\[4mm] \qquad\qquad \displaystyle\sum_{i=1}^{32} \bar{x}_i = 16 \end{cases} \tag{4.57}$$

$$\begin{cases} maximize \quad r_\eta(\bar{X}) = \left| \dfrac{(\eta)_{I=1.8\ Amp} - (\eta)_{I=0\ Amp}}{(\eta)_{I=0\ Amp}} \right| \\[4mm] subject\ to \quad \bar{x}_i\ is\ 0\ or\ 1 \\[4mm] \qquad\qquad \displaystyle\sum_{i=1}^{32} \bar{x}_i = 16 \end{cases} \tag{4.58}$$

Figure 4.10 shows the optimal topology candidates obtained using GA and IP algorithms for the constrained optimization problems. In order to find the true optimized topology configuration among these candidates, the rate of change of the first axisymmetric natural frequency and the corresponding loss factor are evaluated using the developed FE model. The results are presented in Table 4.7. Examining candidates 5 to 8, it can be realized that in all, the circular portion at the center of the core layer is mainly covered by the silicone rubber. Considering this, candidate 9 is also introduced in which the center circle of core layer is completely filled with silicone rubber and MR fluid is concentrated in the two middle annular portions. Further examination of potential optimum topology candidates in Table 4.7 reveals that the optimal topology for the maximum rate of changes in natural frequency is candidate 2 in which the MR fluid concentrated at the center of the core layer and the silicone rubber is located around the MR section near the clamped edge. The reason for this may be attributed to the fact that the MR fluid has the maximum influence in the

98

area that it is under maximum shear deformation. Considering the first axisymmetric motion of the clamped circular panel, the maximum shear deformation occurs in the first two annular sections of the core layer. Thus, locating MR fluid in these sections of the core layer maximizes the rate of change of the first axisymmetric natural frequency. With respect to the loss factor, it is clear that the maximum rate is attributed to the candidate 9. As it was mentioned before, increasing the stiffness causes the loss factor to decrease and consequently the higher rate of change in stiffness for candidate 2 causes the loss factor to reduce.

|	$D - Optimal$	$Random$		$D - Optimal$	$Random$
GA_1	Candidate 1	Candidate 2	IP_1	Candidate 3	Candidate 4
GA_2	Candidate 5	Candidate 6	IP_2	Candidate 7	Candidate 8
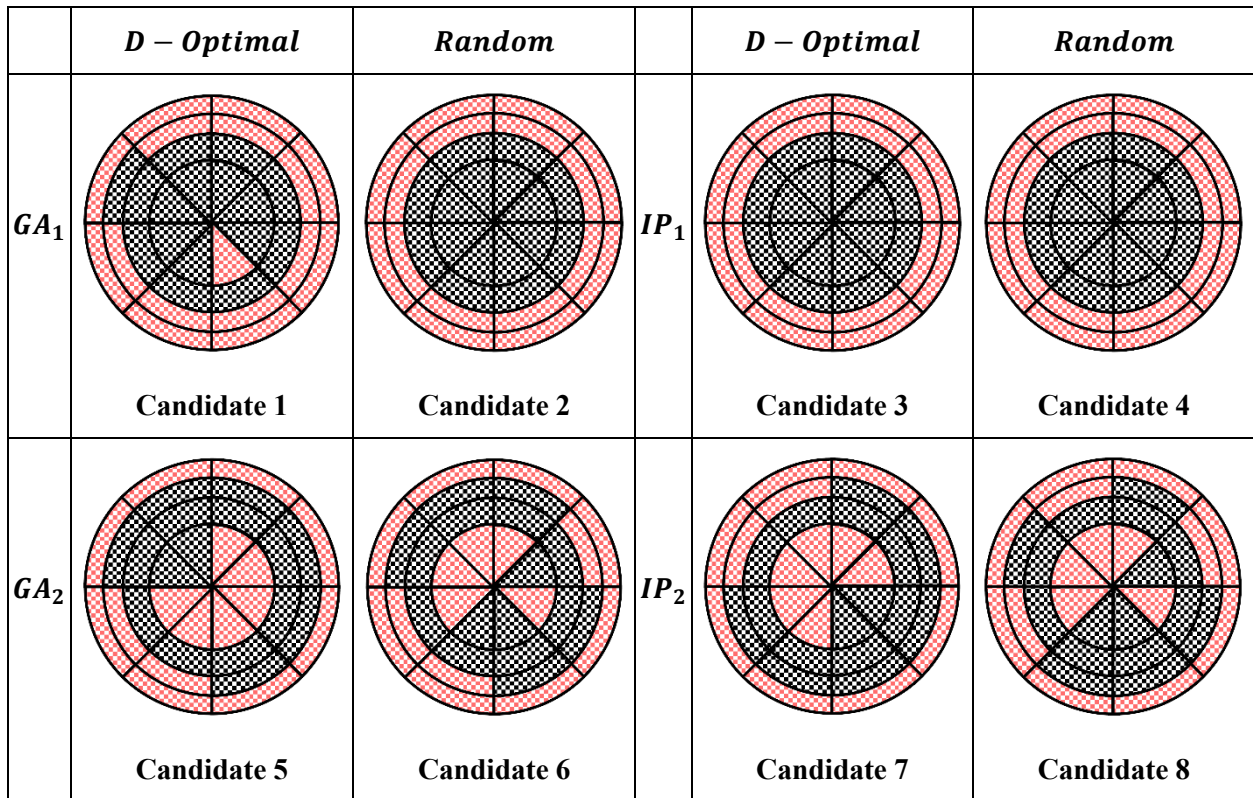
Figure 4.10. The results of topology optimization based on the first axisymmetric natural frequency and loss factor in presence of constraint; MR fluid: ▓, silicone rubber: ▓.

Table 4.7. The rate of changes in the first axisymmetric natural frequency and loss factor due to change in applied magnetic field for optimized topologies with constraint; MR fluid: ▨, silicone rubber: ▨.
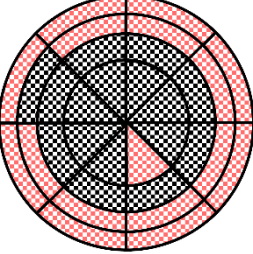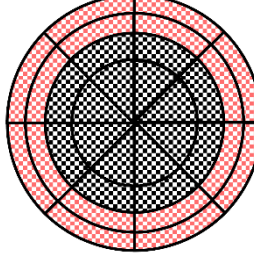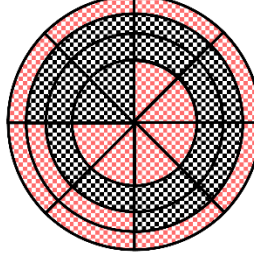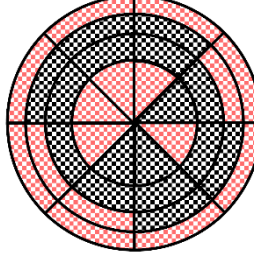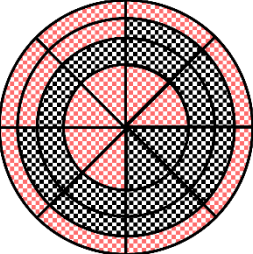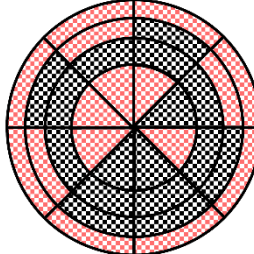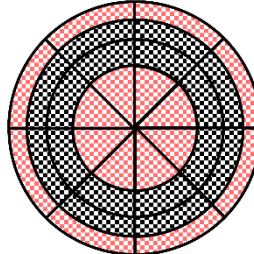
	Candidate 1	Candidate 2, 3 and 4	Candidate 5	Candidate 6
r_ω	0.1975	0.2004	0.1921	0.1906
r_η	1.0776	1.1397	1.0443	1.0079
	Candidate 7	Candidate 8	Candidate 9	
r_ω	0.1937	0.1920	0.1955	
r_η	1.0597	1.0092	1.1422	

Figure 4.11 shows the STL of the optimized topologies obtained for both constrained and unconstrained problems which are the fully treated MR panel, candidate 2 and candidate 9, respectively. The values of the frequencies (Hz) and STLs (dB) at the natural frequencies are presented in the figure as coordinates, X and Y respectively. It can be seen that the panel fully treated with MR fluid core layer has the minimum natural frequency which can be related to higher density of the MR fluid compared with the silicone rubber that causes the first axisymmetric

natural frequency to decrease. Moreover, regardless of some difference near the natural frequencies, the STL of the fully treated panel and candidate 2 are very close to each other at different applied currents. This in addition to the less amount of required MR fluid, make candidate 2 an attractive configuration for noise control applications compared with expensive and heavier fully treated panel. Also partial treatment of the core layer using the topology presented as candidate 2, causes the mass of the structure to reduce about 30 percent compared with that of the fully treated panel.
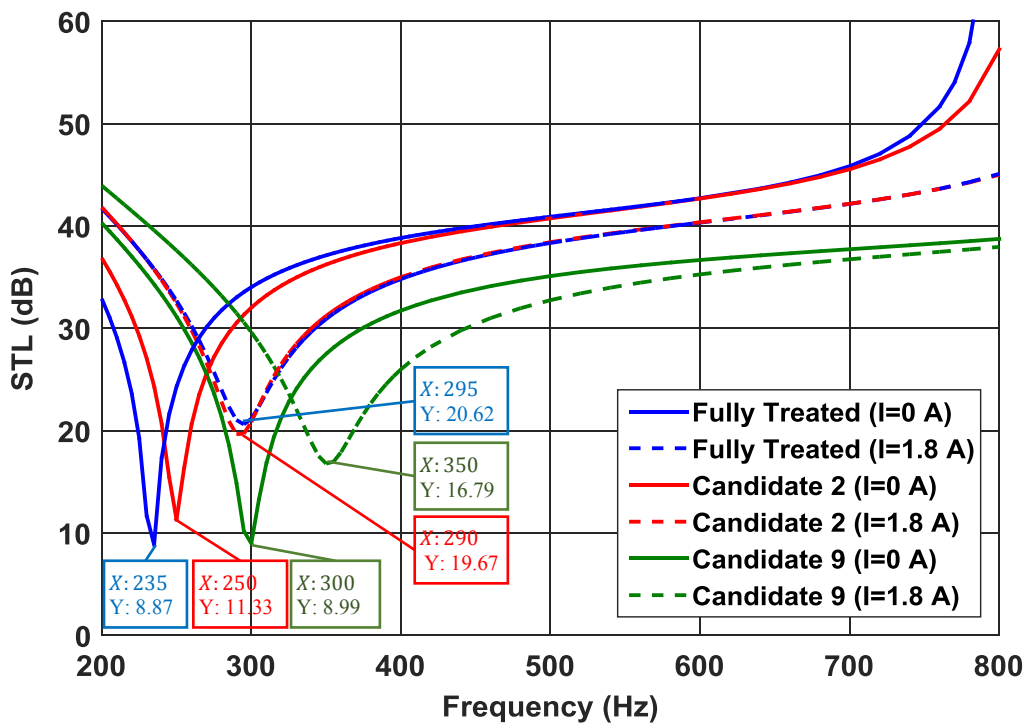
Figure 4.11. STL of the optimized panels based on first axisymmetric natural frequency and loss factor with $0.4\ mm$ aluminum face sheets and $1.35\ mm$ core layer.

Comparing the STL and the rate of changes in the natural frequency of candidates 2 and 9, it can be seen that the rate of change of natural frequency is higher for candidate 9 and the STL is

higher for candidate 2 in almost all the frequency range. Considering that the STL is the main objective, it is reasonable to select candidate 2 as the optimized topology. It is noted that slight difference between the rates of the changes in the natural frequencies mentioned in this figure compared with those provided before is mainly due to the effect of the damping considered in force vibration responses and thus in evaluation of the STL, while it is neglected in the calculation of the natural frequencies using the free vibration equations of motions.

4.6. Conclusions

The topology optimization of a clamped circular sandwich panel with elastic face sheets and partially treated with MR fluid and silicone rubber has been investigated in this chapter. A high fidelity FE model has been developed using circular and 4-node quadrilateral elements to derive the free and forced governing equations of motion in order to evaluate the natural frequencies, loss factors and the STL of the MR-based sandwich panel. The FE model was validated comparing the STL and natural frequencies of the fully treated MR sandwich panel with the experimental and numerical results from the previous chapters. The effect of the location of the MR fluid and silicone rubber in the core layer on the first axisymmetric natural frequency, loss factor and the STL of the panel in absence of magnetic field were then investigated. It was shown that the stiffness and damping of the structure change considerably as the position of the MR fluid and silicone rubber changes in the core layer. To overcome the high computational costs associated with executing the full FE model on many possible combinations, approximate response functions have been proposed using meta-model technique. Linear response functions were proposed for the first

axisymmetric natural frequencies and loss factors under 0 *Amp* and 1.8 *Amp* current input and also their rate of changes due to the applied magnetic field. The D-optimal and random approaches have been utilized to identify the sample design points in the design space. Topology optimization problems, without any constraint and then with a constraint in which the volume of total MR fluid and silicone rubber segments are equal, have been finally investigated. Two linear and nonlinear topology optimization problems have been formulated for each unconstrained and constrained optimization problems and then solved using IP and GA algorithms, respectively. The identified potential candidates for the constrained and unconstrained problems were then evaluated using the developed FE model to select the true optimal topology configuration for the core layer. Finally, the STL of the three eventuated topologies is compared with each other. It was concluded that the optimal topology is the one in which the half central part of the core layer is filled with MR fluid and the other half located near the clamped edge is filled with silicone rubber.

CHAPTER 5

CONTRIBUTIONS, CONCLUSIONS AND RECOMMENDATIONS FOR FUTURE WORK

5.1. Contributions

While there are a number of studies on vibration analysis of MR-based sandwich panels, very limited investigations have been conducted on their vibro-acoustic behavior. The present research has significantly contributed to better understanding of the vibro-acoustic behavior and sound absorption capability of MR sandwich panels. Development of new finite element models and experimental set up to evaluate vibration (natural frequencies and loss factors) and sound (STL) characteristics of MR-based sandwich panels as well as optimization strategies to identify the optimal topology for sandwich panels with partially treated MR fluid configurations are among important contributions in the present research thesis

Circular sandwich panels with aluminum face sheets and clamped boundary condition have been fabricated to experimentally evaluate the effect of the applied magnetic field and thickness of the core layer on the first axisymmetric natural frequency and the STL of the panel using an in-house fabricated anechoic chamber with built-in electromagnet. Also accurate numerical models have been developed to predict sandwich panel's natural frequency and STL for both fully and partially treated MR fluid core layer. Due to high computational cost associated with developed

FE models, approximate response functions (meta-models) have been developed and then utilized in the developed optimization formulations to efficiently identify the optimal topology configurations for different optimization problems.

The research study has resulted to three journal papers, two of which already accepted in well-known journals in the field (Journal of Sound and Vibration and Smart Materials and Structures). The third article is under final review after submitting the revised version. Moreover, the results of the research have been presented in a number of conferences dedicated to the field of smart materials and structures such as the ASME Conference on Smart Materials, Adaptive Structures and Intelligent Systems (SMASIS), SPIE Smart Structures and Materials + Nondestructive Evaluation and Health Monitoring and ECOMAS Thematic Conference on Smart Structures and Materials.

In summary, the development of the Ritz and FE models combined with the experimental studies concluded to one conference paper and two journal papers as follows:

- Hemmatian, M., and Sedaghati, R., "Sound Transmission Loss of Adaptive Sandwich Panels Treated With MR Fluid Core Layer," *Proc. ASME 2016 Conference on Smart Materials, Adaptive Structures and Intelligent Systems, American Society of Mechanical Engineers*, p. V002T03A005.

- Hemmatian, M., and Sedaghati, R., 2017, "Effect of applied magnetic field on sound transmission loss of MR-based sandwich panels," *Smart Materials and Structures*, 26(2), p. 025006.

- Hemmatian, M., and Sedaghati, R., 2017, "Sound transmission analysis of MR fluid based-circular sandwich panels: Experimental and finite element analysis," *Journal of Sound and Vibration*, 408, pp. 43-59.

Moreover, the circular-annular FE model was utilized to investigate the effect of the applied magnetic field on the natural frequency and STL of a sandwich panel partially treated with MR fluid core layer and results were presented in the following conference:

- Hemmatian, M., and Sedaghati, R., "Sound transmission analysis of partially treated MR fluid based-sandwich panels using finite element method," *Proc. SPIE 10164, Active and Passive Smart Structures and Integrated Systems 2017, International Society for Optics and Photonics*, 101642F.

Circular-4-node quadrilateral FE model was developed to investigate the topology optimization of partially treated MR sandwci panel. The investigation on the STL of partially treated MR sandwich panel and the topology optimization concluded to the following conference and journal papers:

- Hemmatian, M., and Sedaghati, R., "Sound transmission loss of sandwich panels partially treated with MR fluid and viscoelastic core layer," *VIII ECOMAS Thematic Conference on Smart Structures and Materials, SMART 2017*, Madrid, Spain.

- Hemmatian, M., and Sedaghati, R., 2017, "Vibro-acoustic topology optimization of sandwich panels partially treated with MR fluid and silicone rubber core layer," *Smart Materials and Structures* (under final review).

106

5.2. Conclusions

The major conclusions that have been achieved from this research dissertation are as follows:

1. As the frequency of the incident sound matches with the axisymmetric natural frequency of the circular sandwich panel, the sandwich panel resonates and consequently the STL significantly decreases. Due to the symmetry of the panel, the STL is not affected by the frequencies corresponding to the non-axisymmetric mode shapes.

2. The stiffness of the MR sandwich panel increases as the applied magnetic field enhances. Considering that the areal density is constant and it is not affected by the magnetic field, the first axisymmetric natural frequency of the panel increases by increasing the applied magnetic field. Thus, the pick and notch in the frequency response and the STL of the panel shift to higher frequencies, respectively.

3. Increasing the applied magnetic field causes the damping of the MR sandwich panel to increase. Therefore the STL at the resonance frequency increases as the applied magnetic field increases.

4. Increasing the applied magnetic field causes the STL to increase and decrease for the frequencies below and above the fundamental natural frequency, respectively. This shows the necessity of designing a semi-active controller to determine the proper applied magnetic field that maximizes the STL in a wide frequency range.

5. The applied magnetic field at middle of a short solenoid is a function of both the radius and the input current to the electromagnet. The magnetic flux density linearly and quadratically changes with respect to the input current and radius, respectively.

6. Increasing the thickness of the core layer causes the stiffness and damping of the sandwich structure to decrease and increase, respectively. Accordingly, the first axisymmetric natural frequency and the STL at the resonance frequency quadratically decreases and increases, respectively. Moreover, increasing the thickness of the core layer enhances the influence of the applied magnetic field on the natural frequency and STL of the MR panel. As the thickness increase, the rate of changes of the natural frequency with respect to the input current to the electromagnet increases.

7. The stiffness of the sandwich panel can be increased by increasing the thickness of the elastic face sheets. The natural frequency of the panel increases almost in proportion to the thickness of the face sheets.

8. The position of the MR fluid in the core layer of the partially treated sandwich panel considerably affects the stiffness and damping of the structure. Locating the MR fluid at the regions with maximum shear deformation increases the influence of the applied magnetic field on the acoustical and vibrational behavior of the structure.

9. Radial distribution of the MR fluid and silicone rubber in the core layer of the partially treated panel has not a significant effect on the STL and also the rate of changes of the first axisymmetric natural frequency and loss factor.

10. The influence of the applied magnetic field on the rate of change of the natural frequency and loss factor of the sandwich panel increases as the treatment of the MR fluid in the core increases. The maximum STL and rate of changes are achieved for the panel in which the core layer is fully treated with MR fluid.

11. For the panel in which the volume of the MR fluid and silicone rubber were considered to be equal, treating the mid-center of the core layer with MR fluid and the other half near the clamped edge with silicone rubber maximizes the STL and the rate of change of the first axisymmetric natural frequency.

5.3. Recommendation for the Future Works

In this dissertation, STL of circular sandwich panels fully and partially treated with MR fluid core layer was investigated. Although the developed theoretical and experimental research work have significantly advanced the state-of-the-art in the field of acoustical behavior of sandwich structures, nevertheless, the following interesting aspects which are natural extension of the current work have been identified:

1. Semi-active control strategies based on various control techniques such as the optimal, fuzzy and robust controllers can be designed and implemented. Accomplishing a closed-loop control system provide the opportunity to determine the appropriate magnetic field based on the feedback signal to reduce the radiated sound from the structure in a wide frequency range for different incident sounds.

2. The STL of circular sandwich panels fully and partially treated with MR fluid core layer can be investigated at high frequencies. The effect of magnetic field on the symmetric and asymmetric coincident frequencies can be theoretically and experimentally studied and be utilized to maximize the STL in high frequency region using semi-active controllers.

3. The developed FE model can be extended to investigate the STL of MR sandwich structures with more complicated geometries which are closer to the application. In this subject,

acoustical behavior of the curved MR sandwich panels including convex and concave circular panels, cylindrical cabins comprising MR sandwich walls and spherical MR sandwich shells can be studied.

4. Providing the required magnetic field is one of the obstacles in the usage of MR sandwich structures. Design optimization can be conducted to design the MR sandwich panel along with the magnetic flux supplier such a way that reduces the mass of the system and maximizes it applicability.

REFERENCES

[1]   "Simoni   Systems: Acoustics,"   [Online],   Available: https://www.simonisystems.com/acoustics.htm (Accessed: 21 August 2017).

[2]   "Acoustic   Glossary: Sound   pressure,"   [Online],   Available: http://www.acoustic-glossary.co.uk/sound-pressure.htm (Accessed: 21 August 2017).

[3] Galgalikar, R., 2012, "Design Automation and Optimization of Honeycomb Structures for Maximum Sound Transmission Loss," Msc Thesis, Clemson University.

[4] Wang, T., 2006, Predictions of the sound transmission loss of composite sandwich panels.

[5] Wang, T., Li, S., Rajaram, S., and Nutt, S. R., 2010, "Predicting the sound transmission loss of sandwich panels by statistical energy analysis approach," Journal of Vibration and Acoustics, 132(1), p. 011004.

[6] Spaggiari, A., 2013, "Properties and applications of Magnetorheological fluids," Frattura ed Integrità Strutturale(23), p. 48.

[7] Mohammadi, N., Mahjoob, M., Kaffashi, B., and Malakooti, S., 2010, "An experimental evaluation of pre-yield and post-yield rheological models of magnetic field dependent smart materials," Journal of mechanical science and technology, 24(9), pp. 1829-1837.

[8] Ford, R., Lord, P., and Walker, A., 1967, "Sound transmission through sandwich constructions," Journal of Sound and Vibration, 5(1), pp. 9-21.

[9] Narayanan, S., and Shanbhag, R., 1981, "Sound transmission through elastically supported sandwich panels into a rectangular enclosure," Journal of Sound and Vibration, 77(2), pp. 251-270.

[10] Narayanan, S., and Shanbhag, R., 1982, "Sound transmission through a damped sandwich panel," Journal of Sound and Vibration, 80(3), pp. 315-327.

[11] Grosveld, F. W., and Mixson, J. S., 1985, "Noise Transmission through an Acoustically Treated and Honeycomb-Stiffened Aircraft Sidewall," Journal of Aircraft, 22(5), pp. 434-440.

[12] Nilsson, A. C., 1990, "Wave propagation in and sound transmission through sandwich plates," Journal of Sound and Vibration, 138(1), pp. 73-94.

[13] Brouard, B., Lafarge, D., and Allard, J.-F., 1995, "A general method of modelling sound propagation in layered media," Journal of Sound and Vibration, 183(1), pp. 129-142.

[14] Tang, Y. Y., Robinson, J. H., and Silcox, R. J., "Sound transmission through a cylindrical sandwich shell with honeycomb core," Proc. 34th AIAA aerospace science meeting and exhibit, pp. 877-886.

[15] Tang, Y. Y., Silcox, R. J., and Robinson, J. H., 1996, "Sound transmission through two concentric cylindrical sandwich shells."

[16] Veeramani, S., and Wereley, N. M., 1996, "Hybrid passive/active damping for robust multivariable acoustic control in composite plates," Proceeding SPIESymp Smart Materials and Structures, pp. 374-387.

[17] Wen-chao, H., and Chung-fai, N., 1998, "Sound insulation improvement using honeycomb sandwich panels," Applied Acoustics, 53(1), pp. 163-177.

[18] Lee, C., and Kondo, K., "Noise transmission loss of sandwich plates with viscoelastic core," Proc. 40th Structures, Structural Dynamics, and Materials Conference and Exhibit, American Institute of Aeronautics and Astronautics, p. 1458.

[19] Thamburaj, P., and Sun, J., 1999, "Effect of material anisotropy on the sound and vibration transmission loss of sandwich aircraft structures," Journal of Sandwich Structures and Materials, 1(1), pp. 76-92.

[20] Thamburaj, P., and Sun, J., 2002, "Optimization of anisotropic sandwich beams for higher sound transmission loss," Journal of Sound and Vibration, 254(1), pp. 23-36.

[21] Klos, J., Robinson, J. H., and Buehrle, R. D., "Sound transmission through a curved honeycomb composite panel," Proc. 9th AIAA/CEAS Aeroacoustics Conference and Exhibit.

[22] Denli, H., and Sun, J., 2007, "Structural-acoustic optimization of sandwich structures with cellular cores for minimum sound radiation," Journal of Sound and Vibration, 301(1), pp. 93-105.

[23] Assaf, S., and Guerich, M., 2008, "Numerical prediction of noise transmission loss through viscoelastically damped sandwich plates," Journal of Sandwich Structures and Materials, 10(5), pp. 359-384.

[24] Wang, T., Li, S., and Nutt, S. R., 2009, "Optimal design of acoustical sandwich panels with a genetic algorithm," Applied Acoustics, 70(3), pp. 416-425.

[25] Zhou, R., and Crocker, M. J., 2010, "Sound transmission loss of foam-filled honeycomb sandwich panels using statistical energy analysis and theoretical and measured dynamic properties," Journal of Sound and Vibration, 329(6), pp. 673-686.

[26] Abid, M., Abbes, M., Chazot, J., Hammemi, L., Hamdi, M., and Haddar, M., 2012, "Acoustic response of a multilayer panel with viscoelastic material," International Journal of Acoustics and Vibration, 17(2), p. 82.

[27] Guerich, M., and Assaf, S., 2013, "Optimization of Noise Transmission Through Sandwich Structures," Journal of Vibration and Acoustics, 135(5), p. 051010.

[28] Kim, Y.-J., and Han, J.-H., 2013, "Identification of Acoustic Characteristics of Honeycomb Sandwich Composite Panels Using Hybrid Analytical/Finite Element Method," Journal of Vibration and Acoustics, 135(1), p. 011006.

[29] Choi, S.-B., Park, Y.-K., and Kim, J.-D., 1993, "Vibration characteristics of hollow cantilevered beams containing an electro-rheological fluid," International journal of mechanical sciences, 35(9), pp. 757-768.

[30] Don, D. L., and Coulter, J. P., 1995, "An analytical and experimental investigation of electrorheological material based adaptive beam structures," Journal of intelligent material systems and structures, 6(6), pp. 846-853.

[31] Berg, C., Evans, L., and Kermode, P., 1996, "Composite structure analysis of a hollow cantilever beam filled with electro-rheological fluid," Journal of intelligent material systems and structures, 7(5), pp. 494-502.

[32] Haiqing, G., and King, L. M., 1997, "Vibration characteristics of sandwich beams partially and fully treated with electro-rheological fluid," Journal of intelligent material systems and structures, 8(5), pp. 401-413.

[33] Yeh, J.-Y., Chen, L.-W., and Wang, C.-C., 2004, "Dynamic stability of a sandwich beam with a constrained layer and electrorheological fluid core," Composite Structures, 64(1), pp. 47-54.

[34] Yeh, Z.-F., and Shih, Y.-S., 2005, "Critical load, dynamic characteristics and parametric instability of electrorheological material-based adaptive beams," Computers & structures, 83(25), pp. 2162-2174.

[35] Vaičaitis, R., Liu, S., and Jotautienė, E., 2016, "Nonlinear random vibrations of a sandwich beam adaptive to electrorheological materials," Mechanics, 71(3), pp. 38-44.

[36] Allahverdizadeh, A., Mahjoob, M. J., Nasrollahzadeh, N., and Eshraghi, I., 2013, "Optimal parameters estimation and vibration control of a viscoelastic adaptive sandwich beam incorporating an electrorheological fluid layer," Journal of Vibration and Control, p. 1077546313483159.

[37] Allahverdizadeh, A., Mahjoob, M., Maleki, M., Nasrollahzadeh, N., and Naei, M., 2013, "Structural modeling, vibration analysis and optimal viscoelastic layer characterization of adaptive sandwich beams with electrorheological fluid core," Mechanics Research Communications, 51, pp. 15-22.

[38] Rezaeepazhand, J., and Pahlavan, L., 2009, "Transient response of sandwich beams with electrorheological core," Journal of Intelligent Material Systems and Structures, 20(2), pp. 171-179.

[39] Rahiminasab, J., and Rezaeepazhand, J., 2013, "Aeroelastic stability of smart sandwich plates with electrorheological fluid core and orthotropic faces," Journal of Intelligent Material Systems and Structures, 24(5), pp. 669-677.

[40] Yeh, J.-Y., and Chen, L.-W., 2004, "Vibration of a sandwich plate with a constrained layer and electrorheological fluid core," Composite structures, 65(2), pp. 251-258.

[41] Yeh, J.-Y., and Chen, L.-W., 2007, "Finite element dynamic analysis of orthotropic sandwich plates with an electrorheological fluid core layer," Composite structures, 78(3), pp. 368-376.

[42] Yeh, J.-Y., 2007, "Vibration control of a sandwich annular plate with an electrorheological fluid core layer," Smart Materials and structures, 16(3), p. 837.

[43] Yeh, J.-Y., 2010, "Vibration and damping characteristics analysis of a rotating annular plate with electrorheological treatment," Smart Materials and Structures, 19(8), p. 085010.

[44] Yeh, J.-Y., 2011, "Free vibration analysis of rotating polar orthotropic annular plate with ER damping treatment," Composites Part B: Engineering, 42(4), pp. 781-788.

[45] Hasheminejad, S. M., and Maleki, M., 2009, "Free vibration and forced harmonic response of an electrorheological fluid-filled sandwich plate," Smart Materials and Structures, 18(5), p. 055013.

[46] Lu, H., and Meng, G., 2006, "An experimental and analytical investigation of the dynamic characteristics of a flexible sandwich plate filled with electrorheological fluid," The International Journal of Advanced Manufacturing Technology, 28(11-12), pp. 1049-1055.

[47] Soleymani, M. M., Hajabasi, M. A., and Elahi Mahani, S., 2015, "Free vibrations analysis of a sandwich rectangular plate with electrorheological fluid core," Journal of Computational & Applied Research in Mechanical Engineering (JCARME), 5(1), pp. 71-81.

[48] Farough, M., and Ramin, S., 2012, "Nonlinear free vibration analysis of sandwich shell structures with a constrained electrorheological fluid layer," Smart Materials and Structures, 21(7), p. 075035.

[49] Mohammadi, F., and Sedaghati, R., 2012, "Vibration analysis and design optimization of sandwich cylindrical panels fully and partially treated with electrorheological fluid materials," Journal of Intelligent Material Systems and Structures, 23(15), pp. 1679-1697.

[50] Mohammadi, F., and Sedaghati, R., "Free Vibration Analysis of Electrorheological Fluid Sandwich Shell Structures Subjected to Large Deformation," Proc. ASME 2013 Conference on Smart Materials, Adaptive Structures and Intelligent Systems, American Society of Mechanical Engineers, pp. V001T003A005-V001T003A005.

[51] Hasheminejad, S. M., and Motaaleghi, M. A., 2014, "Supersonic flutter control of an electrorheological fluid-based smart circular cylindrical shell," International Journal of Structural Stability and Dynamics, 14(02), p. 1350064.

[52] Hasheminejad, S. M., and Motaaleghi, M. A., 2015, "Aeroelastic analysis and active flutter suppression of an electro-rheological sandwich cylindrical panel under yawed supersonic flow," Aerospace Science and Technology, 42, pp. 118-127.

[53] Chen, L., and Hansen, C. H., 2005, "Active vibration control of a magnetorheological sandwich beam," Proc. Acoustics 2005 (Busselton Western Australia), pp. 93-98.

[54] Harland, N. R., Mace, B. R., and Jones, R. W., 2001, "Adaptive-passive control of vibration transmission in beams using electro/magnetorheological fluid filled inserts," IEEE Transactions on Control Systems Technology, 9(2), pp. 209-220.

[55] Yeh, Z.-F., and Shih, Y.-S., 2006, "Dynamic characteristics and dynamic instability of magnetorheological material-based adaptive beams," Journal of Composite Materials, 40(15), pp. 1333-1359.

[56] Lara-Prieto, V., Parkin, R., Jackson, M., Silberschmidt, V., and Zbigniew, K., 2010, "Vibration characteristics of MR cantilever sandwich beams: experimental study," Smart Materials and structures, 19(1), p. 015005.

[57] Bishay, P. L., Tawfik, M., and Negm, H. M., "Experimental and finite element models of an adaptive magnetorheological sandwich beam," Proc. Proceedings of the 17th international congress on sound & vibration.

[58] Rajamohan, V., Sedaghati, R., and Rakheja, S., 2010, "Vibration analysis of a multi-layer beam containing magnetorheological fluid," Smart Materials and Structures, 19(1), p. 015013.

[59] Rajamohan, V., Rakheja, S., and Sedaghati, R., 2010, "Vibration analysis of a partially treated multi-layer beam with magnetorheological fluid," Journal of Sound and Vibration, 329(17), pp. 3451-3469.

[60] Rajamohan, V., Sedaghati, R., and Rakheja, S., 2011, "Optimal vibration control of beams with total and partial MR-fluid treatments," Smart materials and structures, 20(11), p. 115016.

[61] Hu, G., Guo, M., Li, W., Du, H., and Alici, G., 2011, "Experimental investigation of the vibration characteristics of a magnetorheological elastomer sandwich beam under non-homogeneous small magnetic fields," Smart materials and structures, 20(12), p. 127001.

[62] Dyniewicz, B., Bajkowski, J. M., and Bajer, C. I., 2015, "Semi-active control of a sandwich beam partially filled with magnetorheological elastomer," Mechanical Systems and Signal Processing, 60, pp. 695-705.

[63] Eshaghi, M., Rakheja, S., and Sedaghati, R., 2015, "An accurate technique for pre-yield characterization of MR fluids," Smart Materials and Structures, 24(6), p. 065018.

[64] Eshaghi, M., Sedaghati, R., and Rakheja, S., 2015, "The effect of magneto-rheological fluid on vibration suppression capability of adaptive sandwich plates: Experimental and finite element analysis," Journal of Intelligent Material Systems and Structures, p. 1045389X15586449.

[65] Eshaghi, M., Sedaghati, R., and Rakheja, S., 2016, "Analytical and experimental free vibration analysis of multi-layer MR-fluid circular plates under varying magnetic flux," Composite Structures, 157, pp. 78-86.

[66] Eshaghi, M., Sedaghati, R., and Rakheja, S., 2017, "Vibration analysis and optimal design of multi-layer plates partially treated with the MR fluid," Mechanical Systems and Signal Processing, 82, pp. 80-102.

[67] Mahjoob, M., Mohammadi, N., and Malakooti, S., 2009, "An investigation into the acoustic insulation of triple-layered panels containing Newtonian fluids: theory and experiment," Applied Acoustics, 70(1), pp. 165-171.

[68] Mohammadi, N., and Mahjoob, M., 2009, "Transmission loss of multilayer panels containing a fluid using progressive wave model: comparison with impedance progressive model and experiments," Comptes Rendus Mécanique, 337(4), pp. 198-207.

[69] Mahjoob, M. J., Mohammadi, N., and Malakooti, S., 2012, "Analytical and experimental evaluation of magnetic field effect on sound transmission loss of MR-based smart multi-layered panels," Applied Acoustics, 73(6), pp. 614-623.

[70] Hasheminejad, S. M., and Shabanimotlagh, M., 2010, "Magnetic-field-dependent sound transmission properties of magnetorheological elastomer-based adaptive panels," Smart Materials and Structures, 19(3), p. 035006.

[71] Choi, S., Seo, J., Kim, J., and Kim, K., 2001, "An electrorheological fluid-based plate for noise reduction in a cabin: experimental results," Journal of sound and vibration, 239(1), pp. 178-185.

[72] Tang, H., Luo, C., and Zhao, X., 2004, "Tunable characteristics of a flexible thin electrorheological layer for low frequency acoustic waves," Journal of Physics D: Applied Physics, 37(16), p. 2331.

[73] Tang, H., Zhao, X.-p., and Luo, C.-r., 2006, "Sonic responses of an electrorheological layer with one side of grating electrodes," Journal of Physics D: Applied Physics, 39(3), p. 552.

[74] Tang, H., and Lee, S.-Y., 2007, "Direct experimental verification of the sound-induced tunable resonance on a flexible electrorheological layer," Journal of Applied Physics, 101(8), p. 084913.

[75] Zielinski, T. G., and Rak, M., 2010, "Acoustic Absorption of Foams Coated with MR Fluid under the Influence of Magnetic Field," Journal of Intelligent Material Systems and Structures, 21(2), pp. 125-131.

[76] Meeker, D., 2006, "Finite element method magnetics (FEMM 4.0.1)," [Online], Available: http://www.femm.info (Accessed: 5 September 2016).

[77] 2011, "LORD technical data: MRF-132DG magneto-rheological fluid," [Online], Available: http://www.lord.com/sites/default/files/DS7015_MRF-132DGMRFluid.pdf (Accessed: 15 July 2016).

[78] Hjelmstad, K. D., 2005, Fundamentals of structural mechanics, Springer US.

[79] Selmane, A., and Lakis, A., 1999, "Natural frequencies of transverse vibrations of non-uniform circular and annular plates," Journal of sound and vibration, 220(2), pp. 225-249.

[80] Baumann, W. T., Saunders, W. R., and Robertshaw, H. H., 1991, "Active suppression of acoustic radiation from impulsively excited structures," The Journal of the Acoustical Society of America, 90(6), pp. 3202-3208.

[81] Fuller, C. R., 1990, "Active control of sound transmission/radiation from elastic plates by vibration inputs: I. Analysis," Journal of Sound and Vibration, 136(1), pp. 1-15.

APPENDIX A

$$[C^c] = \begin{bmatrix} 1 & 1 & 0 & 0 \\ 0 & \dfrac{2}{r_j} & 0 & 0 \\ 0 & 0 & 1 & 0 \\ 0 & 0 & 0 & 1 \end{bmatrix} \tag{A.1}$$

$$[C^a] = \begin{bmatrix} 1 & y_i^2 & \ln y_i & y_i^2 \ln y_i & 0 & 0 & 0 & 0 \\ 0 & \dfrac{2}{r_j} y_i & \dfrac{1}{r_j y_i} & \dfrac{1}{r_j} y_i(2\ln y_i + 1) & 0 & 0 & 0 & 0 \\ 0 & 0 & 0 & 0 & y_i & y_i^2 & 0 & 0 \\ 0 & 0 & 0 & 0 & 0 & 0 & y_i & y_i^2 \\ 1 & 1 & 0 & 0 & 0 & 0 & 0 & 0 \\ 0 & \dfrac{2}{r_j} & \dfrac{1}{r_j} & \dfrac{1}{r_j} & 0 & 0 & 0 & 0 \\ 0 & 0 & 0 & 0 & 1 & 1 & 0 & 0 \\ 0 & 0 & 0 & 0 & 0 & 0 & 1 & 1 \end{bmatrix}, \quad y_i = \dfrac{r_i}{r_j} \tag{A.2}$$

$$[N_1^c] = \begin{bmatrix} 1 & y^2 & 0 & 0 \\ 0 & 0 & y & 0 \end{bmatrix} \tag{A.3}$$

$$[N_3^c] = \begin{bmatrix} 1 & y^2 & 0 & 0 \\ 0 & 0 & 0 & 0 \end{bmatrix} \tag{A.4}$$

$$[N_1^a] = \begin{bmatrix} 1 & y^2 & \ln y & y^2 \ln y & 0 & 0 & 0 & 0 \\ 0 & 0 & 0 & 0 & y & y^2 & 0 & 0 \end{bmatrix} \tag{A.5}$$

$$[N_3^a] = \begin{bmatrix} 1 & y^2 & \ln y & y^2 \ln y & 0 & 0 & 0 & 0 \\ 0 & 0 & 0 & 0 & 0 & 0 & y & y^2 \end{bmatrix} \tag{A.6}$$

$$[B_i^c] = \begin{bmatrix} -z\dfrac{\partial^2}{\partial r^2} & \dfrac{\partial}{\partial r} \\[10pt] -\dfrac{z}{r}\dfrac{\partial}{\partial r} & \dfrac{1}{r} \\[10pt] 0 & 0 \end{bmatrix} [L_i^{*c}] \quad , \quad i = 1,3 \tag{A.7}$$

$$[B_2^c] = \begin{bmatrix} \dfrac{d}{2h_2}\dfrac{\partial}{\partial r} & \dfrac{1}{h_2} \\[10pt] 0 & 0 \end{bmatrix} [L_1^{*c}] + \begin{bmatrix} \dfrac{d}{2h_2}\dfrac{\partial}{\partial r} & -\dfrac{1}{h_2} \\[10pt] 0 & 0 \end{bmatrix} [L_3^{*c}] \tag{A.8}$$

$$[B_i^a] = \begin{bmatrix} -z\dfrac{\partial^2}{\partial r^2} & \dfrac{\partial}{\partial r} \\[10pt] -\dfrac{z}{r}\dfrac{\partial}{\partial r} & \dfrac{1}{r} \\[10pt] 0 & 0 \end{bmatrix} [L_i^{*a}] \quad , \quad i = 1,3 \tag{A.9}$$

$$[B_2^a] = \begin{bmatrix} \dfrac{d}{2h_2}\dfrac{\partial}{\partial r} & \dfrac{1}{h_2} \\[10pt] 0 & 0 \end{bmatrix} [L_1^{*a}] + \begin{bmatrix} \dfrac{d}{2h_2}\dfrac{\partial}{\partial r} & -\dfrac{1}{h_2} \\[10pt] 0 & 0 \end{bmatrix} [L_3^{*a}] \tag{A.10}$$

$$[L_1^c] = \begin{bmatrix} 1 & y^2 & 0 & 0 \\[10pt] 0 & -\dfrac{2z_1 y}{r_j} & y & 0 \end{bmatrix} [C^c]^{-1} \tag{A.11}$$

$$[L_3^c] = \begin{bmatrix} 1 & y^2 & 0 & 0 \\[10pt] 0 & -\dfrac{2z_3 y}{r_j} & 0 & y \end{bmatrix} [C^c]^{-1} \tag{A.12}$$

$$[L_1^a] = \begin{bmatrix} 1 & y^2 & \ln y & y^2 \ln y & 0 & 0 & 0 & 0 \\[10pt] 0 & -\dfrac{2z_1 y}{r_j} & -\dfrac{z_1}{r_j y} & -\dfrac{z_1 y}{r_j}(2\ln y + 1) & y & y^2 & 0 & 0 \end{bmatrix} [C^a]^{-1} \tag{A.13}$$

$$[L_3^a] = \begin{bmatrix} 1 & y^2 & \ln y & y^2 \ln y & 0 & 0 & 0 & 0 \\ 0 & -\dfrac{2z_3 y}{r_j} & -\dfrac{z_3}{r_j y} & -\dfrac{z_3 y}{r_j}(2 \ln y + 1) & 0 & 0 & y & y^2 \end{bmatrix} [C^a]^{-1} \qquad \text{(A.14)}$$

APPENDIX B

$$L_w = [N_{i_1} \quad [0]_{1\times4} \quad N_{i_2} \quad [0]_{1\times4} \quad N_{j_1} \quad [0]_{1\times4} \quad N_{j_2} \quad [0]_{1\times4}]_{1\times28} \tag{B-1}$$

$$N_{i_k} = \left[N_{i_k}^w \quad N_{i_k}^{\phi r} \quad N_{i_k}^{\phi\theta}\right]_{1\times3} \quad \& \quad k = 1,2 \tag{B-2}$$

$$N_{j_k} = \left[N_{j_k}^w \quad N_{j_k}^{\phi r} \quad N_{j_k}^{\phi\theta}\right]_{1\times3} \quad \& \quad k = 1,2 \tag{B-3}$$

$$L_{u_1}^0 = \left[[0]_{1\times3} \quad N_{i_1}^{u_1} \quad [0]_{1\times6} \quad N_{i_2}^{u_1} \quad [0]_{1\times6} \quad N_{j_1}^{u_1} \quad [0]_{1\times6} \quad N_{j_2}^{u_1} \quad [0]_{1\times3}\right]_{1\times28} \tag{B-4}$$

$$L_{u_3}^0 = \left[[0]_{1\times4} \quad N_{i_1}^{u_3} \quad [0]_{1\times6} \quad N_{i_2}^{u_3} \quad [0]_{1\times6} \quad N_{j_1}^{u_3} \quad [0]_{1\times6} \quad N_{j_2}^{u_3} \quad [0]_{1\times2}\right]_{1\times28} \tag{B-5}$$

$$L_{v_1}^0 = \left[[0]_{1\times5} \quad N_{i_1}^{v_1} \quad [0]_{1\times6} \quad N_{i_2}^{v_1} \quad [0]_{1\times6} \quad N_{j_1}^{v_1} \quad [0]_{1\times6} \quad N_{j_2}^{v_1} \quad 0\right]_{1\times28} \tag{B-6}$$

$$L_{v_3}^0 = \left[[0]_{1\times6} \quad N_{i_1}^{v_3} \quad [0]_{1\times6} \quad N_{i_2}^{v_3} \quad [0]_{1\times6} \quad N_{j_1}^{v_3} \quad [0]_{1\times6} \quad N_{j_2}^{v_3}\right]_{1\times28} \tag{B-7}$$

$$N_{i_1}^w = \frac{1}{8}(1 - \bar{r})(1 - \bar{\theta})(2 - \bar{r} - \bar{r}^2 - \bar{\theta} - \bar{\theta}^2) \tag{B-8}$$

$$N_{i_2}^w = \frac{1}{8}(1 - \bar{r})(1 + \bar{\theta})(2 - \bar{r} - \bar{r}^2 + \bar{\theta} - \bar{\theta}^2) \tag{B-9}$$

$$N_{j_1}^w = \frac{1}{8}(1 + \bar{r})(1 - \bar{\theta})(2 + \bar{r} - \bar{r}^2 - \bar{\theta} - \bar{\theta}^2) \tag{B-10}$$

$$N_{j_2}^w = \frac{1}{8}(1 + \bar{r})(1 + \bar{\theta})(2 + \bar{r} - \bar{r}^2 + \bar{\theta} - \bar{\theta}^2) \tag{B-11}$$

$$N_{i_1}^{\phi r} = \frac{1}{8}\left(\frac{r_2 - r_1}{2}\right)(1 - \bar{r})(1 - \bar{\theta})(1 - \bar{\theta}^2) \tag{B-12}$$

$$N_{i_2}^{\phi r} = -\frac{1}{8}\left(\frac{r_2 - r_1}{2}\right)(1 - \bar{r})(1 + \bar{\theta})(1 - \bar{\theta}^2) \tag{B-13}$$

$$N_{j_1}^{\phi r} = \frac{1}{8}\left(\frac{r_2 - r_1}{2}\right)(1 + \bar{r})(1 - \bar{\theta})(1 - \bar{\theta}^2) \tag{B-14}$$

$$N_{j_2}^{\phi r} = -\frac{1}{8}\left(\frac{r_2 - r_1}{2}\right)(1 + \bar{r})(1 + \bar{\theta})(1 - \bar{\theta}^2) \tag{B-15}$$

$$N_{i_1}^{\phi \theta} = \frac{1}{8}\left(\frac{\theta_2 - \theta_1}{2}\right)(1 - \bar{r})(1 - \bar{\theta})(1 - \bar{\theta}^2) \tag{B-16}$$

$$N_{i_2}^{\phi \theta} = \frac{1}{8}\left(\frac{\theta_2 - \theta_1}{2}\right)(1 - \bar{r})(1 + \bar{\theta})(1 - \bar{\theta}^2) \tag{B-17}$$

$$N_{j_1}^{\phi \theta} = -\frac{1}{8}\left(\frac{\theta_2 - \theta_1}{2}\right)(1 + \bar{r})(1 - \bar{\theta})(1 - \bar{\theta}^2) \tag{B-18}$$

$$N_{j_2}^{\phi \theta} = -\frac{1}{8}\left(\frac{\theta_2 - \theta_1}{2}\right)(1 + \bar{r})(1 + \bar{\theta})(1 - \bar{\theta}^2) \tag{B-19}$$

$$N_{i_1}^{u_1} = N_{i_1}^{v_1} = \frac{1}{4}(1 - \bar{r})(1 - \bar{\theta}) \tag{B-20}$$

$$N_{i_2}^{u_1} = N_{i_2}^{v_1} = \frac{1}{4}(1 - \bar{r})(1 + \bar{\theta}) \tag{B-21}$$

$$N_{j_1}^{u_1} = N_{j_1}^{v_1} = \frac{1}{4}(1 + \bar{r})(1 - \bar{\theta}) \tag{B-22}$$

$$N_{j_2}^{u_1} = N_{j_2}^{v_1} = \frac{1}{4}(1 + \bar{r})(1 + \bar{\theta}) \tag{B-23}$$

$$\bar{r} = \frac{r - \frac{r_i + r_j}{2}}{\frac{r_j - r_i}{2}} \tag{B-24}$$

$$\bar{\theta} = \frac{\theta - \frac{\theta_1 + \theta_2}{2}}{\frac{\theta_2 - \theta_1}{2}} \tag{B-25}$$

APPENDIX C

Table C-1. The identified coefficients for the first axisymmetric natural frequency in the absence and 1.8 *Amp* of the applied current and also the rate of change obtained using D-optimal design points (10-decimal digits).

i	a_{ω_i}	b_{ω_i}	c_{ω_i}	i	a_{ω_i}	b_{ω_i}	c_{ω_i}
0	354.9103928875	359.2197267566	-0.0125545438	17	-1.9545708556	0.7321109768	0.0101503809
1	-8.7457556688	-6.8388981025	0.0107411796	18	-1.9545708556	0.7321109768	0.0101503809
2	-8.7457556688	-6.8388981025	0.0107411796	19	-2.0984262209	0.6083665607	0.0098281337
3	-8.8543980981	-6.8382927490	0.0109817007	20	-2.0984262209	0.6083665607	0.0098281337
4	-8.8543980981	-6.8382927490	0.0109817007	21	-1.9111144589	0.6623310404	0.0099860939
5	-8.7914268232	-6.8820630894	0.0108401809	22	-1.9111144589	0.6623310404	0.0099860939
6	-8.7914268232	-6.8820630894	0.0108401809	23	-1.8998329856	0.6740084067	0.0100364607
7	-8.7487507659	-6.9185033274	0.0107164402	24	-1.8998329856	0.6740084067	0.0100364607
8	-8.7487507659	-6.9185033274	0.0107164402	25	-0.4584121125	0.0788130224	0.0017452553
9	-4.4861544213	-0.6773105484	0.0153558605	26	-0.4584121125	0.0788130224	0.0017452553
10	-4.4861544213	-0.6773105484	0.0153558605	27	-0.3424012183	0.2552954069	0.0018345598
11	-4.5244961304	-0.6807647357	0.0153784518	28	-0.3424012183	0.2552954069	0.0018345598
12	-4.5244961304	-0.6807647357	0.0153784518	29	-0.3314567344	0.1283448949	0.0017968960
13	-4.5567602728	-0.6943289073	0.0154488594	30	-0.3314567344	0.1283448949	0.0017968960
14	-4.5567602728	-0.6943289073	0.0154488594	31	-0.4144889029	0.0543964313	0.0017217882
15	-4.4947763995	-0.7469590649	0.0148108500	32	-0.4144889029	0.0543964313	0.0017217882
16	-4.4947763995	-0.7469590649	0.0148108500				

Table C-2. The identified coefficients for the first axisymmetric loss factor in the absence and 1.8 *Amp* of the applied current and also the rate of change obtained using D-optimal design points (10-decimal digits).

i	a_{η_i}	b_{η_i}	c_{η_i}	i	a_{η_i}	b_{η_i}	c_{η_i}
0	0.0845292528	0.0816293036	-0.4553087633	17	-0.0021914344	0.0002413298	0.0779590572
1	-0.0021020964	0.0001897550	0.0726228832	18	-0.0021914344	0.0002413298	0.0779590572
2	-0.0021020964	0.0001897550	0.0726228832	19	-0.0021213417	0.0002313839	0.0678220722
3	-0.0021798338	0.0002013346	0.0754422906	20	-0.0021213417	0.0002313839	0.0678220722
4	-0.0021798338	0.0002013346	0.0754422906	21	-0.0020748826	0.0002441160	0.0780877456
5	-0.0021361161	0.0001889138	0.0773563346	22	-0.0020748826	0.0002441160	0.0780877456
6	-0.0021361161	0.0001889138	0.0773563346	23	-0.0021281056	0.0002398701	0.0792015802
7	-0.0020733098	0.0001842405	0.0829878481	24	-0.0021281056	0.0002398701	0.0792015802
8	-0.0020733098	0.0001842405	0.0829878481	25	-0.0004057903	0.0000641272	0.0127498775
9	-0.0032869588	0.0001319552	0.1147215798	26	-0.0004057903	0.0000641272	0.0127498775
10	-0.0032869588	0.0001319552	0.1147215798	27	-0.0004050744	0.0000814764	0.0027415318
11	-0.0032420143	0.0001338996	0.1081179387	28	-0.0004050744	0.0000814764	0.0027415318
12	-0.0032420143	0.0001338996	0.1081179387	29	-0.0003313369	0.0000797341	0.0093657346
13	-0.0032790770	0.0001439843	0.1114476630	30	-0.0003313369	0.0000797341	0.0093657346
14	-0.0032790770	0.0001439843	0.1114476630	31	-0.0003687671	0.0000718288	0.0185667099
15	-0.0031540899	0.0001160220	0.1059386764	32	-0.0003687671	0.0000718288	0.0185667099
16	-0.0031540899	0.0001160220	0.1059386764				

Table C-3. The identified coefficients for the first axisymmetric natural frequency in the absence and 1.8 *Amp* of the applied current and also the rate of change obtained using random design points (10-decimal digits).

i	a_{ω_i}	b_{ω_i}	c_{ω_i}	i	a_{ω_i}	b_{ω_i}	c_{ω_i}
0	355.0008798956	359.0672269178	-0.0131590477	17	-1.9697898323	0.5631985275	0.0096878934
1	-8.6173125408	-6.6936772063	0.0110357223	18	-1.9169049261	0.8438494230	0.0102896623
2	-8.5100296103	-6.6495917439	0.0103610062	19	-2.2653713520	0.5274323666	0.0100414986
3	-8.7528561102	-6.7051910317	0.0105315124	20	-1.9906169415	0.6638175216	0.0103096488
4	-8.6381839197	-6.7992811776	0.0104591286	21	-2.3263445418	0.4074343971	0.0099691616
5	-8.8259059695	-6.8403351140	0.0106732548	22	-1.9963633497	0.6352761462	0.0098306869
6	-8.7067778159	-6.6957126050	0.0110079859	23	-1.8995023979	0.8077472971	0.0102772794
7	-8.8065499829	-6.7727227892	0.0112716194	24	-1.9872920265	0.7685190406	0.0102445918
8	-8.8032881346	-6.8229761099	0.0106550676	25	-0.3194260476	0.0354633776	0.0011994189
9	-4.3608593594	-0.6055338728	0.0148514125	26	-0.5898930298	-0.0899414417	0.0017905308
10	-4.5495355813	-0.7586584734	0.0150581029	27	-0.2643126220	0.1096549758	0.0011535443
11	-4.4646892357	-0.8294646818	0.0146189409	28	-0.3981653840	0.0052466246	0.0014803656
12	-4.6653076594	-0.7633820717	0.0154742751	29	-0.3368281543	0.1236787513	0.0013667957
13	-4.6334319673	-0.7159896149	0.0156230118	30	-0.2682610818	0.1442725823	0.0017347022
14	-4.7331628183	-0.9138053421	0.0151200269	31	-0.4816097815	-0.0813855634	0.0015057043
15	-4.8703285657	-0.8692970564	0.0156469659	32	-0.1214905141	0.2183389336	0.0015817552
16	-4.5397745024	-0.6223412287	0.0153035910				

Table C-4. The identified coefficients for the first axisymmetric loss factor in the absence and 1.8 *Amp* of the applied current and also the rate of change obtained using random design points (10-decimal digits).

i	a_{η_i}	b_{η_i}	c_{η_i}	i	a_{η_i}	b_{η_i}	c_{η_i}
0	0.0851868160	0.0817456349	-0.3864376724	17	-0.0020290262	0.0002345517	0.0652295112
1	-0.0021917165	0.0001936860	0.0771766053	18	-0.0022571263	0.0002524444	0.0700978053
2	-0.0020460084	0.0001871702	0.0576340263	19	-0.0020928857	0.0002569584	0.0599377846
3	-0.0020953797	0.0001910549	0.0539611571	20	-0.0022501113	0.0002337239	0.0759265720
4	-0.0020562020	0.0001641434	0.0664762648	21	-0.0020638575	0.0002427420	0.0610368273
5	-0.0021123890	0.0001845207	0.0646336047	22	-0.0021200707	0.0002228874	0.0688158950
6	-0.0022006839	0.0001935435	0.0668556071	23	-0.0021956296	0.0002462361	0.0685628129
7	-0.0021719323	0.0002089810	0.0718913989	24	-0.0022017747	0.0002470235	0.0670205097
8	-0.0021414349	0.0001847742	0.0642743987	25	-0.0001405999	0.0000684025	0.0058013493
9	-0.0031801015	0.0001179080	0.0972598402	26	-0.0003715296	0.0000667845	0.0135894322
10	-0.0031839437	0.0001357577	0.0993612035	27	-0.0002004349	0.0000775638	0.0001597017
11	-0.0029982580	0.0001273794	0.0965983440	28	-0.0002664337	0.0000668502	0.0080795289
12	-0.0033289698	0.0001363592	0.1020599268	29	-0.0002081765	0.0000722309	-0.0020105510
13	-0.0034474894	0.0001201611	0.1093601836	30	-0.0003842992	0.0000654405	0.0146257097
14	-0.0032078735	0.0001190402	0.0984191615	31	-0.0003173589	0.0000463383	0.0134044679
15	-0.0033808810	0.0001330451	0.1034015420	32	-0.0003071328	0.0000716860	0.0170727621
16	-0.0033139125	0.0001366010	0.0975778105				